FACULTY OF ELECTRICAL ENGINEERING
UNIVERSITY OF BANJA LUKA

# ELECTRONICS

VOLUME 23, NUMBER 1, JUNE 2019

**FACULTY OF ELECTRICAL ENGINEERING**
**UNIVERSITY OF BANJA LUKA**

Address: Patre 5, 78000 Banja Luka, Bosnia and Herzegovina
Phone: +387 51 211824
Fax: +387 51 211408
Web: www.etf.unibl.org

# E L E C T R O N I C S

Web: www.els-journal.etf.unibl.org
E-mail: els-journal@etf.unibl.org



*Publisher:*
Faculty of Electrical Engineering, University of Banja Luka, Bosnia and Herzegovina

Number of printed copies: 100

# Editor's Column

Mladen Knezic

Chop your own wood and it will warm you twice.

*Henry Ford*

*Editorial Letter*
*DOI: 10.7251/ELS1923001K*

THIS is the first issue in 2019 and it brings four regular papers that address different challenges in diverse topics within the scope of the *Electronics* journal.

The paper "Mitigation of Fiber Nonlinear Effects in 1.28 Tbps DQPSK Modulated DWDM System" by T. Huszaník, J. Turán, and L. Ovseník explores limiting factors of high capacity multichannel Dense Wavelength Division Multiplexing (DWDM) imposed by fiber nonlinearities. The authors have developed a numerical simulation model of 1.28 Tbps DWDM system in order to address some of the aforementioned challenges and they have presented several methods to mitigate fiber nonlinear effects.

The paper "Two element folded meander line MIMO antenna for Wireless applications" by S. Chouhan and L. Malviya describes a design of compact low profile folded MIMO antenna for 5.2 GHz applications. As reported by the authors, the antenna has bandwidth of 600 MHz, 11.32% fractional bandwidth, compact size, and return loss of -44 dB. The authors also evaluated the radiation effect on human body in different positions for indoor environment.

The paper "DC Hard Faults Detection and Localization in Analog Circuits Using Fuzzy Logic Techniques" by M. Merabet and N. Bourouba demonstrates a novel technique based on the use of a fuzzy logic system and simulation before test (SBT) approach for detecting hard faults in analog electronic circuits. The proposed method has been validated on an example of inverting amplifier with uA741 operational amplifier, and its applicability has been demonstrated through a set of different experiments.

The paper "The Investment Justification Estimate and Techno-economic and Ecological Aspects Analysis of the University Campus Microgrid" by N. Savić, V. Katić, B. Dumnić, D. Milićević, Z. Čorba, and N. Katić presents the plan and design of an idea of microgrid at the Faculty of Technical Sciences in Novi Sad (FTN NS). The authors have described the main technical characteristics, the estimation of electricity generation and the amount of non-polluted gaseous greenhouse effect for each distributed energy source.

I thank the authors for their contribution to this issue of the journal. I also thank all the reviewers for providing valuable comments to the authors, which definitely improved the content quality of this issue.

# Mitigation of Fiber Nonlinear Effects in 1.28 Tbps DQPSK Modulated DWDM System

Tomáš Huszaník, Ján Turán, Ľuboš Ovseník

***Abstract*—The main limitation factor of high capacity multichannel DWDM (Dense Wavelength Division Multiplexing) systems are fiber nonlinear effects. The optical signal is severely degraded due to fiber nonlinear effects also known as Kerr fiber nonlinearity. Nonlinear effects under investigation are self-phase modulation (SPM) and cross-phase modulation (XPM). There are several methods to compensate these nonlinear distorts, some less or more effective. Nonlinear distort due to SPM and XPM can be effectively mitigated through implementation of optical DQPSK modulation over commonly used intensity modulation known as OOK (On-Off Keying). This paper presents a numerical simulation model of 1.28 Tbps DWDM system with optical DQPSK modulation. We present several scenarios and methods to mitigate fiber nonlinear effects including Fractional Fourier Transform (FrFT). Linear and nonlinear effects are considered together, so we implement the inline FrFT module in the optical domain which causes a time-frequency plane rotation to mitigate combined linear and nonlinear effects. The performance of proposed 1.28 Tbps DQPSK modulated DWDM system is evaluated in term of bit error rate (BER) and Q factor value.**

***Index Terms*—chromatic dispersion, DQPSK, DWDM, FrFT, nonlinear effects.**

*Original Research Paper*
*DOI: ELS10.7251/ELS1923003H*

## I. Introduction

THE exponential increase in transmission capacity triggered the era of fast and reliable data transfer techniques through fiber optical networks. This has led to the exploration of new options in the field of spectrally efficient systems suitable for extremely high data rates. Consequently, there is a gradual transition from existing systems with a 10 Gbps transmission rate to 40 Gbps optical transmission systems. However, with the increase in network transmission capacity, the demand for optical signal performance is also increased to ensure acceptable bit error rate (BER) in the receiver. Increasing transmission power, however, leads to distortion of the transmitted signal due to the non-linear Kerr effect or interference between adjacent channels. These are the main limitations that set the upper limit of the maximum effective SNR (signal to noise ratio) of the optical link and limit the performance of the entire system. On the other hand, linear effects, such as chromatic dispersion (CD), spontaneous photon emission, fiber optic loss, or channel overlapping through long stretches of fiber are also important factors when designing the DWDM system. Despite the relatively reliable and efficient modulation formats (intensity modulation), the spectral efficiency of the DWDM system is heavily influenced by linear and nonlinear effects such as self-phase modulation (SPM), cross-phase modulation (XPM) and four-wave mixing (FWM). Nonlinear effects affect not only the backbone networks but also access fiber optic networks and their capacity and transmission range itself. In designing high-speed multi-channel optical transmission, therefore, the impact of linear and nonlinear transmission degrading phenomena has required a great deal of attention from research teams. The influence of nonlinear effects such as XPM and FWM can be controlled in conventional optical communication systems by residual local optical fiber dispersion or by setting the channel spacing to a sufficiently large value. The chromatic dispersion, as a linear effect, can be effectively compensated either periodically along the fiber or on the receiver side [1]-[3].

The current generation of fiber optical networks relies mainly on basic optical modulation techniques such as NRZ-OOK or optical phase modulation (OPM). However, with the increasing transmission rates and capacity basic modulation formats are no more suitable for such transmission. From the study of nonlinear effects, it has been found that the generation of nonlinear effects SPM, XPM and FWM can be minimized if the transmitted signal has some special characteristics. A narrow bandwidth modulation format can increase spectral efficiency and chromatic dispersion resistance. Conversely, the modulation format with constant optical performance may be less prone to SPM and XPM. A multilevel modulation format can capture more information than a binary signal, and thanks to the longer symbol duration, reduce degradation due to chromatic and polarization dispersion. In addition, long-haul transmission is an important factor influencing the occurrence of nonlinear phenomena, as well as the amplification of the optical signal often performed by an erbium doped fiber amplifier (EDFA) or semiconductor optical amplifier (SOA), which also introduces noise into the system and under certain circumstances (the length of doped fiber, the degree of amplification) the nonlinear SPM and XPM effects can build up in the optical fiber. The main difference between doped fiber amplifier and semiconductor one is the in the energy delivery, as in the case of EDFA a laser pump is used. For SOA, the power is supplied by an electric excitation field.

Manuscript received 29 November 2018. Received in revised form 23 January 2019. Accepted for publication 6 February 2019.

T. Huszaník, J. Turán and Ľ. Ovseník are with the Faculty of Electrical Engineering and Informatics, Technical University of Košice, Košice, Slovakia (email: tomas.huszanik@tuke.sk, jan.turan@tuke.sk, lubos.ovsenik@tuke.sk).

The principle of amplifying light is based on the recombination of electrons and holes at the p-n transition. SOAs are produced as chips that are placed in a closed housing capable of maintaining a constant temperature. Therefore, via advanced optical modulation formats and optimization of fiber optical transmission path we can mitigate fiber nonlinear effects [2], [3].

In this paper we present the structure of DWDM system with 32 wavelength channels and capacity of 1.28 Tbps (40 Gbps per channel). Each channel is DQPSK (Differential Quadrature Phase Shift Keying) modulated. Using the simulation tool OptiSystem™ we investigate the nonlinear effects in proposed 1.28 Tbps DQPSK modulated DWDM system. We present several ways to mitigate fiber nonlinear effects in high capacity DWDM system including Fractional Fourier Transform (FrFT) which will be further described in this paper.

The structure of the paper is organized as follows: in the second chapter we discuss related works, the third chapter is dedicated to the brief overview of FrFT and its implementation to the optical DQPSK transmitter, the fourth chapter include the description of mathematical simulation model of DWDM system, followed by results analysis and discussion in the chapter five.

## II. Related Works

Several researchers have contributed their effort to investigate the influence of fiber nonlinear effects on signal transmission in high speed DWDM networks. Sajgalikova et al. compared the different numerical modeling of optical degradation mechanisms in [4]. The fiber nonlinear effects were also investigated by Karar [5]. The self-phase modulations dependence on chromatic dispersion was investigated by Ivaniga et al. [6]. He proved SPM influence in DWDM system with AWG multiplexer and demultiplexer. Zhang et al. [7] studied the impact of fiber nonlinearity on PMD (Polarization Mode Dispersion) penalty in DWDM systems back in 2005. They determined the PMD-induced Q factor penalty in 80 channel DWDM system with transmission rate of 10.67 Gbps. Nain et al. provides the mathematical description of nonlinear Kerr effects in [8]. He also provides the experimental results of SPM, XPM and FWM at 5 Gbps and 10 Gbps over 100 km transmission distance. In [9], Ivaniga et al. performed the simulation of 8 and 16 channel DWDM system. They simulated the two scenarios in which the transmission power was increased. The main contribution of that paper was the monitoring of SPM under two different coding methods – NRZ (Non-Return to Zero) and Miller coding. The influence of FWM in DWDM system with AWG with NRZ and BRZ (Bipolar Return to Zero) was investigated by Ivaniga et al. [10]. Authors put their effort into investigation of FWM influence on Ultra-DWDM system (with channel spacing of 12.5 GHz). Authors of this manuscript published the paper [11] in which they propose a 40 Gbps 16 channel DWDM system with 2-DPSK (Differential Phase Shift Keying) modulation and counter directional EDFA. Authors estimate the optimal parameters of counter directional EDFA such as the optimal length of erbium doped fiber, pump power and pump central wavelength. Lavrinovica et al. [12] also estimated EDFA performance in 40 Gbps DWDM system. Since nonlinear effects, most significantly SPM, are chromatic dispersion dependent, several authors contributed to this area. Spolitis et al. compared several passive chromatic dispersion compensation techniques in 16 channel DWDM in [13]. The study of fiber nonlinear effects controlled by different optical modulation formats in 10 Gbps DWDM systems are provided in [14] by Huszaník et al. The same authors also contributed on investigation of optical IQ modulation in 4 channel DWDM system with the presence of optical fiber nonlinearities [15]. Authors provide comparative analysis of three possible configurations of optical IQ modulator and evaluate its performance in high spectral DWDM system. Optical QPSK was also investigated by Fady El-Nahal [16]. Optical modulation formats for DWDM systems were intensively studied by Kahn [17], Kaur [18], Jawla [19] and Faisal [20]. In 2014, Mohaparta et al. [21] studied digital modulation formats within and beyond 400 Gbps in both DWDM and CWDM (Coarse Wavelength Division Multiplexing). In this paper, authors team, describe the influence of bit rate on different digital modulations.

## III. Overview of Fractional Fourier Transform in fiber optical networks

The main limitation factors of current long-haul fiber optical communication networks are nonlinear effects and chromatic dispersion. Nonlinear effects, especially SPM, are in a very close relationship to CD. The combined effect of CD and Kerr nonlinear effects correspond to time-frequency distortion of transmitted optical pulses. CD affects the amplitude and the width of the optical spectra of transmitted optical pulse. Nonlinear effects such as SPM and XPM do not have influence on the pulse envelope. This contribution of CD and nonlinear effects result in the time-frequency distortion. The correction of transmission affected by time-frequency distortion can be done by introducing a transformation that corrects the time-frequency rotation. This correction can be done by utilizing Fractional Fourier Transform (FrFT) [22]-[23].

FrFT is based on conventional Fourier transform. Fourier transform (FT) is widely used in various fields. It enables to transform signal from time domain to frequency domain. The concept of conventional Fourier transform is very well known. The functions *f* and *F* are Fourier transform pair if [22]:

$$f(x) = \int_{-\infty}^{\infty} F(v) e^{(i2\pi vx)} dv, \tag{1}$$

$$F(v) = \int_{-\infty}^{\infty} f(x) e^{(-i2\pi vx)} dx. \tag{2}$$

The fractional Fourier transform is the general form of conventional Fourier transform. Fractional Fourier transform can be defined as [22]:

$$X_\phi(u) = \int_{-\infty}^{\infty} x(t) K_\phi(t,u) dt, \tag{3}$$

$$X_\phi(u) = \sqrt{\frac{1 - j\cot\phi}{2\pi}} \cdot \exp\left(j\frac{u^2}{2}\cot\phi\right) \int_{-\infty}^{\infty} x(t)\exp\left(j\frac{t^2}{2}\cot\phi - jut\csc\phi\right)dt. \tag{4}$$

In the equation (4), $\phi=p(\pi/2)$, $p$ is the order of FrFT. If $\phi=\pi/2$, FrFT corresponds to the conventional FT. FrFT with parameter $\phi$ can be seen as an angle of rotation in the time-frequency plane (Fig. 1) [22]-[23].

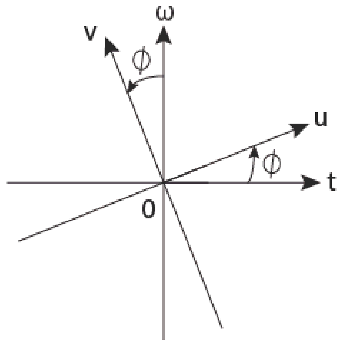


Fig. 1. Time-frequency plane rotation

So, the FrFT is performed as a rotation operation on the time frequency distribution. If the rotation is $\phi=0$, there will be no change when applying FrFT and $\phi=\pi/2$ equals to FT [23].

The FrFT module consists of two optical phase modulators and a dispersive optical medium as shown on Fig. 2. The two optical phase modulators are driven by periodic parabolic electric signal and the dispersive medium (optical fiber) which can act like a filter which performs an approximated operation of convolution [22], [23].

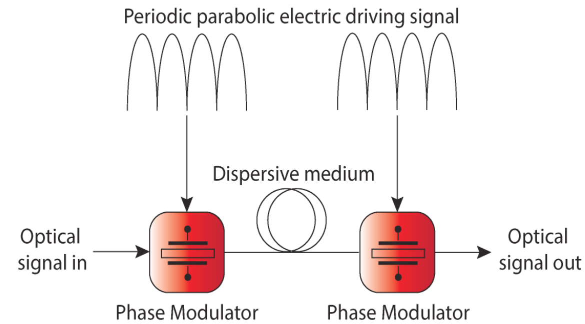


Fig. 2. The structure of FrFT module

## IV. Description of Proposed Simulation Model

The simulation model of 1.28 Tbps DQPSK modulated DWDM system was created within the OptiSystem™ environment. OptiSystem™ is an innovative software package for simulating optical communication systems. It enables to design, test and optimize virtually any type of optical connection in the physical layer of a wide range of optical networks, from analogue video transmission to intercontinental bone fiber optical networks. The simulation is based on Time-Domain Split-Step method (TDSS).

The block scheme of a simulation model is shown on Fig. 3. It consists of three parts: transmitting section, optical fiber section and receiving section. The global parameters of a simulation model are: bit rate – 40 Gbps, time window – 6.4e-09, sample rate – 1.024e+13 Hz, sequence length – 256 bits.

Transmitting section is formed of 32 wavelength channels placed in C-band in the range of (193.0 – 196.1) THz with the

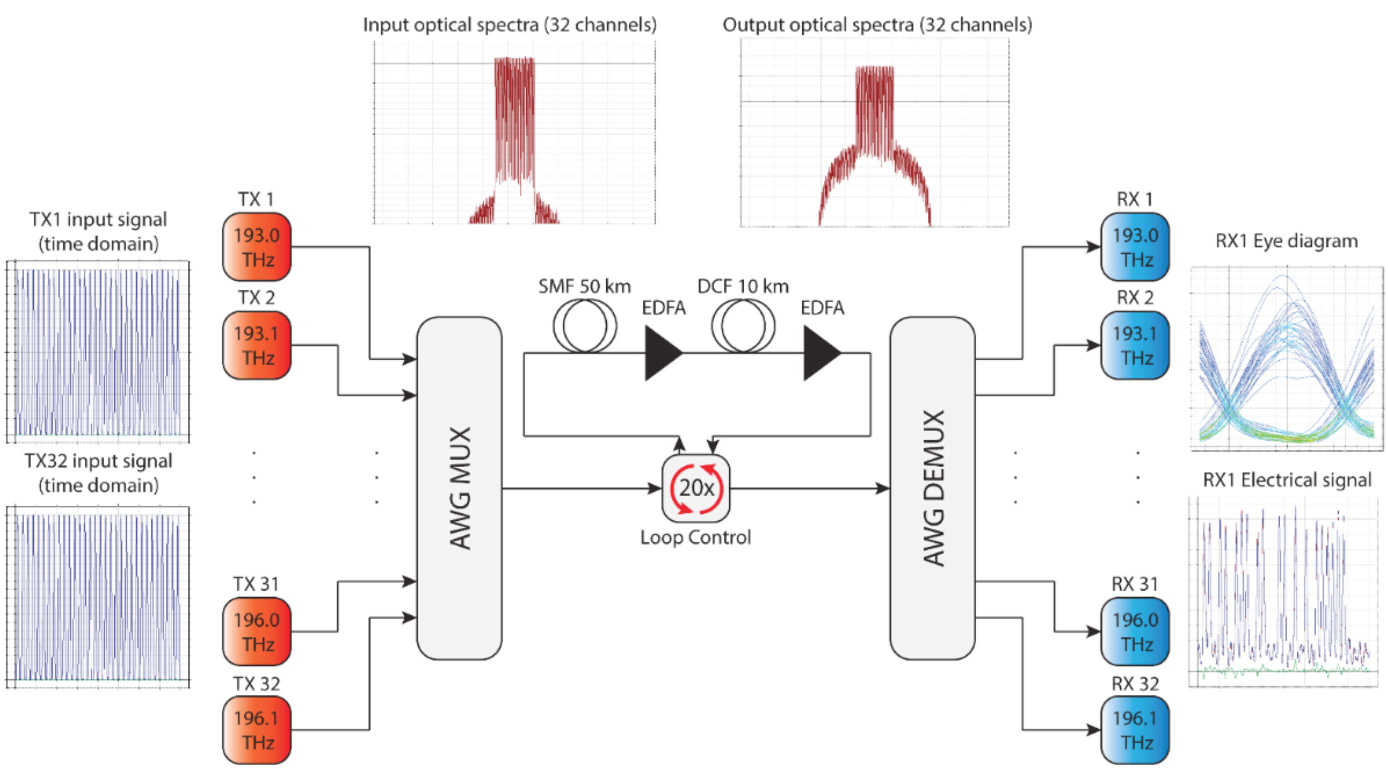


Fig. 3. Simulation model of 1.28 Tbps DQPSK modulated DWDM system

channel spacing of 100 GHz. Each transmitter utilizes optical DQPSK modulator with 40 Gbps bit rate. The block scheme of optical transmitter with DQPSK modulator is on Fig. 4. Optical DQPSK modulator is formed of pseudorandom binary sequence (PRBS) generator generaring pseudorandom bit sequence with 40 Gbps bit rate (per channel). Data are then precoder by 4-DPSK (Differential Phase Shift Keying) precoder and then electrically modulated via NRZ modulator drivers. NRZ signal is then modulated by two $LiNbO_3$ Mach-Zehnder (MZ) modulators. In one of the arms, there is an optical phase shifter to create orthogonal signal to the other arm of the modulator structure and thus create I (In phase) and Q (Quadrature) signal component. Optical carrier is generated by continuous wave (CW) laser.

The induced phase difference between two arms of the IQ modulator is expressed by following equation:

$$\Delta\varphi_I(t) = \frac{u_I(t)}{V_\pi}\pi \cdot \Delta\varphi_Q(t) = \frac{u_I(t)}{V_\pi}\pi, \tag{5}$$

where $\Delta\varphi_I(t)$ and $\Delta\varphi_Q(t)$ are phases of I and Q arms, $u_I(t)$ is the voltage applied on the arms of $LiNbO_3$ MZ modulators and $V_\pi$ is the driving amplitude for switching bias voltage. The transfer function of an IQ (DQPSK) modulator is:

$$\frac{E_{out}(t)}{E_{in}(t)} = \frac{1}{2}cos\left(\frac{\Delta\varphi_I(t)}{2}\right) + j\frac{1}{2}cos\left(\frac{\Delta\varphi_Q(t)}{2}\right). \tag{6}$$

Then, the amplitude modulation $A_{IQM}(t)$ (3) and phase modulation $\varphi_{IQM}(t)$ (4) of DQPSK modulator is:

$$A_{IQM}(t) = \left|\frac{E_{out}(t)}{E_{in}(t)}\right| = \frac{1}{2}\sqrt{cos^2\left(\frac{u_I(t)}{V_\pi}\pi\right) + cos^2\left(\frac{u_Q(t)}{V_\pi}\pi\right)}, \tag{7}$$

$$\varphi_{IQM}(t) = arg\left[cos^2\left(\frac{u_I(t)}{V_\pi}\pi\right) \cdot cos^2\left(\frac{u_Q(t)}{V_\pi}\pi\right)\right]. \tag{8}$$

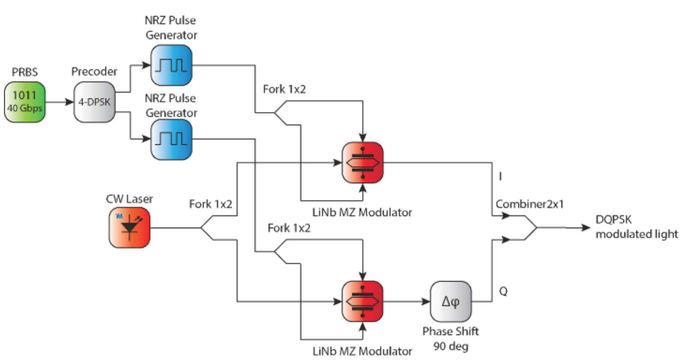


Fig. 4. The block model of optical DQPSK transmitter

The structure of optical DQPSK transmitter is modified with FrFT module to mitigate the influence of fiber nonlinear effects. In general, the FrFT module consists of two optical phase modulators driven by periodic parabolic electric signal and dispersive medium. However, OptiSystem™ does not allow to use an arbitrary waveform generator for generating periodic parabolic electric signal. To produce periodic parabolic signal, we used the sine pulse generator with the binary NOT and binary OR components. PRBS generates the stream of binary ones and zeros, which does not produce periodic parabolic signal by connecting the sine pulse generator. However, by using binary NOT and binary OR components as shown on Fig. 5, the sine pulse generator is driven by binary ones only so the periodic parabolic signal can be produced. The dispersive medium (SMF) is 0.1 km long. All 32 wavelength channels are multiplexed by AWG (Arrayed Waveguide Grating) multiplexer and then transmitted through the optical fiber section. The insertion loss of an AWG is 5.5 dB.

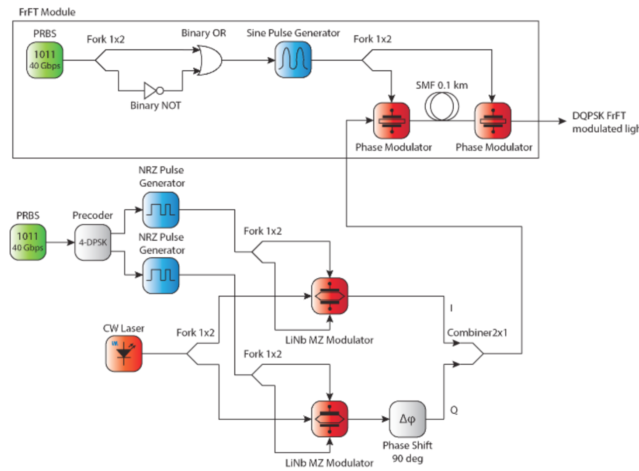


Fig. 5. The block model of optical DQPSK transmitter with FrFT

Optical distribution path (seen on Fig. 3) is formed of a loop component with number of loops 20. Each loop consists of 50 km of highly nonlinear optical fiber (HNLF), two in-line erbium doped fiber amplifiers (EDFAs) and dispersion compensation fiber (DCF). An SMF has attenuation of 0.22 dB/km, chromatic dispersion is set to 17 ps/km-nm$^2$, nonlinear refractive index is $n_2$ = 2.6e-20 m$^2$/W and effective cross section area of the fiber is $A_{eff}$ = 80 μm$^2$. Induced chromatic dispersion is fully compensated in dispersion compensation fiber. DCF is an optical fiber that has opposite value of dispersion to the main transmission fiber, in this case, the value of chromatic dispersion of DCF is -80 ps/km-nm$^2$, $n_2$ is 2.6e-20 m$^2$/W and $A_{eff}$ is 30 μm$^2$. The length of DCF is 10 km. In each loop, there are two EDFAs. The first one, in-line EDFA having the noise figure of 6 dB and output power 20 dB is used to compensate the power loss of the SMF. The second EDFA is used to compensate the power loss of DCF and its output power is 5 dB and noise figure is 6 dB.

The signal is demultiplexed using AWG demultiplexer. The block scheme of optical DQPSK receiver is illustrated on Fig. 6. The receiver is formed of one-bit delay line with double balanced photodiode. Data are precoded differentially at the transmitter. That means, that at the receiver side, we can compare and restore the phase of current transmitted symbol with the phase of previously transmitted symbol. The phase difference between current and previous symbol may be 0, π/2, -π/2 or π. The signals detected by two photodiodes (I and Q) are multiplied and regenerated. Receiver sensitivity is -30 dBm.

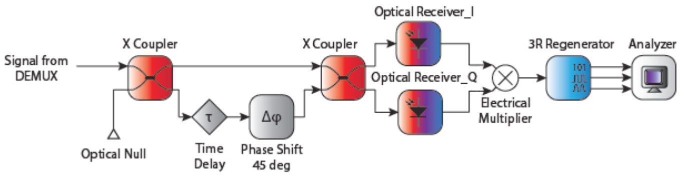


Fig. 6. The block model of optical DQPSK receiver

The received signal is analyzed in electrical domain and compared to the originally transmitted signal. Analyzer component is used to generate the eye diagram. From the eye diagram we extract bit error rate (BER) and Q factor. The calculation of BER and Q factor is based upon these equations [2]:

$$Q = \frac{I_1 - I_0}{\sigma_1 + \sigma_0}, \tag{9}$$

In the equation (9), $I_1$ is the mean value and $\sigma_1$ is the deviation of the pulse 1, $I_0$ is the mean value and $\sigma_0$ is the deviation of pulse 0. The relationship between the BER and the Q factor itself can be determined by a linear combination of probabilities that the receiver is decrypting the incorrect symbol [2]:

$$BER = \frac{1}{2}[P(1|0) + P(0|1)], \tag{10}$$

$$BER = \frac{1}{2} erfc\left(\frac{Q}{\sqrt{2}}\right) \approx \frac{1}{\sqrt{2\pi}Q} exp\left(-\frac{Q^2}{2}\right). \tag{11}$$

## V. Simulation Results and Discussion

The proposed simulation model of 1.28 Tbps DQPSK modulated DWDM system is evaluated in three different scenarios. In all scenarios we consider the fiber nonlinear effects. The objective is to investigate the impact of intensity fluctuations of channel 1 (193.0 THz) on the phase of the signal in channel 2 (193.1 THz). In all simulation scenarios we consider the case without nonlinear effects and chromatic dispersion, the case with nonlinear effects and chromatic dispersion and the case in which we add FrFT module to the DQPSK modulator structure while considering nonlinear effects and chromatic dispersion.

### *A. Scenario 1*

In the first scenario, we set the simulation model to 20 loops. Each loop consists of 50 km of SMF and 10 km of DCF. The performance of the DWDM system is evaluated independently in each loop. The aim of this scenario is to evaluate the influence of fiber nonlinear effects depending on the transmission distance. Fig. 7 shows the optical spectra of 32 wavelength channels transmitted on 250 km and 500 km. Chromatic dispersion cumulated by transmission through the SMF is compensated at the end of each loop by dispersion compensation fiber. From the given spectra we can see that the impact of FWM is weak and thus is neglected. However, the influence of SPM and XPM due to chromatic dispersion is considerably higher. The signal spectra distort as the transmission distance is increased. It is caused due to the in-line amplification. The contribution of SPM and XPM is increasing after each loop. As a consequence, the quality of the received signal, measured by BER and Q factor, is decreasing at each loop.

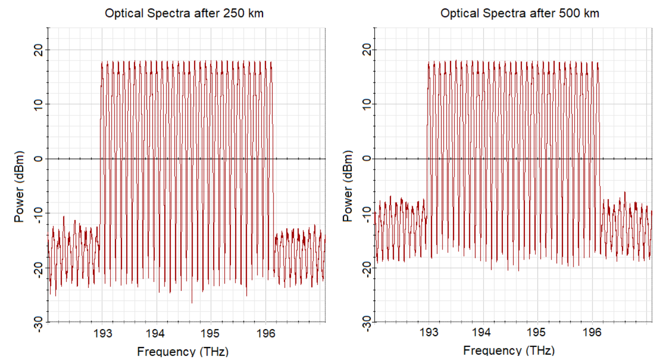


Fig. 7. Optical signal spectra after 250 km and 500 km

Fig. 8 shows the eye diagrams of received signals distorted by nonlinear effects after 550 km and 800 km. The BER values are 3.26e-12 at 550 km and 1.37e-06 at 800 km. In general, the minimum required value of BER is 1e-10. When we do not take nonlinear effects on account, the maximum reach of the proposed DWDM system is over 1000 km. However, due to nonlinear effects the reach is reduced almost by half – 600 km with nonlinear effects and 750 km with nonlinear effects with FrFT module DQPSK transmitter.

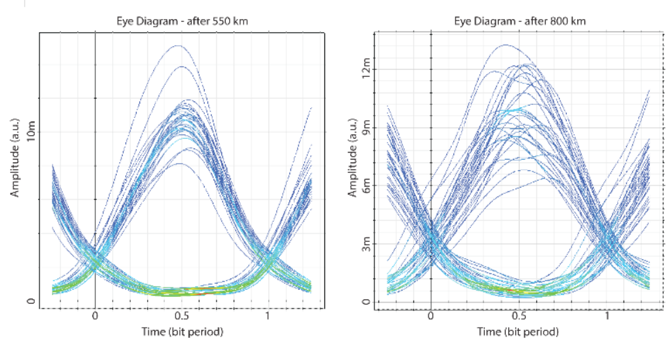


Fig. 8. Eye diagrams of received signals after 550 km and 800 km

The dependence between optical fiber length and BER is illustrated on Fig. 9. There were three calculations made. The first calculation (blue line) does not take nonlinear effects into equation. Thus, the performance of the DWDM system is influenced only by linear effects – attenuation, chromatic dispersion and optical noise and induced by EDFAs. In the second calculation (red line) we consider nonlinear effects, while the nonlinear refractive index $n_2$ = 2.6e-20 $m^2/W$. The maximum acceptable reach is 600 km which is 400 km difference to the case without nonlinear effects. The reason of 400 km drop is the nonlinear interaction in SMF. The nonlinear interaction depends on the length and the cross-section area of the optical fiber. The influence of nonlinear effects increases, the longer the length of the fiber connection. However, as the signal spreads along the line, its performance decreases due to the fiber attenuation. So most nonlinear effects occur at the beginning of the optical path and gradually fade away as the signal propagates through the optical fiber. By utilizing FrFT into optical DQPSK modulator, there is a slight improvement in the performance and the transmission distance has been extended to 750 km (yellow line). Above the 750 km, the transmission quality is no more sufficient for today's standards.

Values of Q factor are provided in Table I. The threshold in Table I. is calculated from equation (11): for 1e-10 BER, the Q-factor is 6.36.

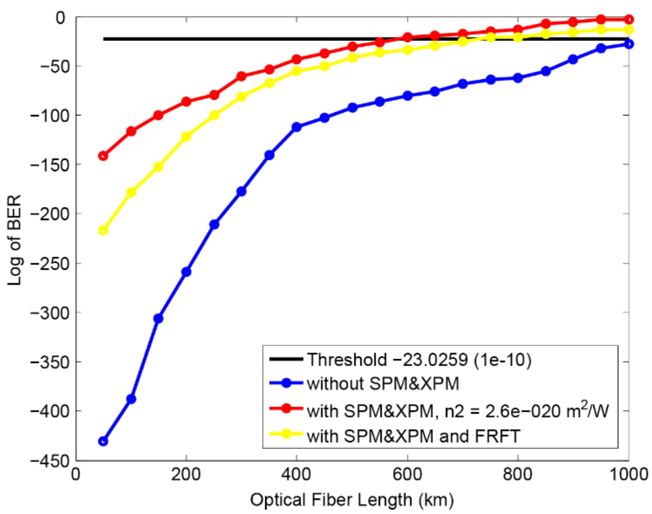


Fig. 9. System performance comparison of three different scenarios

TABLE I
VALUES OF Q FACTOR

| Transmission distance (km) | Q factor | | |
|---|---|---|---|
| | No SPM&XPM | With SPM&XPM | With SPM&XPM + FrFT |
| 50 | 29.20 | 16.61 | 20.65 |
| 100 | 27.70 | 15.02 | 18.68 |
| 150 | 24.56 | 13.90 | 17.23 |
| 200 | 22.57 | 12.84 | 15.33 |
| 250 | 20.33 | 12.30 | 13.88 |
| 300 | 18.63 | 10.71 | 12.44 |
| 350 | 16.56 | 10.05 | 11.30 |
| 400 | 14.70 | 8.95 | 10.20 |
| 450 | 14.06 | 8.24 | 9.71 |
| 500 | 13.32 | 7.38 | 8.81 |
| 550 | 12.87 | 6.87 | 8.23 |
| 600 | 12.37 | 6.03 | 7.85 |
| 650 | 12.02 | 5.78 | 7.26 |
| 700 | 11.41 | 5.46 | 6.76 |
| 750 | 11.05 | 4.92 | 6.08 |
| 800 | 10.82 | 4.69 | 5.98 |
| 850 | 10.24 | 3.32 | 5.41 |
| 900 | 8.97 | 2.80 | 5.12 |
| 950 | 7.68 | 1.54 | 4.72 |
| 1000 | 7.06 | 1.54 | 4.73 |
| Threshold | | 6.36 | |

*B. Scenario 2*

A common way to avoid the creation of fiber nonlinear effects is to keep launch powers low. The main goal is to keep propagation linear. Kerr nonlinear effects, SPM and XPM, are power sensitive. The phase shift difference due to SPM, when propagating single channel over optical fiber is [1]:

$$\Delta\varphi = -2\pi n_1 \frac{L}{\lambda A} P, \tag{12}$$

where $n_1$ is fiber core refractive index, $L$ is the length of the optical fiber, $A$ is the cross-section area of the optical fiber, λ is the wavelength of transmitted signal and $P$ is the power of transmitted signal. SPM and XPM are very similar depending on the refractive index of the optical fiber from the optical signal intensity. However, for XPM, the total phase shift of the transmitted optical pulse in one channel is affected by the properties of the adjacent channels. The refractive index of the optical fiber is also determined by the total intensity of all transmitted channels. Cross-phase modulation actually causes fluctuations in power at a certain wavelength to phase fluctuations at other channels. The result of XPM may be an excessive displacement of the spectral line and the impulse shape deformation. So, in 32 channel DWDM system is the phase shift of the i-channel through the XPM expressed by following equation [1]:

$$\phi_{nl}^{i} = k_{nl} L_e \left( P_i + 2 \sum_{n=i+1}^{32} P_n \right). \tag{13}$$

In the equation (13), $k_{nl}$ is the nonlinear propagation coefficient, $L_e$ is the effective length of the fiber and $P$ is the power. The first part of the equation (13) represents the contribution of the SPM and the second part the contribution of the XPM. The second part of equation (13) also expresses the non-linear sensitivity, and indicates that XPM is two times more efficient than the SPM at given energy.

To evaluate the influence of the launch power on the nonlinear effects, we swept the output power of CW laser of each channel in the range of -10 – 12 dBm. To mitigate nonlinear effects, the launch power must be low. However, it is impractical for long-haul links. With higher launch levels we can transmit further and the detection is more efficient. To fully evaluate the launch power dependence on nonlinear effects we opted for 550 km long transmission (11 loops). Fig. 10 shows the eye diagrams of received signals after 550 km with 10 dBm launch power. BER of received channel is 3.76e-81 without consideration of nonlinear effects and 1.67e-07 with nonlinear effects.

For low launch levels (-10 – 0 dBm) we get BER values above the threshold for all three cases. The signal is not well detectable for the receiver. The lowest possible launch level, for

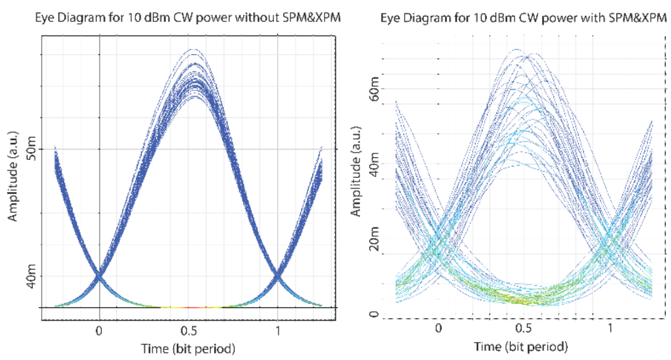


Fig. 10. Eye diagrams of received signals for 10 dBm CW power without and with nonlinear effects

which the performance of the proposed DWDM is acceptable is -3 dBm. In the case without nonlinear effects, BER values increase as the launch power increases. However, SPM and XPM cause severe signal distortion as the launch power increases. This distortion is cause primarily due to phase interaction between adjacent channels induced by XPM. The optimal launch power of the case with nonlinear effects is 5 dBm according to this experiment. The BER in this case is 5.37e-20. As we increase launch power even further, the effect of SPM and XPM increases. The slight correction of the transmission affected by phase shift caused by SPM and XPM and time-frequency distortion respectively can be mitigated by utilization of FrFT. We can see slight improvement of BER in this case – BER 8.51e-22 for 5dBm. Values of calculated Q factor are in Table II.

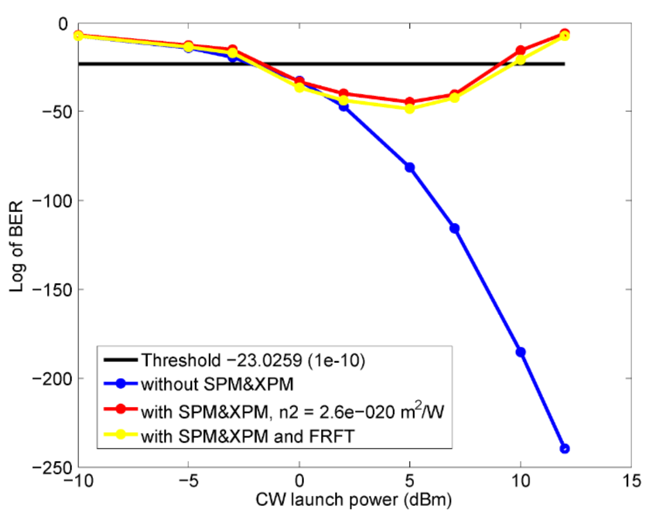


Fig. 11. CW launch power sweep vs BER of three different scenarios

### C. Scenario 3

Since SPM occurs in a close association with chromatic dispersion, it is important to take SPM into account in high-speed systems which are particularly limited in chromatic dispersion. In systems with a transmission rate above 10 Gbps and in systems with high power SPM significantly increases the effects of chromatic dispersion, i.e. overlapping of the transmitted optical pulses. Deployment of appropriate dispersion compensating

TABLE II

VALUES OF Q FACTOR FOR DIFFERENT VALUES OF CW LAUNCH POWER

| CW Launch power (dBm) | Q factor | | |
|---|---|---|---|
| | No SPM&XPM | With SPM&X-PM | With SPM&X-PM + FrFT |
| -10 | 3.16 | 3.10 | 3,27 |
| -5 | 4.78 | 4.47 | 4.66 |
| -3 | 5.75 | 5.03 | 5.38 |
| 0 | 7.68 | 7.76 | 8.17 |
| 2 | 9.35 | 8.55 | 9.00 |
| 5 | 12.48 | 9.08 | 9.52 |
| 7 | 14.97 | 8.63 | 8.85 |
| 10 | 19.04 | 5.10 | 5.98 |
| 12 | 21.70 | 2.74 | 3.28 |
| Threshold | | 6.36 | |

modules in the fiber link limits the signal degradation. In the third scenario we present the way of mitigating nonlinear effects through the chromatic dispersion compensation. There are three possible configurations of DCF compensation technique shown on Fig. 12.

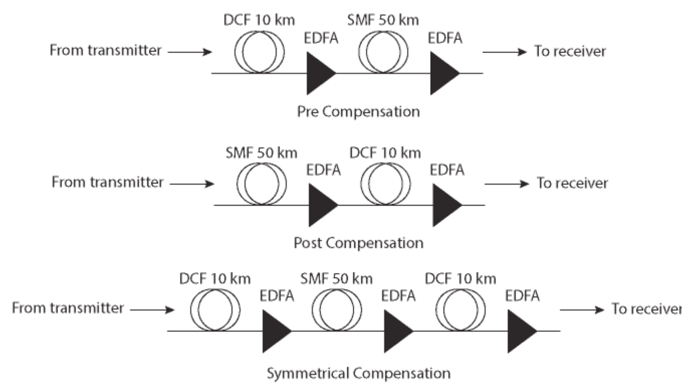


Fig. 12. Schematic of three simulation setups

To simplify calculations, we do not consider nonlinear effects in DCF, since its length is shorter and its nonlinear contribution will be negligible. The nonlinear effects and the resulting distortions occur only in SMF. The simulation setup of this scenario is: length of transmission path – 550 km (11 loops), CW launch power 5 dBm. The most effective DCF compensation techniques are post-compensation and symmetrical compensation. The BER of the DWDM system without CD compensation is above the threshold (-23.0259 / 1e-10). The values of BER and Q factor for different DCF configurations are provided in Table III.

## VI. CONCLUSION

This paper successfully demonstrates the 1.28 Tbps DQPSK modulated DWDM system in the presence of optical fiber nonlinearities. Using the OptiSystem™ the simulation model has been established to estimate the transmission performance of the proposed system in relation to mitigation of fiber nonlinear

TABLE III
Values of Q factor and BER for different CD compensation techniques

| DCF setup | 550 km, CW power – 5 dBm | |
|---|---|---|
| | Q factor | BER |
| No compensation | 5.58 | 1.02e-09 |
| Pre-compensation | 7.81 | 8.25e-15 |
| Post-compensation | 9.04 | 5.37e-20 |
| Symmetrical compensation | 9.30 | 4.56e-21 |

effects. We show that spectrally efficient DQPSK modulated optical signal is robust against the nonlinear effects such as SPM and XPM and linear effect of chromatic dispersion. The higher capacity can be achieved by utilization of optical DQPSK modulation format but the influence of nonlinear effects is still not negligible. The maximum reach of DWDM is limited by nonlinear effects and the power must be kept low enough no to generate nonlinearities. FrFT has been applied on the tested channel in all cases and it is noted that there are improvements in the performance. Nonlinear effects can be mitigated by utilization of FrFT to the optical transmitter. The right choice of launch power along with CD compensation technique can significantly reduce the nonlinear distort due to SPM and XPM.

## ACKNOWLEDGEMENTS

This work was supported by following research grants: KEGA 023TUKE-4/2017 and the Slovak Research and Development Agency under the contract no. "APVV-17-0208 - Resilient mobile networks for content delivery".

## References

[1] R. Ramaswami, K. N. Sivarajan, G. H. Sasaki. *Optical Networks*, 2010. 928p. ISBN 978-0-12-374092-2.

[2] J. M. Simmons, *Optical Network Design and Planning*, 2014, 529 p. ISSN: 1935-3847, DOI: 10.1007/978-3-319-05227-4.

[3] S. P. Singh and N. Singh, "Nonlinear Effects in Optical Fibers: Origin, Management and Applications," *Progress In Electromagnetics Research*, vol. 73, pp. 249-275, 2007. DOI:10.2528/PIER07040201.

[4] J. Sajgalikova, M. Dado, J. Litvik, "Comparison of Numerical Modelling of Degradation Mechanisms in Single Mode Optical Fibre Using MATLAB and VPIphotonics," *Advances in Electrical and Electronic Engineering,* vol. 13, no. 3, pp. 268-272, 2015. DOI: 10.15598/aeee.v13i3.1330.

[5] A. S. Karar, S. Gazor, Y. Gao, J. C. Cartledge, M. O'Sullivan, C. Laperle, A. Borowiec, K. Roberts, "Polynomial Pulses for Mitigating Fiber Nonlinearity in Coherent Optical Fiber Communications," in *IEEE Photonics Technology Letters*, vol. 27, no. 15, pp. 1653-1655, 2015. DOI: 10.1109/LPT.2015.2433834.

[6] T. Ivaniga, J. Turán, Ľ. Ovseník, "Verification of the SPM Impact in DWDM System Using AWG Multiplexer / Demultiplexer," *Acta Electrotechnica et Informatica*, Vol. 17, No. 1, 2017, 17–22, DOI:10.15546/aeei-2017-0003.

[7] G. Zhang, J. T. Stango, X. Zhang, X. Chongjin, "Impact of fiber nonlinearity on PMD penalty in DWDM transmission systems," *IEEE Photonics Technology Letters*, vol. 17, no. 2, pp. 501-503, 2005. DOI: 10.1109/LPT.2004.839010.

[8] H. Nain, U. Jadon, V. Mishra, "Performance investigation of Kerr effects on to WDM fiber optical networks," *IEEE International Conference on Recent Trends in Electronics, Information and Communication Technology*, 2016, pp. 2018-2022, DOI: 10.1109/RTEICT.2016.7808193.

[9] T. Ivaniga, Ľ. Ovseník, J. Turán, "Influence of self-phase modulation on 8 and 16-channel DWDM system with NRZ and miller coding," *Carpathian Journal of Electronic and Computer Engineering,* vol. 8, no. 1, pp. 17-22, 2015.

[10] P. Ivaniga, T. Ivaniga, J. Turán, Ľ. Ovseník, M. Márton, D. Solus, J. Oravec, T. Huszaník. "The Influence of FWM with AWG Multiplexor in DWDM System," *Przeglad Elektrotechniczny*, vol. 2018, no. 4, pp. 113-117, 2018. DOI:10.15199/48.2018.04.28.

[11] O. Kováč, J. Mihalík, I. Gladišová, "Convolution implementation with a novel approach of DGHM multiwavelet image transform," *Journal of Electrical Engineering*, vol.68, no.6, pp. 455-462, 2017. DOI: 10.1515/jee-2017-0080.

[12] I. Lavrinovica, J. Porins, G. Ivanovs, "Estimation of EDFA Performance in 40 Gbit/s 8 channel DWDM Transmission System," *PIERS Proceedings*, pp. 502-505, Prague, Czech Republic, 2015.

[13] V. Spolitis, V. Bobrovs, P. Gavars, G. Ivanovs, "Comparison of passive chromatic dispersion compensation techniques for long reach dense WDM-PON system," *Elektronika ir Elektrotechnika*, vol. 122, no. 6, pp. 65–70, 2012.

[14] O. Kováč, P. Lukács, I. Gladišová, "Textures classification based on DWT," *Proc. 28th Int. Conf. Radioelektronika, RADIOELEKTRONIKA 2018*, Prague; Czech Republic; 19-20 April 2018; pp. 1-5. DOI: 10.1109/RADIOELEK.2018.8376379.

[15] T. Huszaník, J. Turán, Ľ. Ovseník, "Comparative analysis of optical IQ modulation in four-channel DWDM system in the presence of fiber nonlinearities," *Proceedings of the 2018 19th International Carpathian Control Conference, ICCC 2018*, pp. 468-473, 2018. DOI:10.1109/CarpathianCC.2018.8399675.

[16] Fady El-Nahal, "Coherent Quadrature Phase Shift Keying (QPSK) Optical Communication Systems", *Optoelectronics letters*, Vol. 14, No. 5, pp: 372-375, 2018.

[17] J. Kahn, K. P. Ho. "Spectral Efficiency Limits and Modulation/Detection Techniques for DWDM Systems," *IEEE. Journal of Selected Topics in Quantum Electronics*, vol. 10, no. 2, pp. 259-272, 2004. ISSN: 1558-4542. DOI: 10.1109/JSTQE.2004.826575.

[18] A. Kaur, S. Dewra. "Comparative Analysis of Different Modulation Techniques in Coherent Optical Communication System," *International Journal of Innovative Research in Computer and Communication Engineering,* vol. 3, issue 8, pp. 7193 – 7200, August 2015. ISSN: 2320-9801.

[19] S. Jawla, R. K. Singh. "Different Modulation Formats Used In Optical Communication System," *IOSR Journal of Electronics and Communication Engineering (IOSR-JECE)*, vol. 8, no. 4, pp. 15-18, 2013. e-ISSN: 2278-2834, p-ISSN: 2278-8735.

[20] M. Faisal, T. Faruque, M. A. R. Khan, "Post mitigation performance comparison of RZ-DPSK and CSRZ-DPSK DWDM systems," *8th International Conference on Electrical and Computer Engineering*, Dhaka, pp. 433-436, 2014. DOI: 10.1109/ICECE.2014.7026971.

[21] S. K. Mohapatra, R. R. Choudhury, R. Bhojray, P. Das. "Performance analysis and monitoring of various advanced digital modulation and multiplexing techniques of F.O.C within and beyond 400 GB/s," *International Journal of Computer Networks & Communications (IJCNC)*, vol.6, no.2, pp. 159 – 181, India, 2014. ISSN: 0974-9322.

[22] B. T. Krishna, "Fractional Fourier transform: a survey," *Proceedings of the International Conference on Advances in Computing, Communications and Informatics (ICACCI '12)*, Chennai, India, 2012, pp. 751-757. DOI: http://dx.doi.org/10.1145/2345396.234551.

[23] A. Yang, L. Xiang, X. Chen, "A FrFT based method for measuring chromatic dispersion and SPM in optical fibers," *Optical Fiber Technology,* vol. 34, pp. 59-64, 2017. DOI: 10.1016/j.yofte.2017.01.002.

# Two element folded meander line MIMO antenna for Wireless applications

Sanjay Chouhan and Leeladhar Malviya

*Abstract*— **Compact antenna, appropriate gain, high efficiency, wide bandwidth, minimum envelope correlation coefficient (ECC), large total active reflection coefficient (TARC) bandwidth, and low specific absorption rate (SAR) are certain conditions set on the present/future generations of wireless communication antennas with the lowest cost of implementation. A compact low profile folded MIMO antenna has been designed using CST tool to cover application at 5.2 GHz. The reported folded MIMO antenna has bandwidth of 600 MHz (5.0-5.6 GHz) and has fractional bandwidth of 11.32 % along with the compact size of 37.5 × 17.0 mm$^2$. The reported MIMO antenna has ECC of < $10^{-2}$. The proposed folded MIMO antenna resonates at 5.2 GHz and has return loss of -44.0 dB. The inter-port isolation in antenna ports is > 11.50 dB in the defined frequency band. The response of TARC shows > 580 MHz of bandwidth with pair of excitation angles at antenna ports. The gain of antenna is > 3.0 dBi in the operating band. The reported radiating geometry makes the design very compact. To check the radiation effect on human body in different positions, the SAR is evaluated for indoor environment.**

***Index Terms***— **MIMO, ECC, TARC, WLAN, SAR.**

*Original Research Paper*
*DOI: 10.7251/ELS1923011C*

## I. Introduction

VARIETIES of wireless communicating devices are presently available in market and the continuous research work is also carried out in different parts of the world for fastest communication to reduce the delay and loss of signaling using multiple input multiple output (MIMO) antennas. Various MIMO radiators are offered for WLAN applications. Previously, an antenna system based on single-input-single-output (SISO) was used in wireless communication, which had low data/bit rate, low capacity and average quality of transmission and reception of signals. MIMO antenna has high data rate, high channel capacity, medium latency, and good connection reliability over the slow/fast fading [1]. Various MIMO antenna factor like, gain efficiency, dimension of antenna and radiation distribution are decided according to the length of antenna [2]. A defected ground structure and metamaterial (MTM) plays important role in MIMO antenna design system. It limits the objectionable port coupling effects and surface wave [3].

Sometimes multi-layered substrate like Polydimethylesiloxane (PDMS) used to produce the effects like the defected ground and MTM in MIMO antenna system [4]. Some square shaped antenna produced >15 dB of isolation without supporting decoupling element [5]. A virtually touched element like parasitic element (PE) provides frequency shifts by inductive effect and produces in-band mutual coupling from 5.8 GHz frequency band to some undesired bands [6].

Various types of meander line antenna have been designed in last few years. Sometimes miniaturization is achieved in travelling wave tube using meander line structures, and it increases the bandwidth about 53.5% [7]. The ultra wideband (UWB) application is fulfilled by monopole antenna using two-dimensional meander line structures [8]. The low profile meander line with defected ground structure (DGS) was used to miniaturize the design structure by 23.8% [9]. Some other meander line based antenna with meandered feeding lines [10], MIMO antenna with dual band meander line [11], and meander line frequency selective surface [12] etc., are used with folding for compactness. Some UWB [13], circularly polarized [14], offset planner antenna [15], and terahertz antenna [16] are used for isolation enhancement.

The paper covers $0.66\lambda \times 0.3\lambda$ mm$^2$ substrate size for 2-element folded MIMO antenna for wireless application. The proposed antenna has return loss of -44.0 dB at resonant. The good isolation between ports is achieved in reported frequency band. The compactness in design is achieved by partial ground.

The initial part of paper covers proposed antenna geometry, then simulation and measured results are discussed. The detailed MIMO antenna parameters with SAR are presented and analyzed in further sections.

## II. Meander Line Mimo Antenna Design

The folded MIMO antenna design parameters are optimized using CST version 15.0. The FR-4 dielectric substrate has thickness, permittivity, and loss tangent of 1.524 mm, 4.4, and 0.025 respectively. The proposed antenna takes complete size of 37.5 x 17.0 mm$^2$. The compactness in the design is achieved by overlapping of meander lines and small ground. The limited ground plane is considered for proposed antenna to contribute in size reduction and return loss. For the same frequency of operation full ground takes large size as compared to presented antenna ground. The optimized parameters are specified in Table 1. The schematic and fabricated folded MIMO antenna views are shown in Fig. 1 and Fig. 2.

Manuscript received 19 October 2018. Received in revised form 11 January and 7 February 2019. Accepted for publication 8 February 2019.

Sanjay Chouhan is with the Faculty of Electronics and Communication Engineering, Jawaharlal Institute of Technology, Borawan-Khargone, M.P, India. (09752752988 ; e-mail: sanjaychouhanjit@yahoo.co.in).

Leeladhar Malviya is with Faculty of Electronics and Telecommunication Engineering, S.G.S.I.T.S, Indore, MP, India. (e-mail: ldmalviya@gmail.com).

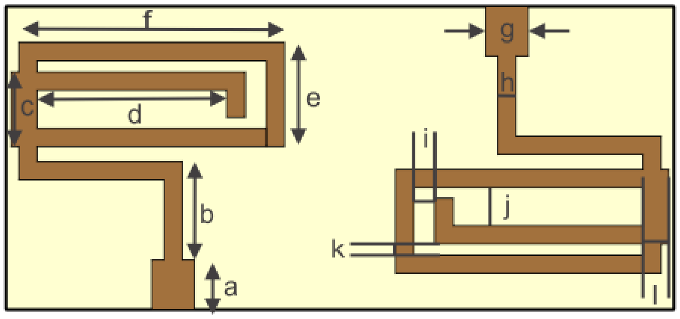


(a)

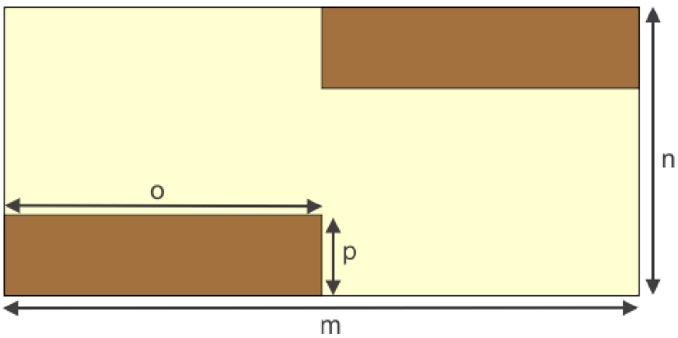


(b)

Fig. 1. Schematic views (a) Folded MIMO Front (b) Folded MIMO Back

Table 1. Optimized Design Parameters

| Design parameter | a | b | c | d | e | f | g | h |
|---|---|---|---|---|---|---|---|---|
| Size (mm) | 2.8 | 5.5 | 4.2 | 10.6 | 5.8 | 14.8 | 2.4 | 1.0 |
| Design parameter | i | j | k | l | m | n | o | p |
| Size (mm) | 1.1 | 2.1 | 0.6 | 1.5 | 37.5 | 17 | 18.7 | 4.8 |

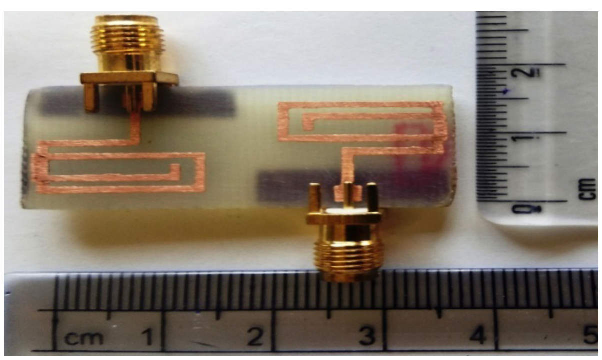

(a)

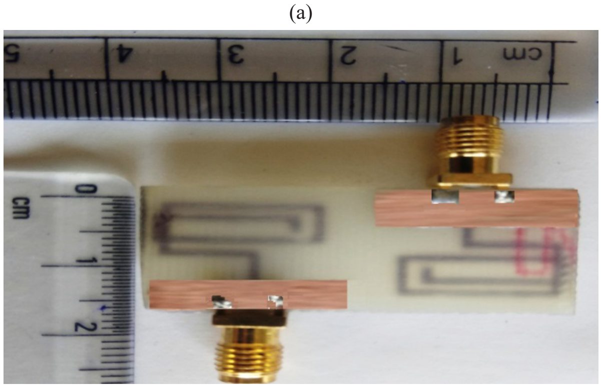

(b)

Fig. 2. Fabricated views of proposed design (a) Front, (b) Back

## III. Simulated And Measured Results

The proposed two port antenna with microstrip feed is $180^0$ upturned to control the field and surface current accountable for mutual coupling. As the entire antenna elements are equal in size and identical, therefore only $S_{11}$, and $S_{12}$ parameters are considered. The proposed folded MIMO antenna with limited antenna ground has band of 5.0-5.6 GHz. The total bandwidth is 600 MHz. The designed folded antenna has return loss and inter-port isolation of -44.0 dB and 11.9 dB at 5.2 GHz frequency. In the working band, the inter-port isolation is > 11.5 dB. The results are presented in Fig. 3 for simulated and measured S-parameters. The fabricated folded antenna resonates at 5.27 GHz. The minor mismatch in results is due to coupling in port or may be due to fabrication errors.

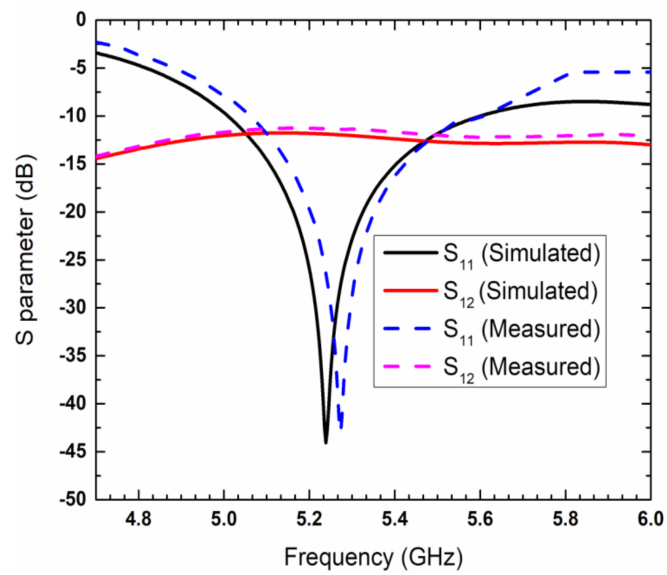


Fig. 3. S-parameters of proposed MIMO antenna.

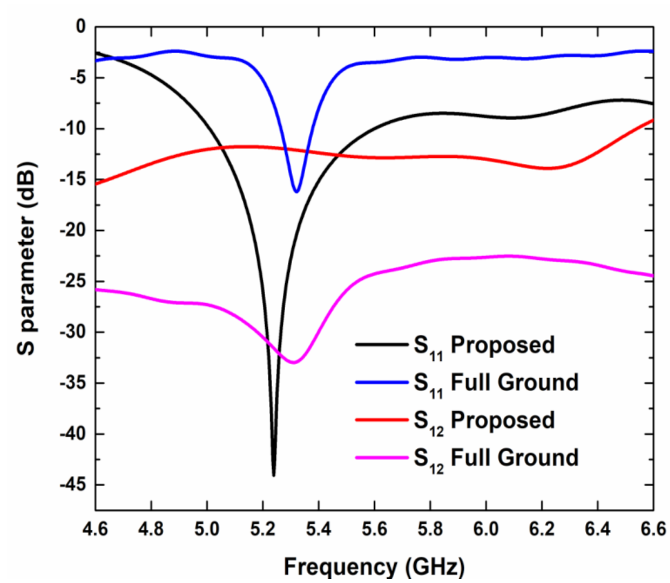


Fig. 4. S-parameter with partial ground and full ground.

In Fig. 4, results of proposed MIMO S-parameters are compared with full ground. The full ground shows the band of 5.26-5.38 GHz which has bandwidth of 114 MHz and resonates at 5.3 GHz. It is therefore evident that the full ground has very less bandwidth and very less return loss.

The E-field and H-field patterns are discussed to show the radiation behavior of the designed folded antenna. Fig. 5 (a) shows the radiation field (E-field for $\phi=0^0$) for port 1 at 5.2 GHz resonant frequency. The other port has the same field pattern. The results show that $259^0$ and 12.8 dBV/m main lobe direction and magnitude respectively at port 1. The 3 dB angular width of proposed MIMO antenna at port 1 is $184^0$. Similarly, Fig. 5 (b) gives the radiation field (H-field for $\phi=90^0$) at 5.2 GHz frequency. The H-field magnitude of MIMO antenna at port 1 is 33.9 dBA/m with direction of $261^0$.

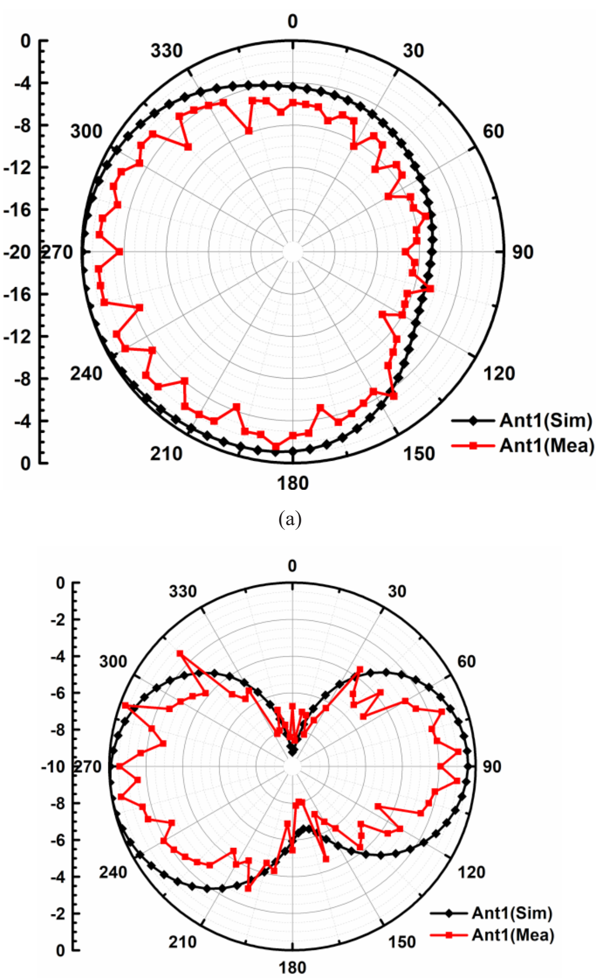


(a)

(b)

Fig. 5. Far-field (a) E-Field (b) H-Field (Sim: Simulated, and Mea: Measured)

The distribution of current sharing on the patch surfaces reveal the idea of isolation. The lower mutual coupling indicates higher isolation among antenna ports. For the proper analysis of surface current, port 1 is energized and port 2 is terminated with 50 ohm load. The current distribution in patch is shown in Fig. 6. The effect of surface current is very less at other ports on the corresponding antenna arms. The port 2 has equal current values due to same antenna geometry. The distribution of surface current at port 1 is in the range of 0 to 97.4 Ampere/meter.

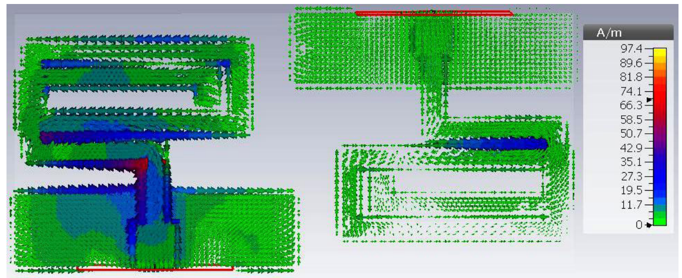


Fig. 6. Surface current distribution (SCD) of MIMO antenna.

The gain of antenna is typically the power ratio produced by the antenna from a far-field source on the antenna's beam axis to the power produced by a hypothetical lossless isotropic antenna. Generally this ratio is expressed in decibels, and these units are referred to as "decibels-isotropic" (dBi). The measurement of gain of the proposed design is obtained in an anechoic chamber using substitution method. The proposed antenna is used as a receiver and pyramidal horn antenna as transmitter. The measured value of gain is > 3 dBi in presented band, and is 4.0 dBi at resonant. The simulated-measured results of gain are presented in Fig. 7. The radiation efficiency and total efficiency are > 80 % and > 65 % in proposed operating band.

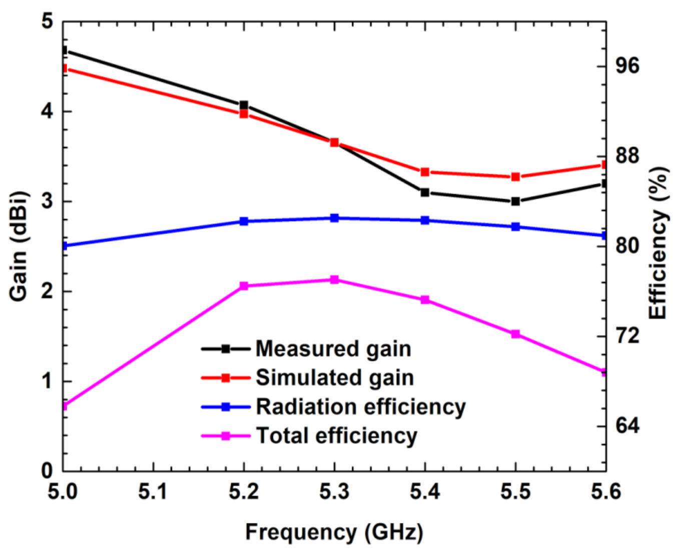


Fig. 7. Proposed MIMO antenna gain and efficiency.

The overall mutual coupling of MIMO antenna is evaluated by ECC. The ECC is calculated using all S-parameter coefficients, and it shows the correlation between ports 1and 2. The individual isolation coefficient is unable to give all the diversity information, thus ECC plays a very important role for the same. It is calculated by using (1) [17]:

$$|\rho_e(i,j,N)| = \frac{\left|\sum_{n=1}^{N} S_{i,n}^{*} S_{n,j}\right|}{\sqrt{\left|\prod_{k(=i,j)}\left[1-\sum_{n=1}^{N} S_{i,n}^{*} S_{n,k}\right]\right|}} \quad (1)$$

where N is the number of antennas and i, j are the antenna elements.

The two port correlation ($\rho_{e12}$) can be calculated by equation (2):

$$\rho_{e12} = \frac{\left|S_{11}^{*}S_{12}+S_{21}^{*}S_{22}\right|^{2}}{\left(1-|S_{11}|^{2}-|S_{21}|^{2}\right)\left(1-|S_{22}|^{2}-|S_{12}|^{2}\right)} \tag{2}$$

where $S_{11,}$ $S_{22}$ are return loss coefficients and $S_{12,}$ $S_{21}$ is isolation coefficients.

The simulated-measured results of ECC are presented in Fig. 8. The simulated result of ECC for the ports (1, 2) is given as 0.01 at 5.2 GHz. The ECC result shows minute difference between simulated and measured one. Therefore, the proposed folded antenna is appropriate for WLAN application in the given frequency band. The simulated and measured ECCs in the whole frequency band are < $10^{-2}$.

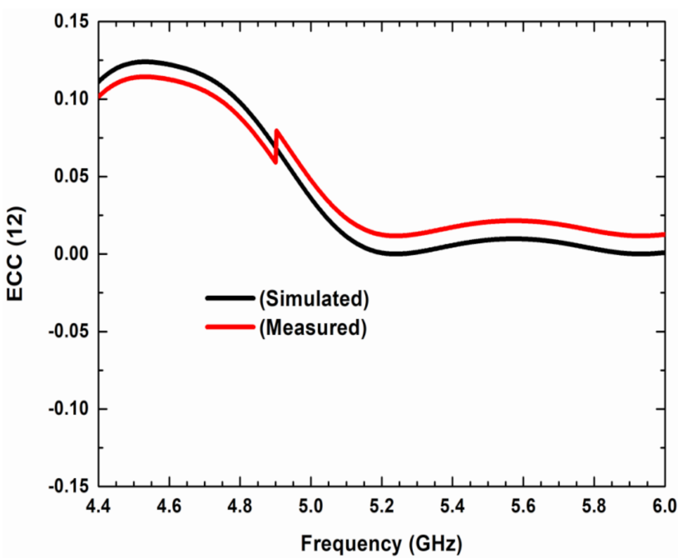


Fig. 8. Simulated-measured results of ECC.

The frequency response description of MIMO antenna with the random signals and their excitation angles can be analyzed using the parameter TARC. The TARC is defined in terms of square root of total reflected power to total incident power. The TARC is expressed in (3) and (4) [18]:

$$\Gamma = \sqrt{\frac{Available\ Power - Radiated\ Power}{Available\ power}} \tag{3}$$

$$\Gamma_a^t = \frac{\sqrt{\sum_{i=1}^{N}|b_i|^2}}{\sqrt{\sum_{i=1}^{N}|a_i|^2}} \tag{4}$$

where [b]=[S][a], [b], [s] and [a] is the scattering vector, scattering matrix, and excitation vector respectively.

The TARC value of 1 represents total reflection in the defined frequency band, while 0 for no reflection. Fig. 9 shows the TARC results for the two port MIMO antenna for various excitation angles. The TARC bandwidth is 580 MHz. From the TARC graph, the best condition for the excitation angle combination of $45^0$, $45^0$ is obtained.

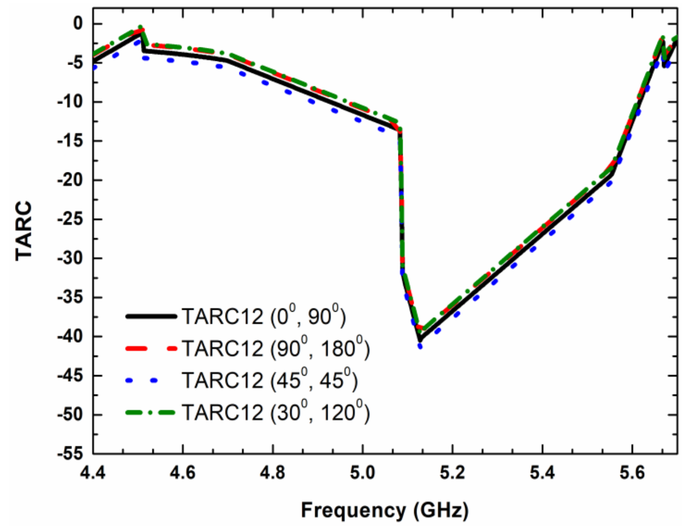


Fig. 9. Proposed MIMO antenna TARC.

The effect of radiation on the human body is analyzed using SAR. The SAR is a sign of electromagnetic energy absorbed by the biological tissues, mainly in the human head/body/palm. Fig. 10 presents the CST simulated SAR results by the IEEE/ICE 62704-1 averaging method. The results of SAR are calculated by placing antenna 140 mm away from human head. The maximum SAR for 1g is 0.283 W/Kg and SAR for 10 g is 0.144 W/Kg near the human head and ear. The obtained SAR values of proposed antenna satisfy the standard safety limit over 1 g of tissue.

The SAR performance near palm and fingers are calculated in Fig. 11. The maximum SAR values near palm and fingers are 0.264 W/Kg and 0.137 W/Kg for 1g and 10g tissues respectively. The SAR calculation near body parts are given in Table 2.

Table 2. SAR Calculation Near Human Body Parts

| SAR near | SAR | |
|---|---|---|
| | At 5.2 GHz | |
| | 1 (g) W/Kg | 10 (g) W/Kg |
| Head | 0.12 | 0.07 |
| Ear | 0.28 | 0.14 |
| Palm | 0.13 | 0.10 |
| Finger | 0.26 | 0.13 |
| Wrist | 0.08 | 0.07 |

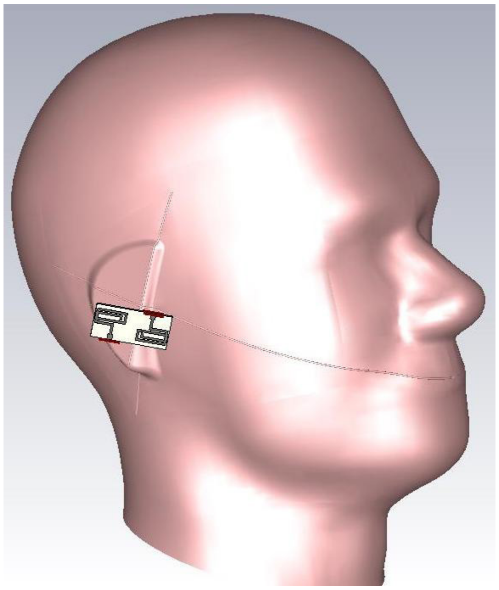

(a)

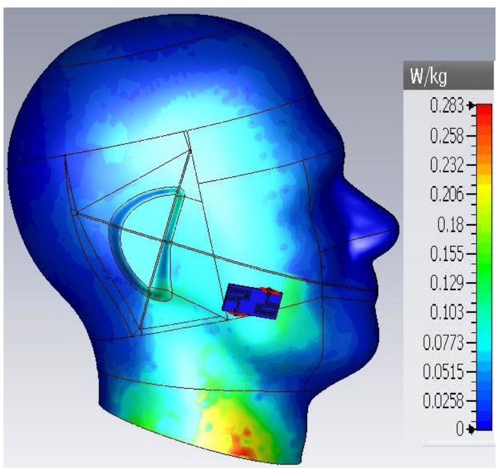


(b)

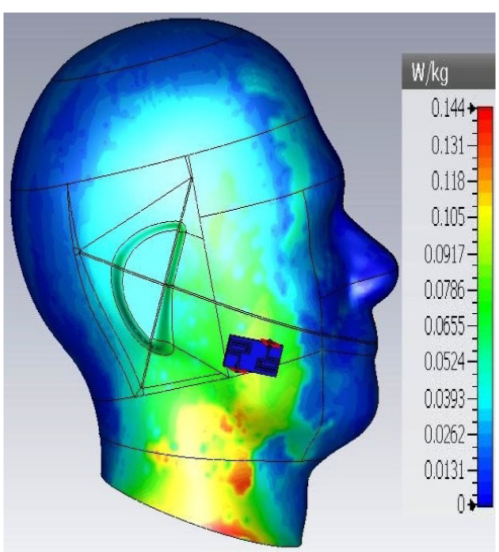


(c)

Fig. 10. SAR Results near human head at 5.2 GHz (a) antenna positioned near head (b) SAR 1 g (c) SAR 10 g.

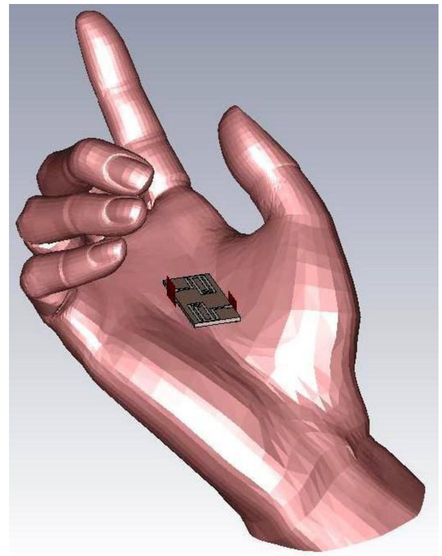

(a)

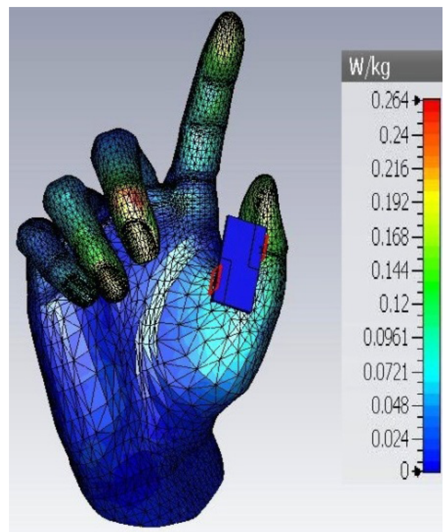


(b)

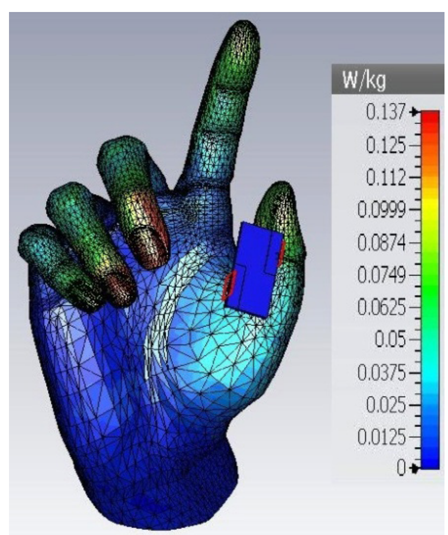


(c)

Fig. 11. SAR Results near palm and fingers (a) antenna positioned near palm (b) SAR 1 g near palm (c) SAR 10 g near palm.

Similarly, the input power and radiated power are given in Fig. 12. The MIMO antenna is simulated for 0.5 watt of power and radiates in the range of 0.34-0.38 watt, which shows good performance. The 0.16 [W] of power is absorbed, returned and lost.

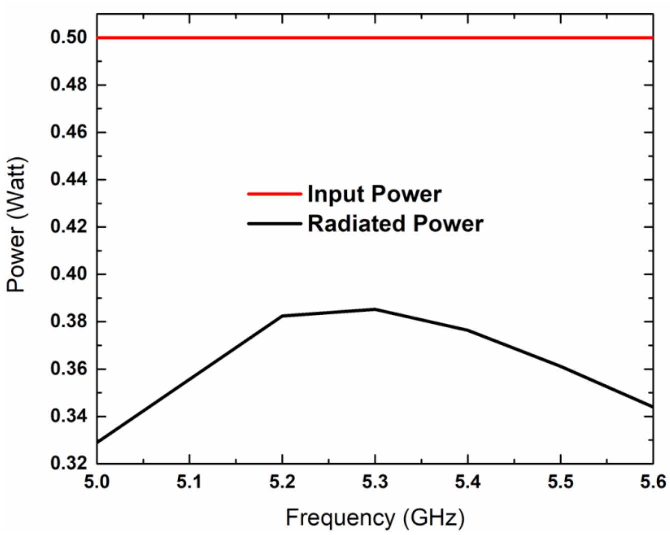


Fig. 12. Proposed MIMO antenna power distribution.

Some existing designs are compared with the proposed folded MIMO antenna, given in Table 3. The given references except [3] have bigger sizes in comparison with proposed MIMO antenna. The size reduction factor has also been given and compared. The radiation effect on human body also gives results below the safety limits.

## IV. Conclusion

The folded antenna elements placed in opposite direction to each other produces good isolation. Good radiation performance is achieved with low mutual coupling. The surface current distribution of MIMO antenna showed the low correlation among the antenna elements. The proposed folded MIMO structure showed the suitability for IEEE 802.11 for 5.2 GHz. Also, it has very low value of SAR for different modes of operation/handling and is as per the standard set by the ITU. The presented results in the paper showed meaningful research contribution for wireless technology.

Table 3. Comparison of Proposed Work with earlier Reported Works

| S. No. | Ref. | $f_H$(GHz) | $f_L$(GHz) | Size ($mm^2$) | Size reduction (%) | Isolation (dB) | ECC | Gain (dBi) | TARC (GHz) | SAR (W/Kg) |
|---|---|---|---|---|---|---|---|---|---|---|
| 1. | [3] | 5.75 | 5.84 | 0.5 λ x 0.45 λ | -4 | 55 | - | -3.0 | - | - |
| 2. | [4] | 5.7 | 6.1 | 2.5 λ x 1.4 λ | 92 | 31 | 1 x $10^{-6}$ | 11.5 | - | - |
| 3. | [5] | 5.5 | 6.2 | 0.57 λ x 0.94 λ | 54 | 15 | 1x $10^{-2}$ | 4.7 | 1.0 | - |
| 4. | [6] | 5.75 | 5.85 | 0.7 λ x 0.6 λ | 41 | 42 | - | 4.9 | - | - |
| 5. | [19] | 5.49 | 6.024 | 0.53 λ x 1.85 λ | 76 | 33 | 5 x $10^{-4}$ | 5.3 | - | - |
| 6. | [20] | 5.3 | 6.7 | 0.76 λ x 0.76 λ | 56 | 13 | 4 x $10^{-4}$ | 5.43 | 1.24 | - |
| 7. | Proposed | 5.0 | 5.6 | 0.66 λ x 0.3 λ | - | 11.8 | 1x $10^{-2}$ | 4.0 | 0.58 | 0.28 |

## References

[1] R. Bhagavatula, R. W. Heath Jr, and K. Linehan, “Performance evaluation of MIMO base station antenna designs”, Antenna systems and technology magazine, vol. 11, pp. 14-17, 2008.

[2] N. Valizade, and H. Oraizi, “A design of reconfigurable CPW-fed planar antenna for multiband MIMO applications”, IET microwaves antennas & propagation, vol. 14, pp. 1-20, 2016.

[3] M. A. Abdalla and A. A. Ibrahim, “Compact and closely spaced Metamaterial MIMO antenna with high isolation for wireless applications”, IEEE antennas and wireless propagation letters, vol. 12, pp. 1452-1455, 2013.

[4] S. M. Alqadami, M. F. Jamlos, P. J. Soh, and G. A. E. Vandenbosch, “Assessment of PDMS technology in a MIMO antenna array”, IEEE antennas and wireless propagation letters, vol. 15, pp. 1939-1942, 2015.

[5] Y. Sharma, D. Sarkar, K. Saurav, and K. V. Srivastava, “Three element MIMO antenna system with pattern and polarization diversity for WLAN applications” IEEE antennas and wireless propagation letters, vol. 16, pp. 1163-1166, 2016.

[6] X. bao Sun and M. Yong Cao, “Low mutual coupling antenna array for WLAN application”, Electronics letters, vol. 53, pp. 368-370, 2017.

[7] Ding Chong, Wei Yanyu, Li Qian, Zhang Luqi, G. Guo and Gong Yubin, “A dielectric-embedded microstrip meander line slow-wave structure for miniaturized traveling wave tube”, Journal of Elec. Waves and App., https://doi.org/10.1080/09205071.2017.1358109, August 2017.

[8] Dalia M. Elsheakh and Amr M. E. Safwat, “Meander line-loaded planar monopole antennas”, Microwave and optical technology letters, vol. 54, pp. 1851-1854, 2012.

[9] A. Ghosh, A. Mitra, and S. Das, “Meander line-based low profile RIS with defected ground and its use in patch antenna miniaturization for wireless applications” Microwave and optical technology letters, vol. 59, pp. 732-738, 2017.

[10] Muhammad Saeed Khan, Antonio-Daniele Capobianco, Adnan Iftikhar, Raed M. Shubair, Dimitris E. Anagnostou, Benjamin D. Braaten, “Ultra-compact dual-polarised UWB MIMO antenna with meandered feeding lines”, IET Microw. Ant. Propag, vol. 11, pp. 997-1002, 2017.

[11] Mohamed M. Morsy, Ahmed M. Morsy, “Dual-band meander-line MIMO antenna with high diversity for LTE/UMTS router” IET Microw. Antennas Propag., vol. 12, pp. 395-399, 2018.

[12] Welyson T. S. Ramos, Renato C. Mesquita and Elson J. Silva, “Frequency selective surface using meander line inclusions”, Journal of electromagnetic waves and applications, DOI: 10.1080/09205071.2018.1442261, 2018.

[13] C. Mao, Q. Chu, “Compact co-radiator UWB-MIMO antenna with dual polarization”, IEEE Tran. on Ant. and Prop., vol. 62, pp. 4474-4479, 2014.

[14] Leeladhar Malviya, Rajib K. Panigrahi, and Machavaram V. Kartikeyan, “Circularly Polarized 2×2 MIMO antenna for WLAN Applications”, Progress In Electromagnetics Research C., vol. 66, pp. 97-107, 2016.

[15] L.D Malviya, M. V. Kartikeyan, and R. K. Panigrahi, “Offset planar

MIMO antenna for omnidirectional radiation patterns", Int. Journal of RF and Microwave Comp. aided Engg., https://doi.org/10.100-2/mmce.21274, 2018.

[16] R. K. Kushwaha, P. Karuppanana, and L.D. Malviya, "Design and analysis of novel microstrip patch antenna on photonic crystal in THz", Physica B: Condensed Matter, vol. 545, pp. 107-112, 2018.

[17] Sanjay Chouhan, Debendra Kumar Panda, Manish Gupta, Sarthak Singhal, "Multiport MIMO antennas with mutual coupling reduction techniques for modern wireless transreceive operations: A review", Int J RF Microw Comp. Aided Engg., doi.org/10.1002/mmce.21189, 2017.

[18] M. Manteghi, Y.R. Sami, "Broadband characterization of the total active reflection coefficient of multiport antennas", Antennas and propagation society international symposium, pp. 20-23, 2003.

[19] Mohammad S. Sharawi, "A 5-GHz 4/8-Element MIMO antenna system for IEEE 802.11ac devices", Microwave and optical technology let., vol. 55, 1589-1594, 2013.

[20] Sanjay Chouhan, Debendra Kumar Panda, Manish Gupta and Sarthak Singhal, "Meander line MIMO antenna for 5.8 GHz WLAN application", International Journal of RF Microwave Computer Aided Engineering, vol. 28, 2018.

# DC Hard Faults Detection and Localization in Analog Circuits Using Fuzzy Logic Techniques

Mohammed Merabet and Nacerdine Bourouba

*Abstract*— **This paper demonstrates a novel technique based on the use of a fuzzy logic system and the simulation before test (SBT) approach for hard faults detection and localization in analog electronic circuits comprising bipolar transistors. For this purpose, first, simulations of the circuit under test (CUT) are performed before the test stage by investigating the response of the circuit under test in faulty and fault-free conditions. Following this, two signatures parameters—output voltage and supply current—are observed and used for the fault diagnosis; the CUT is simulated using the OrCAD/PSpice software, and the output is analyzed in the DC domain. This method is validated through an inverter amplifier based on the uA741 operational amplifier. Then the results of different experiments are presented to demonstrate the applicability of the proposed method by increasing its efficiency.**

*Index Terms*— **Analog circuits, fuzzy logic, hard faults, fault detection, fault diagnosis, fuzzy inference system, simulation before test.**

*Original Research Paper*
*DOI: 10.7251/ELS1923018M*

## I. Introduction

The subject of analog circuit fault diagnosis had gained popularity among researchers from the late 1970s to the early 1980s [1]–[2] due to the growing complexity of electronic circuits. Since then, fault detection and classification has been invoking a great deal of interest, becoming one of the largest domains of analog testing [3], [1]. However, it still faces some difficulties, e.g., in terms of inaccuracy of measurement, circuit nonlinearities, consideration of component tolerances, and poor fault models [4]. With respect to these difficulties, fuzzy logic seems to be one of the most effective tools that can be effectively employed to build an appropriate fuzzy inference system (FIS) that will have the potential to detect and locate faults depending on the inputs assigned to it.

A fault is a change in the value of a component with respect to its regular value that causes failure of the circuit. Faults in analog circuits are generally classified into two categories: hard faults and soft faults (i.e., catastrophic and parametric). Hard faults are attributed to short or open circuits; they lead to failures that manifest themselves in an altogether malfunctioning circuit [5]–[6]. Conversely, soft faults are those changes that hinder the performance of a circuit. This type of faults causes the parameters to deviate from their nominal value that can consequently leave their tolerance band [7]–[8].

Fault diagnosis in analog circuits is conducted using two broad approaches [4]: the simulation before test approach (SBT) and the simulation after test approach (SAT). SAT approach consists of calculating the circuit parameters from the measured responses obtained via the circuit under test (CUT) to observe if they exhibit the expected behavior [2], [9]. On the other hand, in the SBT approach, the response of the CUT is measured in the presence of a pre-selected set of faults, and the results are stored in a fault dictionary. The fault location is detected by comparing the circuit responses with the correspondents in the fault dictionary [9]–[10].

In this article, a strategy for hard fault detection and localization in analog circuits is presented, and a system based on fuzzy logic is used for this purpose. The proposed method is a part of the SBT approach, and experimental results indicate it has a high capacity. Moreover, using fuzzy logic makes it possible to distinguish between different faults even if their values are very close to each other; therefore, the ambiguity rate is zero.

## II. Fault Detection and Localization Algorithm

To locate faults, the following successive steps have been assumed:

1) Simulation of the CUT in the DC domain.
2) Extraction of the output voltage and supply current for fault-free and other faulty conditions.
3) Creation of the fault dictionary.
4) The parameters extracted from the fault dictionary are presented as inputs in a fuzzy logic system that detects and localizes the fault.

The block diagram for the proposed approach has been illustrated in Figure 1.

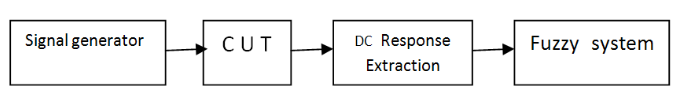


Fig. 1. Block diagram of the proposed algorithm.

Manuscript received 29 January 2019. Received in revised form 16 April 2019 and 16 May 2019. Accepted for publication 18 May 2019.

Mohammed Merabet is with the Laboratory of Scientific Instrumentation (LIS), Faculty of Technology, Ferhat Abbas Setif 1 University, 19000, Setif, Algeria. (phone: +213-770-66-44-06; e-mail: merabet_moh2005@yahoo.fr).

Nacerdine Bourouba is with the Laboratory of Scientific Instrumentation (LIS), Faculty of Technology, Ferhat Abbas Setif 1 University, 19000, Setif, Algeria (e-mail: bourouband@yahoo.fr).

## III. Fuzzy Logic Approach

The fuzzy approach is used to localize hard faults in analog circuits; these faults are caused by open or short components in bipolar transistors [11]. A fault dictionary is a priori produced by collecting signatures of different fault conditions that are simulated in the DC domain. A FIS is utilized to process the CUT's response.

The basic architecture of a fuzzy logic system is shown in Figure 2.

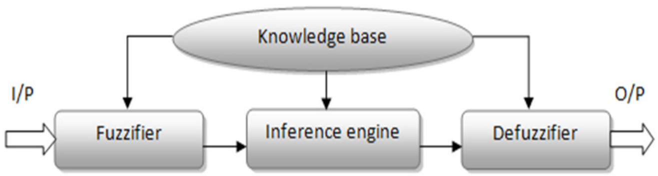


Fig. 2. Basic architecture of a fuzzy system.

The main component of fuzzy logic is the fuzzifier, which transforms real value inputs into members of fuzzy values by applying the membership functions of the fuzzy knowledge base [12]. Several types of membership functions can be used for the fuzzification process, such as triangular, trapezoidal, and Gaussian membership functions. The triangular shape has been used in this work. This function is frequently encountered in practice—e.g., [9]–[10], [13], [16]—given its efficiency with respect to calculation time. This efficiency can be attributed to its simple structure consisting of simple straight-line segments.

The inference engine takes the fuzzy input and converts it into fuzzy output by applying IF-Then type fuzzy rules (Figure 3). The process of converting the fuzzy output of the inference engine into a crisp value is called defuzzification [3].

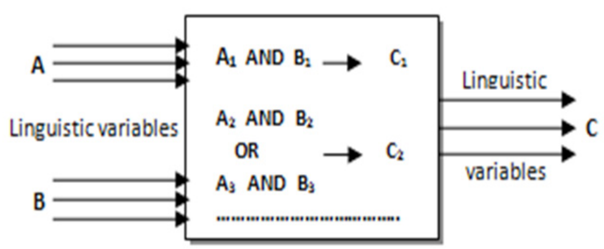


Fig. 3. Fuzzy inference process.

There are a number of defuzzification methods [3], [9], such as centroid of area (COA), bisector of area (BOA), mean of maximum (MOM), smallest of maximum (SOM), and largest of maximum (LOM). Centroid defuzzification (COA) is the most commonly used method, as it is very accurate [10], [12]. The defuzzified values obtained through COA, unlike the values obtained through other methods, divide the area under the membership function into two equal parts (see Figure 4), which can directly compute the crispest value of the fuzzy quantity [10].

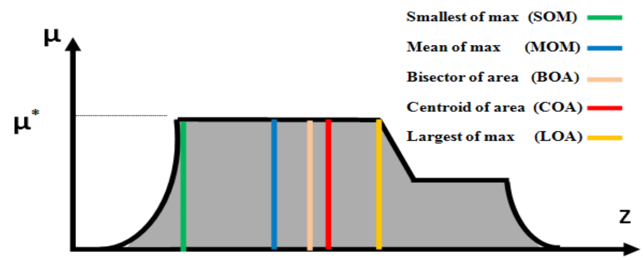


Fig. 4. Defuzzifying methods.

Although there are mainly two types of fuzzy inference methods, namely, Mamdani and Sugeno methods, the Mamdani method was chosen to create the FIS due to the transparency of its rules between the inputs and outputs and its simple implementation steps [13]. It allows us to describe the knowledge in a more intuitive and human-like manner [9]. As opposed to the Sugeno model, the Mamdani model expresses the output using fuzzy terms instead of mathematical combinations of the input variables.

Mamdani uses an inference strategy that is generally termed as the max-min method. The format of the rule base for the Mamdani fuzzy systems has been provided below:

Where $x_{pi}$ ($p$ = 1, 2, 3 … n) is the input, $y_l$ is the output of fuzzy rule, and $A_{pl}$ ($p$ = 1, 2, 3 … n) is the fuzzy membership function that is associated with linguistic variables. Figure 5 illustrates the max-min composition and centroid defuzzification methods [9], which have been used in this study.

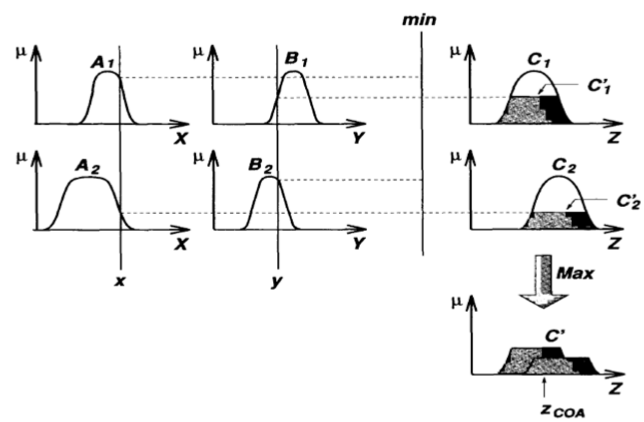


Fig. 5. Max-min composition and centroid defuzzification.

## IV. Experiments And Results

To verify the feasibility of the proposed approach, we apply the steps mentioned in Section II to the operational amplifier uA741, which is operated in an inverting configuration and widely employed as building block components for many analog systems [14]. The simulation circuit is then simulated using the PSpice software. The data obtained from these simulations was transferred to the MATLAB environment for use in the building of the FIS system. Additionally, the fuzzy toolbox was used to locate faults, as described below.

### *A. Inverting Amplifier Circuit*

Figure 6 depicts the configuration of an inverting amplifier. The closed-loop gain of the amplifier is set by two resistors: the feedback resistor, R2, and the input resistor, R1. The component parameters are R1 = 1 k and R2 = 4.7 k. Figure 7 demonstrates the transistor-level circuit of the uA741 amplifier that was used in this study. The chosen test vector includes the input voltage signal whose value ranges from − 5V to + 5V, which represent the limit values that can be accepted by the circuit and whose variation step is sufficient and necessary to explore the fault's effect.

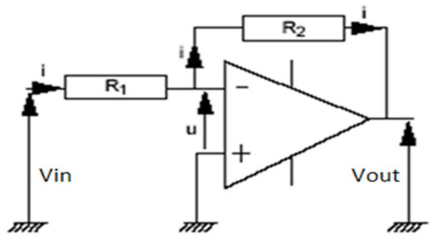


Fig. 6. Inverting amplifier.

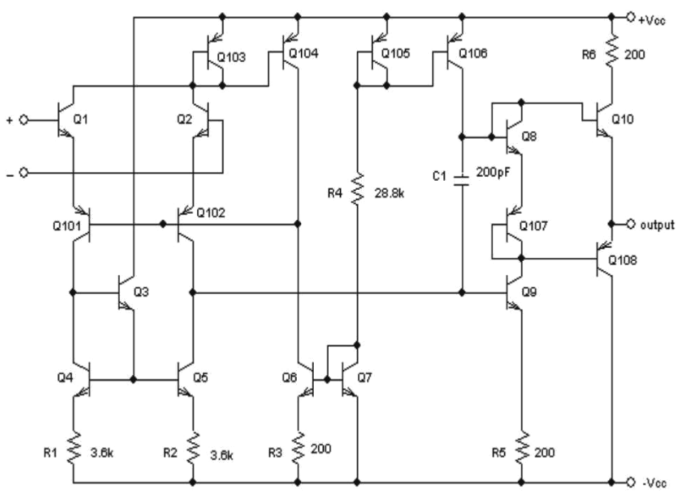


Fig. 7. The uA 741 operational amplifier circuit at the transistor level.

### *B. Faults Applied*

In this experiment, the faults that were considered were mostly short circuits and open circuits, which were applied to the active components (transistors). The short circuits were materialized by resistors of low values (1 Ohm), whereas open connection lines or resistors with high value (100 Mohm) were used for the open circuit [15]. Therefore, for each transistor in the circuit, six faults have been included in the fault list as illustrated in Figure 8 and as listed as follows:

- emitter contact open (EO);
- collector contact open (CO);
- base contact open (BO);
- base to collector short (BCS);
- base to emitter short (BES);
- collector to emitter short (CES).

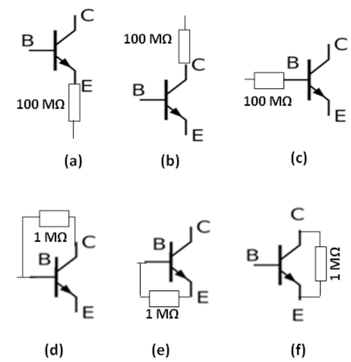


Fig. 8. Open and short transistor faults.

The inverting amplifier is an assembly of 18 transistors and, as the number of faults specific to each transistor is 6, these many components leads to the observation of the effects of 108 theoretical faults. However, the number of faults was reduced to 70 due to its electronic configuration:

- Some short or open faults measured individually at the level of an element are considered to be a duplicate fault because they affect another element that shares a common node with the first.
- Other short circuits associated with the same transistor are considered to be duplicate faults due to the way this element is connected in the circuit; for example, the diode element Q7 (shorted B-C junction) affects a short between B and E and is also treated as a short between E and C.

### *C. Building the Fault Dictionary*

*1. Output Voltage:* A priori, the analysis of the transfer function is performed to detect the test vector (stimulus) at the input that allows the effect of faults to propagate to the output. The following findings will clarify this procedure:

- The input voltage range and measurement of the corresponding output voltage can be applied to reproduce the transfer characteristic (see Figure 9).
- This task is taken up by a set of faults that are yet to be explored to measure the characteristics of the circuit under its different fault conditions, some of which are presented in Figure 10.

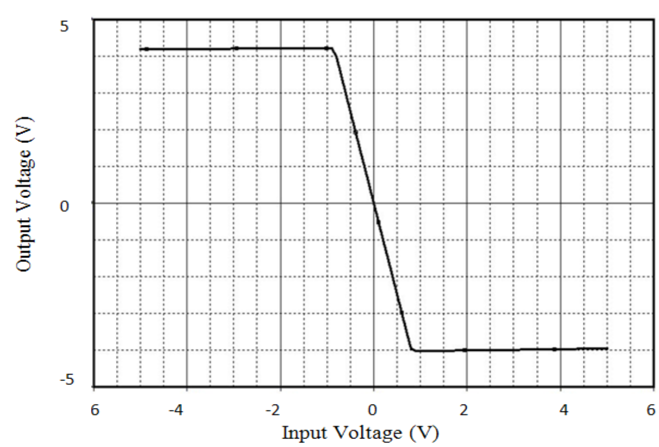


Fig. 9. Transfer function of the circuit for fault free.

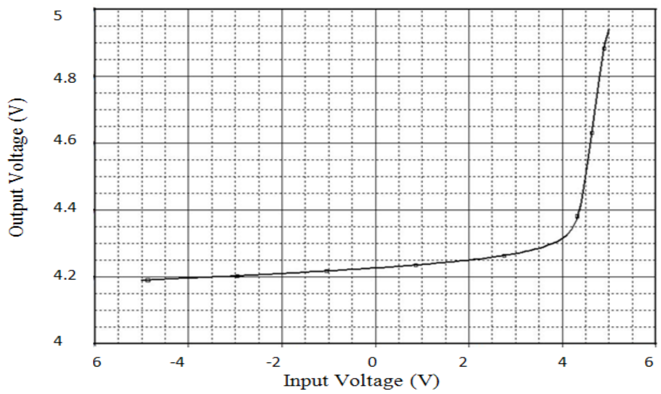


(a)

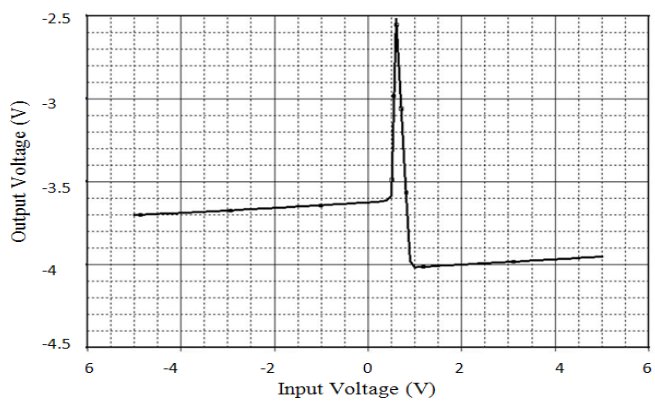


(b)

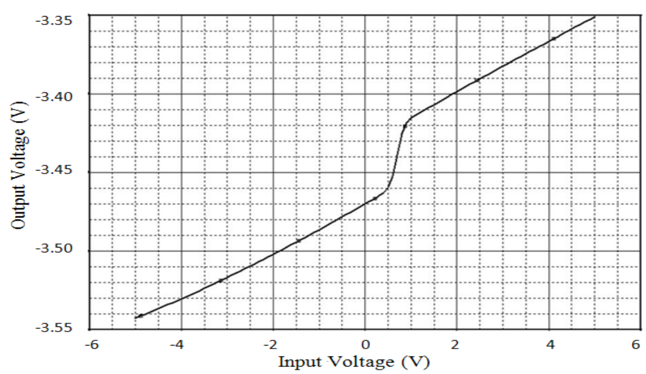


(c)

Fig. 10. Transfer function of the circuit for some fault conditions: (a) BOQ101 (b) BESQ8 (c) BCSQ10.

*2. Supply Current:* The power supply current test applied to the inverting amplifier consists of measuring the current at the negative power supply to ensure that faults that were not detected by the first mode test (output voltage) are detected. The same test vectors that were used in the previous test were imposed here.

Figures 11 and 12 demonstrate the simulation results of the good circuit and the faulty circuits, respectively. The supply current has been plotted with respect to the input voltage *Vin*.

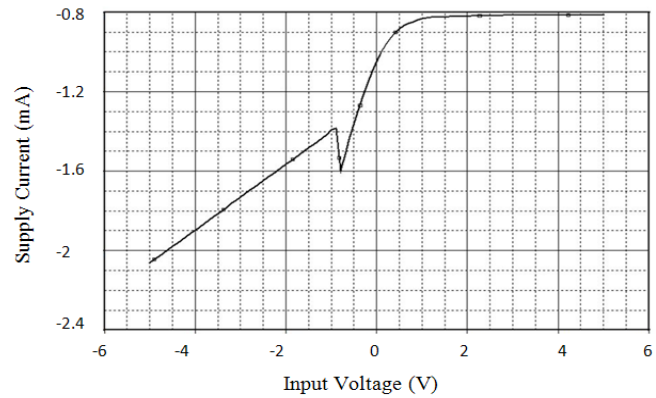


Fig. 11. The supply current plots in terms of the input voltage.

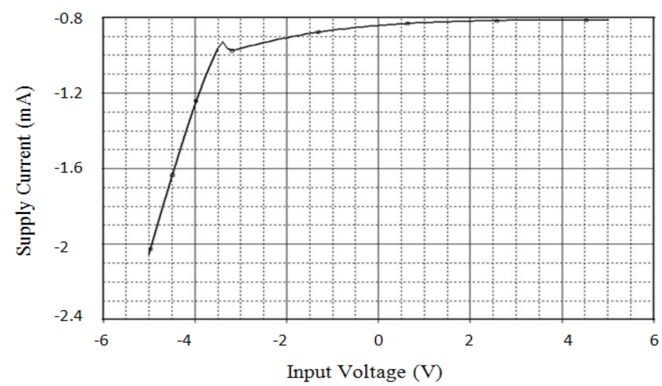


(a)

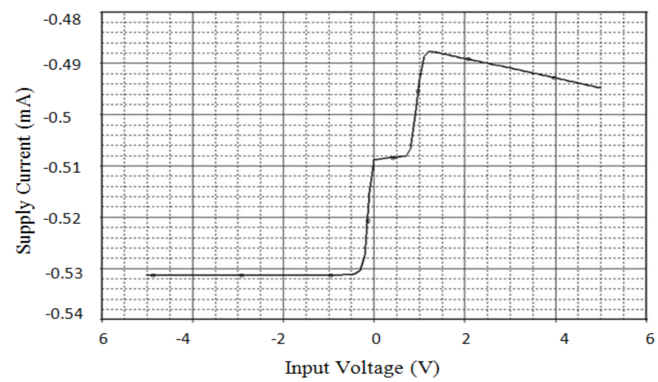


(b)

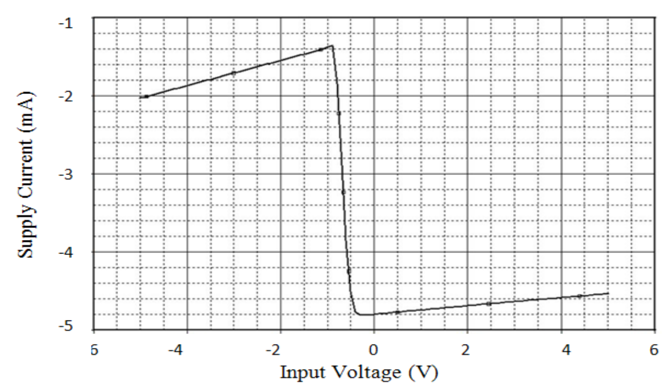


(c)

Fig. 12. Supply current of the circuit for some fault conditions: (a) CESQ3 (b) EOQ2 (c) ECSQ107.

The faults dictionary that was constructed has been depicted in Table I. The results concern the fault coverage evaluation obtained using the classic method. The criterion on which this method is based is defined as a deviation of +/- 1.5% from the nominal value for the two fault analysis parameters (the supply current and the output voltage). This implies that any fault is considered to be detected if it produces a deviation on the nominal value of one of these parameters, which is equal to or greater than this tolerance value. Such a tolerance choice is made from the concept of a current or voltage meter for laboratory use, requiring a precision class of no more than 1.5%. This resulted in a 78% fault coverage by using output voltage as a fault signature. An improvement in this fault detection rate was achieved by implying the supply current as the second fault signature—the combination of these two parameters allowed the detection of 85% faults.

Table 1. Fault Dictionary Of The Inverting Amplifier Circuit

| Fault ID | Fault conditions | Output Voltage(V) | Supply Current(mA) | FIS Output |
|---|---|---|---|---|
| f0 | FF | -3,9424 | -0,8489 | 0 |
| f1 | **BOQ1** | **-4,0182** | -0,8306 | 1.1 |
| f2 | **COQ1** | **-4,0111** | -0,8531 | 2.06 |
| f3 | **BOQ2** | **4,236** | -1,1036 | 2.95 |
| f4 | **COQ2** | **-3,5003** | -0,8756 | 3.98 |
| f5 | **BOQ3** | **-3,9924** | -0,8407 | 5.02 |
| f6 | **COQ3** | **-3,9919** | -0,8568 | 6.05 |
| f7 | **BOQ4** | **-2,9597** | -0,8573 | 7.15 |
| f8 | **COQ4** | **-3,5118** | -1,0312 | 8.05 |
| f9 | **BOQ5** | **-3,9707** | -0,7608 | 8.99 |
| f10 | **COQ5** | **-3,9732** | -0,8307 | 10.1 |
| f11 | **BOQ6** | **4,236** | -0,8705 | 11 |
| f12 | **COQ6** | **4,236** | -0,8708 | 12.1 |
| f13 | **BOQ7** | **-3,7581** | -10,008 | 13 |
| f14 | **COQN7** | **-3,9957** | -0,9774 | 14.05 |
| f15 | **BOQ8** | **-3,5436** | -6,473 | 15.1 |
| f16 | **COQ8** | **-4,0209** | -0,83 | 16.1 |
| f17 | **BOQ9** | **4,2359** | -0,9567 | 17 |
| f18 | **COQ9** | **4,2358** | -1,066 | 18.2 |
| f19 | **BOQ10** | **-3,938** | -0,8202 | 19 |
| f20 | **COQ10** | **-3,9652** | -0,8207 | 20 |
| f21 | **BOQ103** | **4,2352** | -0,9752 | 20.99 |
| f22 | **COQ103** | **-3,6747** | -0,8012 | 22.02 |
| f23 | **BOQ104** | **-3,868** | -3,8562 | 23.1 |
| f24 | **COQ104** | **-3,868** | -3,8563 | 24.05 |
| f25 | **BOQ105** | **3,9108** | -4,7673 | 25 |
| f26 | **COQ105** | **-3,8371** | -1,1471 | 26 |
| f27 | **BOQ106** | **-4,1335** | -0,5057 | 26.98 |
| f28 | **COQ106** | **-4,1336** | -0,5066 | 28.1 |
| f29 | **COQ107** | **-3,9429** | -0,8897 | 29 |
| f30 | **BOQ108** | **0,7821** | -0,8047 | 30.02 |
| f31 | **COQ108** | **-3,5723** | -0,8226 | 31 |
| f32 | **BCSQ1** | **1,1978** | -116,873 | 32.1 |
| f33 | **BESQ1** | **-3,6525** | -4,0572 | 33.1 |
| f34 | **CESQ1** | **4,236** | -1,1124 | 34.05 |
| f35 | **BCSQ2** | **4,3241** | -3,7096 | 35 |
| f36 | **BESQ2** | **-3,9472** | -0,8389 | 35.9 |
| f37 | **CESQ2** | **-4,0163** | -0,8426 | 37 |
| f38 | **BCSQ3** | **4,2143** | -1,1517 | 38 |
| f39 | **BESQ3** | **-3,9924** | -1,1447 | 39.1 |
| f40 | **BCSQ4** | **-3,9585** | -0,8308 | 40 |
| f41 | **BESQ4** | **-3,9923** | -1,7371 | 41.1 |
| f42 | **CESQ4** | **-3,9914** | -0,8305 | 42 |
| f43 | **BCSQ5** | **0,2217** | -56,044 | 42.9 |
| f44 | **CESQ5** | **1,3334** | -66,861 | 44 |
| f45 | **BCSQ6** | **-2,9332** | -53,567 | 45.1 |
| f46 | **BESQ6** | **4,2359** | -0,8925 | 45.9 |
| f47 | **CESQ6** | **-3,1548** | -25,823 | 47 |
| f48 | **BESQ7** | **4,2359** | -0,8947 | 48 |
| f49 | **BESQ8** | **-3,9367** | -0,8228 | 49.1 |
| f50 | **BCSQ9** | **-3,4253** | -0,8481 | 50 |
| f51 | **CESQ9** | **-4,1369** | -0,8491 | 51 |
| f52 | **BCSQ10** | **3,4321** | -4,7524 | 52.05 |
| f53 | **BESQ10** | **-4,096** | -0,825 | 53 |
| f54 | **CESQ10** | **2,1206** | -15,167 | 54 |
| f55 | **BCSQ101** | **-3,3445** | -11,241 | 55 |
| f56 | **BESQ101** | **-0,0297** | -0,8869 | 56.2 |
| f57 | **CESQ101** | **-3,0194** | -16,107 | 57 |
| f58 | **BCSQ102** | **-2,2499** | -16,667 | 58 |
| f59 | **BESQ102** | **4,2359** | -0,9569 | 59.3 |
| f60 | **CESQ102** | **-2,0382** | -15,561 | 60 |
| f61 | **BESQ103** | **-3,8677** | -3,8572 | 61.05 |
| f62 | **BCSQ104** | **4,236** | -0,9716 | 62.1 |
| f63 | **CESQ104** | **4,236** | -0,9719 | 63 |
| f64 | **BESQ105** | **-4,1347** | -0,5416 | 64.2 |
| f65 | **BCSQ106** | **3,4074** | -4,7131 | 64.9 |
| f66 | **CESQ106** | **4,2232** | -4,8967 | 66 |
| f67 | **BESQ107** | **-3,9367** | -0,823 | 67.1 |
| f68 | **BCSQ108** | **-4,2057** | -0,8491 | 67.9 |
| f69 | **BESQ108** | **4,1556** | -3,0547 | 69 |
| f70 | **CESQ108** | **-5** | -6,6342 | 69.98 |
| number of faults (detected/injected) | | 55/70 | 60/70 | 70/70 |

However, there were problems that arose that need to be resolved. These problems include 15% of faults escaping this test mode (f9, f10, f14, f20, f29, f39, f41, f42, f49, f67) and the indistinguishable detected faults constituting groups of ambiguous faults such as (f11, f12, f62, f63), (f5, f39), (f23, f24), making it more difficult to locate them. The data of this dictionary is processed via the FIS to provide solutions to these problems. These solutions have been detailed in the following sections.

### *D. Simulation Results*

All hard faults have been obtained from the DC response and tabulated in Table I. The faults have been coded and can be identified through the following abbreviations: EOQn, BOQn, COQn, EBSQn, ECSQn, and BCSQn, where E, B, and C, respectively, denote the emitter, the base, and the collector of the transistor, which can be identified by the letter Q and its position number n in the configuration. From the simulation results (Table I), it can be seen that the output voltage and supply current are different for different fault conditions. The extracted features are then fed as inputs into the FIS.

The FIS that has been suggested to solve the problem of fault detection and localization is shown in Figure 13. It has been created through three steps [3], which have been listed as follows: defining the input membership function (output voltage and supply current), defining the output membership functions and, finally, creating the rule base.

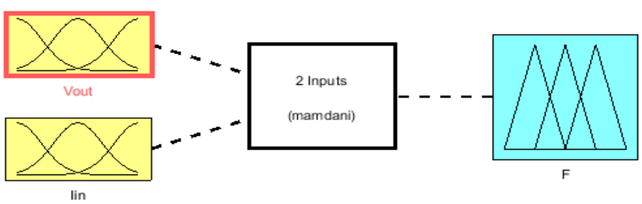


Fig. 13. Mamdani fuzzy inference system (two inputs).

The values of the input parameters are divided into different intervals according to different fault groups. After a number of experiments, this distribution has led to a suitable choice of 18 intervals for the output voltage parameter (Figure 14) and 7 for the supply current parameter (Figure 15). Each value region undergoes a transformation into linguistic parameters, which are provided as input in Madani's FIS. We would like to remind that for each of these regions, a triangular membership function TMF is assigned.

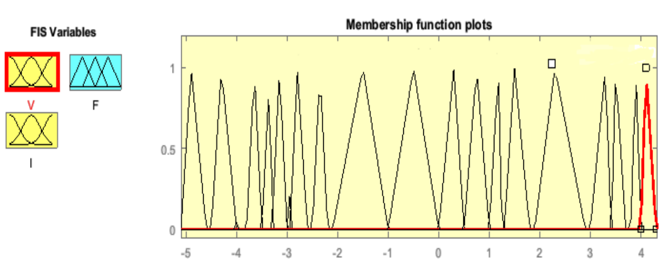


Fig. 14. Membership function of output voltage.

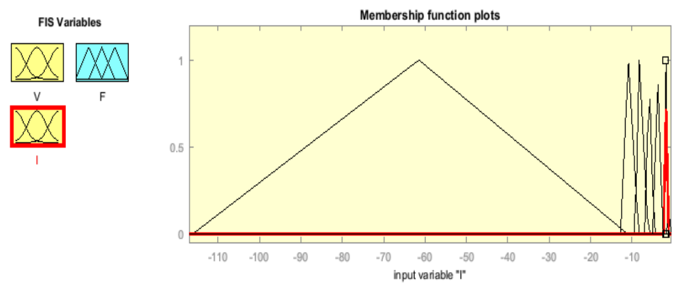


Fig. 15. Membership function of supply current.

The output membership functions are also assigned to the output variables; the membership function is divided into areas, as shown in Figure 16, that characterize the different faults' identities, which can be obtained using the fuzzy rule base. As there are 70 different configurations of the CUT in the fault dictionary, there must be 70 fuzzy rules for the problem under consideration. The fuzzy rule base defines the relationship between the input and the output fuzzy sets. As a result, the use of fuzzy IF-THEN rules imitates the ability of the human mind to make decisions [13]. Finally, the centroid defuzzification method was used on the fuzzy set "fault" to obtain a crisp value, which can be used to easily identify the faults. The output of the FIS for the given inputs is demonstrated in Figure 17.

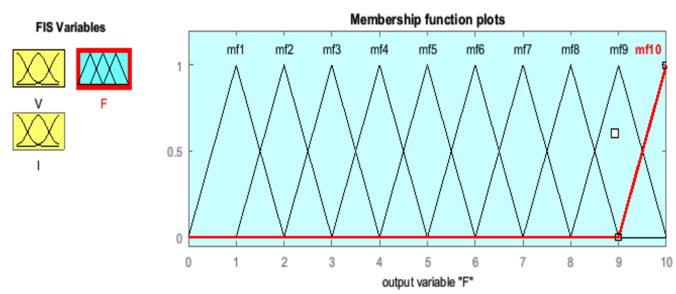


Fig. 16. Membership Function for Fault ID (display range [0 10]).

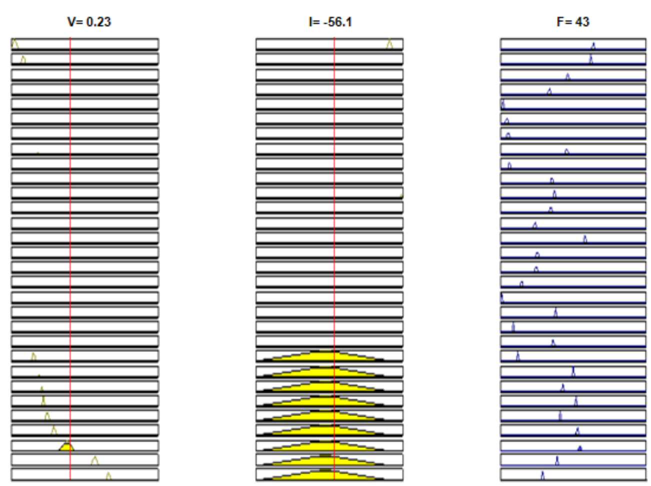


Fig. 17. Output of the FIS.

The fault case F18 has been chosen to illustrate the approach. The FIS for index fault 18 (F18) is 4.2358, − 1.066. For this input, the triangular membership functions (TMF) for the output voltage and supply current are 4.1, 4.23, 4.5 and − 1.2, − 1, − 0.8, respectively.

The TMF for the output is defined as 17, 18, 19 by setting the fault index (in this case, 18) as the center of the TMF. The fuzzy rule for this fault has been provided as follows:

"If $V_{out}$ is in the range 4.1 to 4.5 and $I_{in}$ is in the range − 1.2 to − 0.8, then the fault range is 17 to 19."

The FIS output has a value of 18.2 after defuzzification whose rounded number corresponds to the defect index 18 as a fault identifier (fault ID).

To support the practicality of the approach, the results of some fault cases have been resumed in Table II and agree well within the corresponding fault ID.

Table 2. FIS Inputs and Outputs for Test Cases F4, F49, and F52.

| Fault ID | Input FIS | | TMF output voltage | | TMF supply current | | TMF output | FIS output |
|---|---|---|---|---|---|---|---|---|
| F4 | [-3,5003 -0,8756] | IF | [-3.6 -3.5 -3.4] | AND | [-1 -0.7 0] | THEN | [3 5] | 3.98 |
| F49 | [-3,9367 -0,8228] | | [-4 -3.8 -3.6] | | [-0.9 -0.75 -0.7] | | [48 50] | 49.1 |
| F52 | [3,4321 -4,7524] | | [3.3 3.4 3.5] | | [-5 -4.5 -4] | | [51 53] | 52.05 |

The same applies to other faults where the input and output TMF are determined from the values of the output voltages and supply current and the fault index, respectively.

The FIS outputs exhibited in Table I clearly indicate that the totality (100%) of faults being investigated in the present work have been detected and successfully dispatched to each other. This has been conducted on zero groups of ambiguous faults and, thus, will help in a good fault location.

To verify the efficiency of the method proposed in this paper, Table III compares the fault coverage of the proposed method with that of the classical test method and an earlier method [16] using the time-mode simulation for the same circuit. The fault coverage is found to be 100% for the proposed technique, whereas for the classical testing and time-mode testing method, it is not more than 90%.

Table 3. Comparison of Fault Coverage for Proposed Method, an Earlier Method [16] and Classical Test Methods.

| Earlier method [16] | Classical test | | Proposed method |
|---|---|---|---|
| | Output voltage | Supply current | |
| Fault coverage | | | |
| 90% | 78% | 85% | 100% |

## V. Conclusion

This paper applies fuzzy logic in the detection and localization of hard faults in analog circuits in the DC domain.

The FIS can display the diagnostic result visually and directly. Moreover, the results presented in this research work are very conclusive, as 100% of the entire volume of faults being examined was detected using both DC supply current and output voltage as the fault signature parameters.

Furthermore, applying the FIS approach as the fault classification tool has led to more accurate fault location in comparison to the aforementioned approaches, as all the examined faults had been successfully dissociated from each other.

This experiment indicates that this technique can quickly detect hard faults in analog circuits, as it requires one DC input voltage (a single test vector) instead of an entire voltage range. Our future work will focus on expanding the proposed approach to other analog circuits.

## References


[1] A. Torralba, J. Chavez, and L.G. Franquelo, "Fault detection and classification of analog circuits by means of fuzzy logic-based techniques," in *Proceedings of ISCAS '95—International Symposium on Circuits and Systems*, pp. 1828–1831, 1995.

[2] Y. Lifen, H. Yigang, H. Jiaoying, and S. Yichuang, "A new neural-network-based fault diagnosis approach for analog circuits by using kurtosis and entropy as a preprocessor," *IEEE Trans. on Instrumentation and Measurement*, vol. 59, no. 3, pp. 586–595, 2010.

[3] A. Kumar and A.P. Singh, "Fuzzy classifier for fault diagnosis in analog electronic circuits," *ISA Trans.*, vol. 52, no. 6, pp. 816–24, 2013.

[4] M. Tadeusiewicz, M. Ossowski, "A Verification Technique for Multiple Soft Fault Diagnosis of Linear Analog Circuits" *International Journal of Electronics and Telecommunications*, vol. 64, pp. 82–89, 2018.

[5] G. Zhao, X. Liu, B. Zhang, Y. Liu, G. Niu, C. Hu, "A novel approach for analog circuit fault diagnosis based on Deep Belief Network" *Measurement*, vol. 121, pp. 170–178, 2018.

[6] B. Han, J. Li, and H. Wu, "Diagnosis method for analog circuit hard fault and soft fault," *TELKOMNIKA Indonesian Journal of Electrical Engineering*, vol. 11, no. 9, 2013.

[7] W. He, Y. He, B. Li, and C. Zhang, "Analog circuit fault diagnosis via joint cross-wavelet singular entropy and parametric t-SNE," *Entropy*, vol. 20, no. 8, 2018.

[8] D.E. Grzechca, "Construction of an Expert System Based on Fuzzy Logic for Diagnosis of Analog Electronic Circuits" *International Journal of Electronics and Telecommunications*, vol. 61, pp. 77–82, 2015.

[9] A. Kavithamani, V. Manikandan, and N. Devarajan, "Analog circuit fault

diagnosis based on bandwidth and fuzzy classifier," *in TENCON 2009—2009 IEEE Region 10 Conference*, pp. 1–6, 2009.

[10] M.A. El-Gamal and M. Abdulghafour, "Fault isolation in analog circuits using a fuzzy inference system," *Computers & Electrical Engineering*, vol. 29, no. 1, pp. 213–229, 2003.

[11] A. Rathinam, S. Vanila, and V. Padmanabha Sharma, "Fault classification in mixed signal circuits using artificial neural networks," *Indian Journal of Science and Technology*, vol. 9, no. 38, 2016.

[12] N. Walia, H. Singh, and A. Sharma, "ANFIS: Adaptive neuro-fuzzy inference system—a survey*," International Journal of Computer Applications*, vol. 123, pp. 32–38, 2015.

[13] R.B. Ram, V.P. Moorthy, and N. Devarajan, "Fuzzy based time domain analysis approach for fault diagnosis of analog electronic circuits*," in 2009 International Conference on Control, Automation, Communication, and Energy Conservation*, pp. 1–6, 2009.

[14] Y.J. Chang, C L. Lee, J E. Chen, and c. Su, "A behavior-level fault model for the closed-loop operational amplifier," *Journal of Information Science and Engineering*, vol. 16, pp. 751–766, 2000.

[15] J. Cui and Y. Wang, "A novel approach of analog fault classification using a support vector machines classifier," *Metrology and Measurement Systems*, vol. 17, no. 4, pp. 561–582, 2010.

[16] A. Arabi, N. Bourouba, A. Belaout, and M. Ayad, «Catastrophic faults detection of analog circuits." In *2015 7th International Conference on Modelling, Identification and Control (ICMIC)*, pp. 1–6, 2015.

# The Investment Justification Estimate and Techno-economic and Ecological Aspects Analysis of the University Campus Microgrid

Nemanja Savić, Vladimir Katić, Boris Dumnić, Dragan Milićević, Zoltan Čorba, and Nenad Katić

*Abstract*—**The paper presents the plan and design of the idea of the microgrid at the Faculty of Technical Sciences in Novi Sad (FTN NS) in the university campus, which is based on the application of several different distributed energy sources. The main distributed energy sources used and planned for the distributed electricity generation in the microgrid "FTN NS" are the photovoltaic power plant with a nominal output of 9.6 kW, a photovoltaic power plant with a nominal output power of 16.3 kW, a wind power plant with a nominal output power of 2 kW, a cogeneration plant for combined heat and power production of the nominal output power of 10 kWe + 17.5 kWt, two electric vehicles of 4 kW and 2.5 kW power, and battery energy storage system with a total capacity of 36 kWh. The paper describes the main technical characteristics, the estimation of electricity generation and the estimation of the amount of non-polluted gaseous greenhouse effect for each distributed source of energy. In order to verify the justification of the application of the proposed microgrid concept, a detailed techno-economic and ecological analysis of the aspects of the application of distributed energy sources in the microgrid "FTN NS" was carried out in the paper.**

*Index Terms*—**distributed energy resources, distributed generation, microgrid, renewable energy sources, energy efficiency, techno-economic and ecological analysis**

*Original Research Paper*
*DOI: 10.7251/ELS1923026S*

## I. Introduction

HUMANITY is increasingly and intensively faced with global problems of dynamic increase in the consumption of electricity and heat, which is a consequence of the rapid increase of the human population on the planet Earth and its irrational and uneconomical relation to the limited capacities of fossil fuels, as well as the dynamic development different fields of industry and economy.

In addition, the standard way of planning and building traditional electricity systems requires a very long implementation period, which involves the implementation of various complicated processes and procedures, as well as the acquisition of licenses in the fields of construction, energy, mechanical engineering, ecology, law, etc.

In order to solve all of the above problems, especially global problems of increased energy consumption, greenhouse gas emissions (GHG), the concept of distributed electricity production based on the application of renewable energy sources has been developed.

Nowadays, one of the most effective and most efficient solutions that involves the application of the concept of renewable energy sources (RES) and energy efficiency (EE) are microgrids.

The microgrid (MG) represents a new concept in the field of clean energy technologies, which implies the application of different types of distributed energy sources (DESs) and distributed electricity production in the vicinity of electricity consumption [1]-[3].

The MG represents a small energy system based on the application of the following distributed energy technologies:

- distributed generators,
- systems and devices for storing electricity,
- systems and devices for interconnection, operation and control of MG and main distribution grid (MDG), and
- electricity consumers.

Distributed generators (photovoltaic panels, wind turbines, microturbines for combined heat and power production, hydroturbines, fuel cells, electric vehicles, etc.), their integration and application in MGs will result in increased reliability and security of power supply to consumers, improvement of power balance and frequency in the system reduction of power flows and power losses, and improvement of the quality of electricity in normal operation and cases of failure/outage in the energy system.

Energy storage systems (battery storage systems, energy and super capacitors, super magnets, flywheels, etc.) are an integral part of a MG that is used to store surplus produced electricity from distributed generators and its application in planned and/ or unplanned situations (disconnection from the MDG and

Manuscript received 21 May 2019. Received in revised form 22 June 2019. Accepted for publication 23 June 2019.

Nemanja Savić is with the Faculty of Technical Sciences, University of Novi Sad, Novi Sad, Serbia (corresponding author, e-mail: nemanja.savic@uns.ac.rs).

Vladimir Katić is with the Faculty of Technical Sciences, University of Novi Sad, Novi Sad, Serbia (e-mail: katav@uns.ac.rs).

Boris Dumnić is with the Faculty of Technical Sciences, University of Novi Sad, Novi Sad, Serbia (corresponding author, e-mail: dumnic@uns.ac.rs).

Dragan Milićević is with the Faculty of Technical Sciences, University of Novi Sad, Novi Sad (e-mail: milicevd@uns.ac.rs).

Zoltan Čorba is with the Faculty of Technical Sciences, University of Novi Sad, Novi Sad, Serbia (corresponding author, e-mail: zobos@uns.ac.rs).

Nenad Katić is with the Faculty of Technical Sciences, University of Novi Sad, Novi Sad (e-mail: nenadkatic@uns.ac.rs).

island mode of operation, disturbance of some of the distributed generators in MG, increased consumption, etc.).

Systems and devices in MGs for interconnecting, operating and controlling the MG and the MDG (power converters, power electronics, power transformers, controllers, etc.) are one of the key parts and factors for stable, reliable and safe operation and synchronization of MGs and MDGs in terms of voltage, frequency, active and reactive power flows. For the sake of better illustration, the look of the structure and architecture of a MG based on different types of DES is shown in Fig. 1.

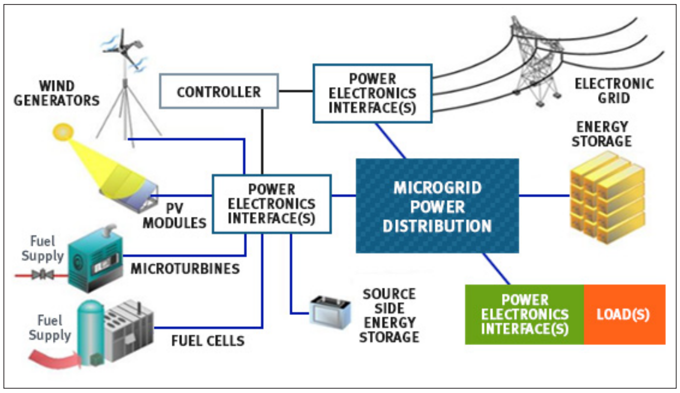


Fig. 1. Structure and architecture of the microgrid concept –an example [4].

The aim of this paper is to present the proposal of the conceptual plan and design of the MG based on the application of different DESs (in particular, two PV power plants, wind power plant, combined heat and power production plant, two electric vehicles, battery energy storage system, and electricity consumers) whose construction and realization is planned in the university campus at the Faculty of Technical Sciences Novi Sad (FTN NS), to process and analyze the main technical characteristics of the used and planned DES, with a special focus on the estimation of electricity production and the assessment of the avoidance of GHG emissions based on adequate technical, economic and ecologic analysis of the aspects the application of DES within the proposed MG. In addition, in order to better illustrate the principles of MG operation and distributed generation, the paper presents the potentials of RESs in the Republic of Serbia, as well as the classification of MGs.

## II. Renewable Energy Potential In Serbia

The Republic of Serbia is located in Southeast Europe, in the central part of the Balkan Peninsula, with the territory which represents the shortest natural link between Eastern and Western Europe, northern and Southern Europe. Considering the latitude, relief, land layout and distance from the sea, the temperate climate (continental, moderate-continental and mountainous) is maintained in the Republic of Serbia with a uniformly distributed four seasons. Spatial distribution of climate parameters in the territory of the Republic of Serbia is a geographical position, relief and local influence, as a result of a combination of relief, the distribution of air pressure of larger proportions, the exposure of the terrain, the presence of river systems, vegetation, urbanization and other factors [5].

Based on a very suitable geographical location, there are more than significant potentials of different types of RESs in the Republic of Serbia. According to [6], the largest share in the total available technical potential of RESs has biomass energy of about 61.03% (3.448 million tonnes of oil equivalent (Mtoe)/year), hydropower 29.72% (1.667 Mtoe/year), solar energy 4.25% (0.240 Mtoe/year), geothermal energy 3.19% (0.180 Mtoe/year), while the share of wind energy is estimated at around 1.82% (0.103 Mtoe/year).

Total available technical potentials, used available technical potentials and unused available technical potentials of RESs in the Republic of Serbia are shown in Fig. 2.

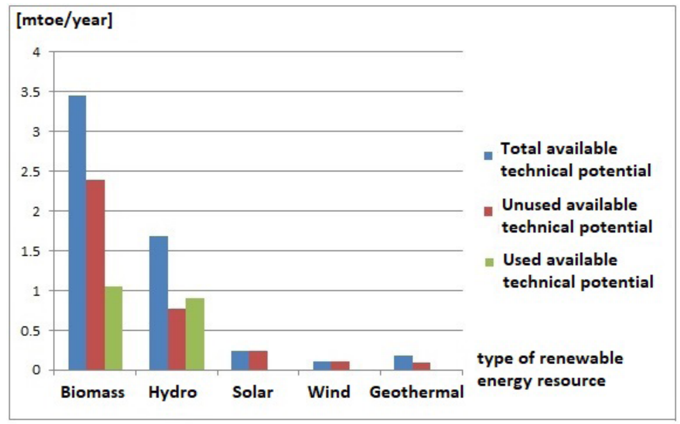


Fig. 2. Potential of RESs in Serbia.

### A. Solar energy potential

Regarding the energy potential, the Republic of Serbia has a significant amount of solar energy that can be used for the production of heat and electricity. Compared to the average in other European countries, solar radiation on the territory of the Republic of Serbia is between 35 % and 40 %, with an annual number of hours of solar radiation between 1,500 and 2,200 hours.

The average daily intensity of solar radiation in the territory of Serbia on the horizontal surface in the winter period (January) is in the range between 1.1 kWh/m$^2$ and 1.7 kWh/m$^2$ in the north, and in the summer period (month July) between 5.9 and 6.6 kWh/m$^2$ in the south, while the average annual energy of solar radiation in the territory of Serbia is around 1,200 kWh/m$^2$ in the northwest, to about 1,550 kWh/m$^2$ in the southeast, and about 1,400 kWh/m$^2$ in the central parts [6]. For the purpose of better illustration, the map of the annual average of the daily energy of global solar radiation in the territory of the Republic of Serbia is shown in Fig. 3.

Regarding the energy potential of the territory of the Autonomous Province of Vojvodina of the Republic of Serbia, where the Faculty of Technical Sciences Novi Sad is located, there are significant solar power capacities.

The average daily energy of global radiation in the territory of Vojvodina for a flat surface during the winter period (December - January) ranges between 1.0 kWh/m$^2$ in the north, 1.45

kWh/m² in the south, and up to 3.55 kWh/m² (in March), and in the summer period between 5.70 kWh/m² in the north and 6.85 kWh/m² in the south (June-August), while the average annual energy of global radiation in the territory of the Autonomous Province of Vojvodina on the horizontal surface is 1.294 kWh/m² in the north, 1.335 kWh/ m² in the south, 1,281 kWh/m² in the west, and 1,294 kWh/m² in the east [9]. For the purpose of better illustration, the annual average of the daily energy of global solar radiation in the territory of the Autonomous Province of Vojvodina in the Republic of Serbia is shown in Fig. 4.

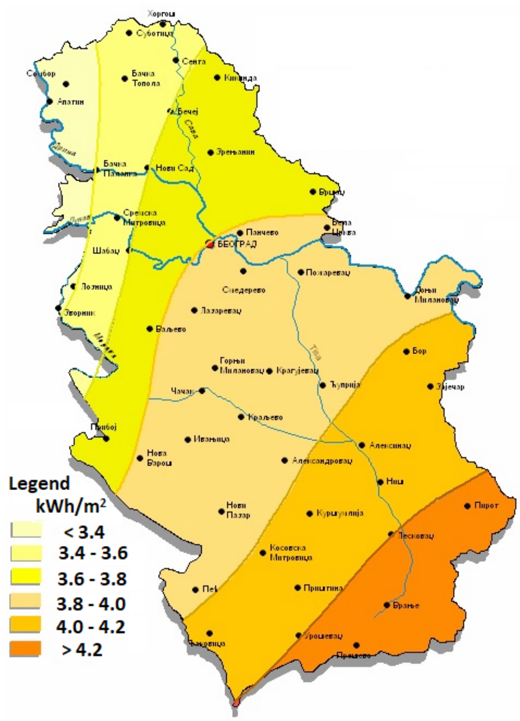


Fig. 3. Annual average daily energy of global solar radiation to the horizontal surface in Serbia [8].

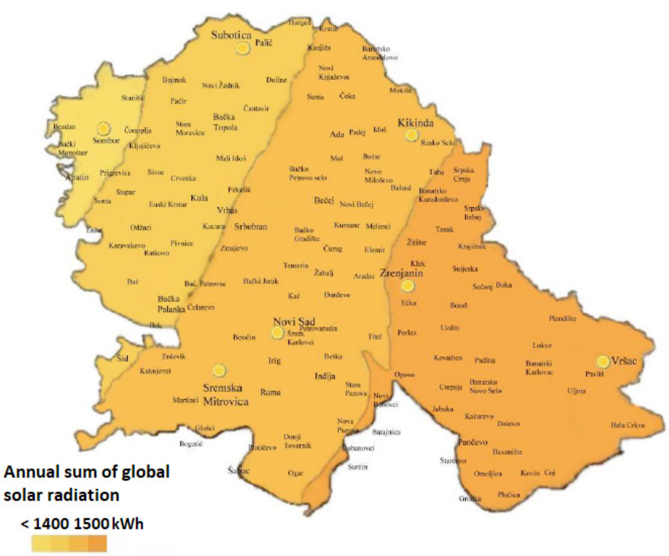


Fig. 4. Annual average daily energy of global solar radiation to the horizontal surface on the teritory of Serbia [9].

### B. Wind energy potential

Regarding the energy potential, the Republic of Serbia has a significant amount of wind energy that can be used for electricity generation.

The largest wind power in the territory of the Republic of Serbia was measured and determined in the area of southern Banat, in eastern Serbia, on the eastern side of the mountain Kopaonik, in the area of the mountain Zlatibor, on the Pešter Plateau, as well as at the locations of mountain passes at altitudes above 800 m [8]. For the purpose of better illustration, the map of the average annual wind energy in the territory of Serbia at a height of 100 meters is shown in Fig. 5.

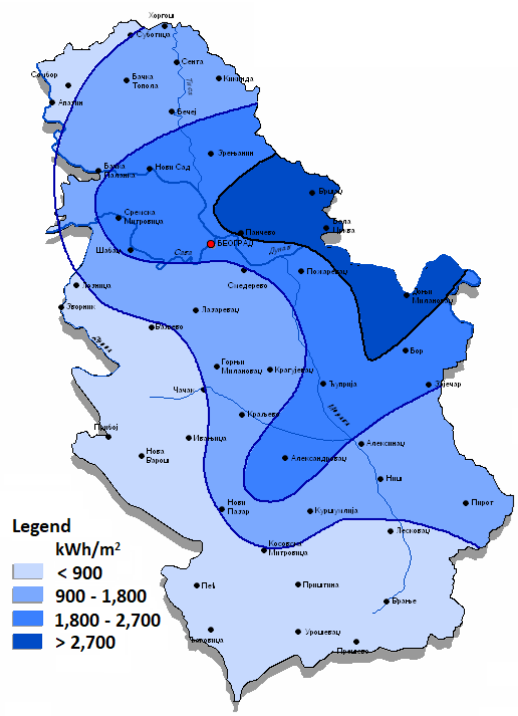


Fig. 5. Average annual wind energy in the teritory of Republic of Serbia [8].

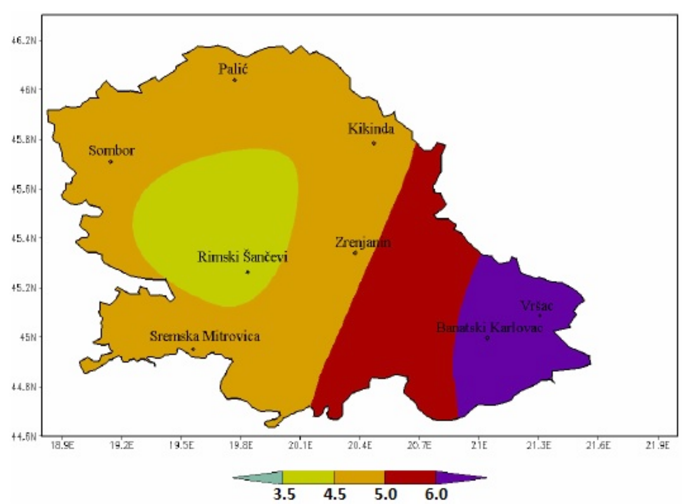


Fig. 6. Mean annual wind speed on the teritory of Vojvodina in m/ s at height of 100 m. [11].

Regarding the energy potential of the territory of the Autonomous Province of Vojvodina of the Republic of Serbia, where the Faculty of Technical Sciences Novi Sad is located, there are significant wind power capacities. According to [10], in most of the territory of Vojvodina, wind velocity was measured in the range from 3.5 m/s to 4.5 m/s in the area of Fruska Gora mountain, Vrsački Breg and southern Banat in the range 4.5 m/s to 6 m/ s, while on two locations on Vršački Breg plateau measured and determined wind speeds were more than 6 m/s. For the purpose of better illustration, mean annual wind speed in the territory of the Republic of Serbia is shown in Fig. 6.

## III. Microgrid Classification

In terms of classification, MGs can be divided according to the following three main factors:

- operating mode,
- type of energy supply, and
- control mode.

For the sake of better understanding and illustration, the classification of the MG is shown in Fig. 7. A detailed description of the classification of the MG is given below.

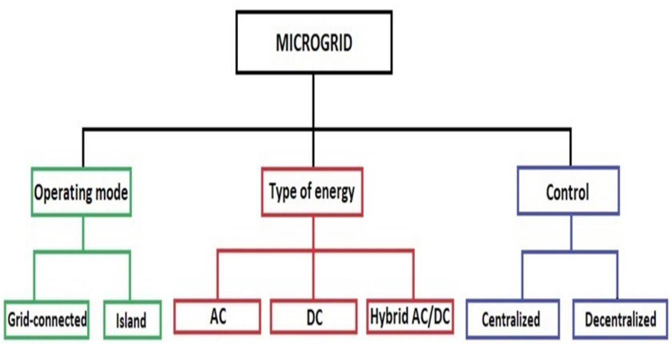


Fig. 7. Classification of the MG.

### A. Microgrid operation modes

Regarding the mode of operation, MGs can be divided into two basic groups:

1. grid-connected mode, and
2. islanded mode.

The grid-connected mode represents the first and, in practice, the most common mode of operation of the MGs, in which the MG is connected to the MDG through the central switch, Point of Common Coupling (PCC) and the transformer. In a grid-connected mode, the MG is dependent on the MDG that defines and dictates the MDG requirements that must be met. In this regard, the main goal in the grid-connected mode of operation is to optimize the operation of the MG according to technical, economic and ecological criteria.

The technical criteria of the operation of the complete energy system of the MDG and MG include enabling and ensuring the stability of the main parameters within the defined (set) technical limits (voltage, frequency, flows of active and reactive power), economic labor criteria imply the achievement of a common profit through incentive measures for production electricity and heat from RESs, while economic criteria are aimed at reducing GHG emissions through the use of DES.

In the grid-connected mode of operation, between the MG and the MDG there is a exchange of active and reactive power and electricity exchange flows, in accordance with the given technical limits of voltage and frequency. Depending on the type of contract defined between the MG and the MDG, in grid-connected mode of operation completely produced and/or the surplus of produced electricity from the MG is delivered to the MDG. In the case that the electricity consumption in the MG is greater than the electricity generation in the MG, the amount of electricity that is missing in the MG is supplied from the MDG. The main role in the case of covering the maximum loads in the grid-connected mode of operation is provided by systems and devices for storing electricity in MGs, which represent a particularly effective and efficient techno-economic and ecological solution.

The islanded mode of operation is the second and, in practice, the type of mode of operation of the MG, in which the MG is excluded from the MDG. In the island mode, the MG is independent of the MDG and without interconnection works within the technical, economic and ecological limits in a stable, secure and reliable manner. In this regard, the main task of MGs in the island mode is to enable and secure the production of electricity that will fully meet the requirements of the electricity consumers. The main objective in the island mode is the stable, reliable and safe operation of the MG while maintaining the voltage and frequency within the defined (set) technical limits.

In the island mode of operation, in addition to designing the production capacity of DESs, the main role in covering the maximum load in the MG is provided by systems and devices for energy storage, which enable and provide the necessary reserve and power supply for consumers in case of planned/unplanned failure (outage) of production units in the MG. An example of the MG architecture in grid-connected and island mode is shown in Fig. 8.

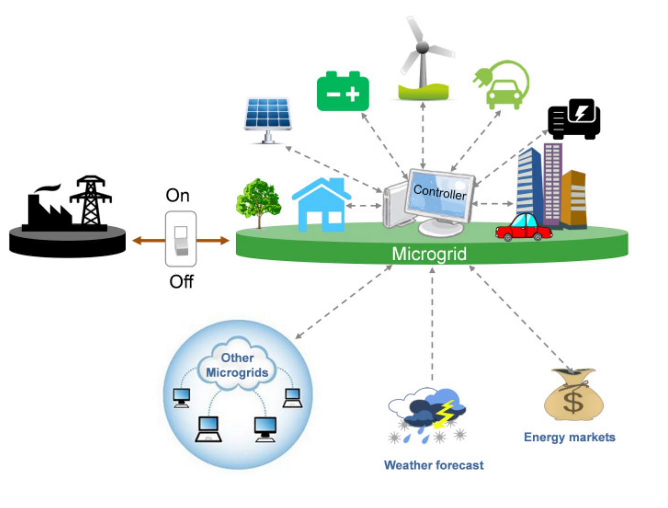


Fig. 8. Appearance of the MG and PCC with the MDG in grid-connected and island mode – an example [12].

*B. Microgrid topology*

In terms of the type of power supply system, MGs can be divided into three basic groups:

1. alternating current (AC) MG,
2. direct current (DC) MG, and
3. hybrid (AC/DC) MG.

The AC MG represents the first type of MG that is based on the application of different types of DESs, systems and devices for interconnection of the MG and MDG, and consumers of electricity. Given that AC MG is dominated mostly by AC DESs that produce AC electricity at their output (wind turbines, combined heat and power generation, diesel generators, etc.), in case of existence and use of DC DES (PV panels, fuel cells, energy storage systems, electric vehicles) AC/DC power converters are used in AC MGs. The main tasks of the DC/AC converters in AC MGs are focused on converting energy from DC DESs into AC energy to the AC bus and adjusting the AC power used by the AC consumers.

The DC MG represents second type of MG that is based on the application of different types of DESs, systems and devices for interconnection of MG and MDG, and DC consumers of electricity. Given that DC MGs are dominated mostly by DC DESs that produce DC electricity at their output (PV panels, electric vehicles, energy storage systems, fuel cells, etc.) in the case of the existence and use of AC DESs (wind turbines, combined heat and power production, diesel generators, etc.) in DC MGs are used AC/DC power converters. In DC MGs, the main tasks of the AC/DC power converter are focused on converting energy from AC DESs into DC energy on the DC bus and adjusting the DC power used by the DC consumers.

Regarding the principles of operation and control, AC and DC MGs are characterized by practically identical characteristics, with the only difference in terms of the applied energy inverter (DC/AC power converter in AC MGs, and AC/DC power converter in DC MGs).

Within basic types of MGs, the additional feature and techno-economic benefit is the fact that DC DES in DC MGs can be connected directly to the DC bus without the use of DC/DC power converters, while AC DES in AC MGs can be connected to AC bus without using AC/AC power converters. In this regard, an example of the appearance of the architecture of the AC MG (black line) and DC MG (green line) is shown in Fig. 9.

Hybrid MG represent the third type of MG that is based on the application of different types of DESs, systems and devices for interconnection of the MG and the MDG, as well as AC and DC electricity consumers. In terms of structure and architecture, hybrid MG represents a combination of a separate AC MG and separate DC MG that are interconnected in a hybrid AC/DC MG. Realization of the interconnection of AC MG and DC MG is done by means of a Bidirectional Interlink Converter (BIC) (AC/DC power power converter). In most cases of interconnection of AC MGs and DC MGs, in practice, a Back-to-Back (B2B) power converter is provided which provides and enables for the conversion of energy and the energy flow from the AC MG to the DC MG, and vice versa.

In terms of the type of concept, hybrid MGs can be implemented as AC hybrid MGs and as DC hybrid MGs. As with the case of standard (basic) types of MGs, DC DES in DC hybrid MGs can be connected directly to the DC bus without the use of DC/DC power converters, while AC DES in AC hybrid micro MGs can be connected to the AC bus without the use of AC/AC power converters, thus achieving a certain economic benefit. An example of the architecture of the hybrid AC/DC MG architecture is shown in Fig. 10.

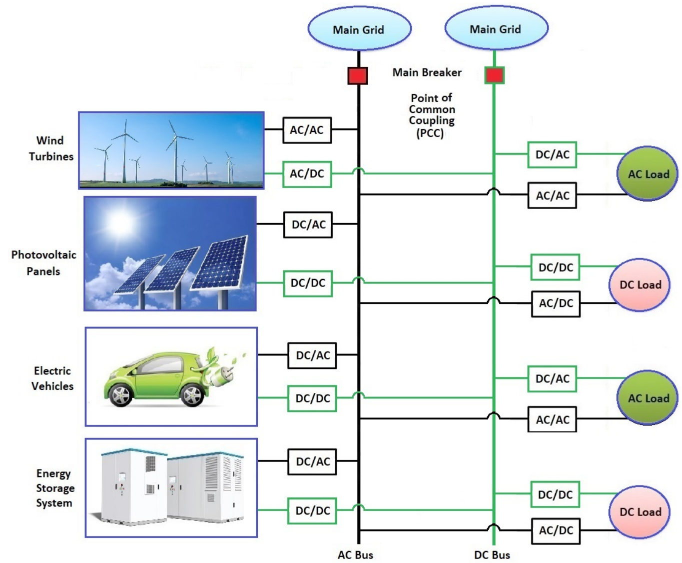


Fig. 9. An example of the architecture of an AC MG (black line) and an DC MG (green line).

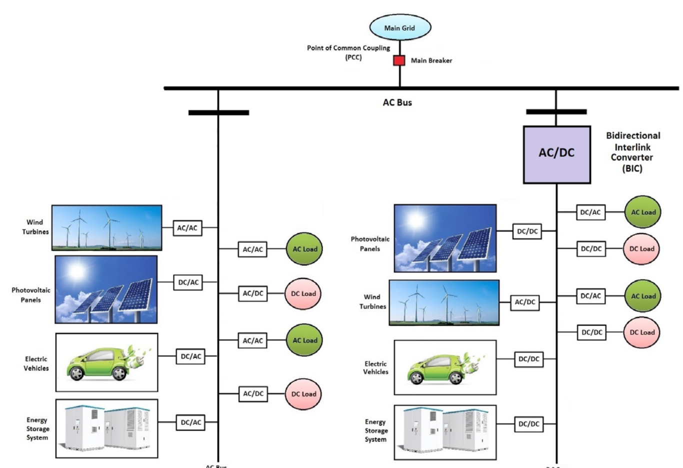


Fig. 10. An example of the architecture of hybrid AC/DC microgrid.

*C. Microgrid control*

In terms of control, MGs can be divided into two basic groups:

1. centralized, and
2. decentralized.

Centralized control represents the first type of MG control, in which the control of the complete energy system between the MG and the MDG, and the complete production of all DESs, is realized by one central control unit. In centralized control, the central control unit and main device used to connect, operate and control all types of DESs and MG in grid-connected mode and island mode, and which is responsible for the stability, reliability, security and protection of the complete energy system (MG and MDG) is microgrid central controller (MGCC).

MGCC represents the energy electronic device and the main interface between the MDG and the MG and other participants in the energy system (distribution system operator, market operator, power suppliers), whose main principle and goal of work are focused on maximizing the value of the MG (maintenance of voltage and frequency, active and reactive power), optimizing the operation of the MG, minimizing the operating costs of MG, respecting the prices in the open electricity market, demand and supply of distributed generators [1], [13]. Based on electricity prices in the electricity market and fuel prices, characteristics of production units in terms of GHG, technical requirements of the distribution grid and demand for ancillary services by the MDG, the MGCC determines the amount of energy that the MG should import from the MDG, optimizing local production, energy storage systems and/or consumption.

Decentralized control represents another type of MG control, in which the management of individual production unit and the production of an individual distributed energy source is carried out by means of individual (decentralized) control units. Decentralized MG control enables and ensures intelligent and independent operation and control of each production unit in the MG, so that the energy system continues to operate normally in the event of a failure, malfunction, outage, planned and/or unplanned interruptions/interventions of the distributed generation of one of the DESs in the energy system. In a decentralized control, the decentralized control unit and the main device used to connect individual distributed energy source and MG management in a grid-connected and island mode is the micro source controller (MSC).

MSC is an energy electronic device and a main interface between the MG and the MDG used to operate and control different types of production units of DESs in the system and/or energy storage system at the individual level. In MGs, the main principle and goal of MSCs operation and management are focused on controlling the voltage and frequency of the MG and maintaining their stability in conditions of a transient state (failure, planned/unplanned interruption of the individual distributed generator and/or complete system, load change, etc.), whereby all MSCs have the autonomy to perform local optimization of active and reactive energy from DESs (based on MGCC set and sent requests), while in the island mode of operation they have autonomy of rapid load monitoring after switching from a grid-connected mode [1], [13]. An example of the hierarchical control layout of the architecture and structure of the microgrid with MGCC and MSC is shown in Fig. 11.

Within the MG, there are three ways of hierarchical management and regulation of a MG:

1. primary regulation,
2. secondary regulation, and
3. tertiary regulation.

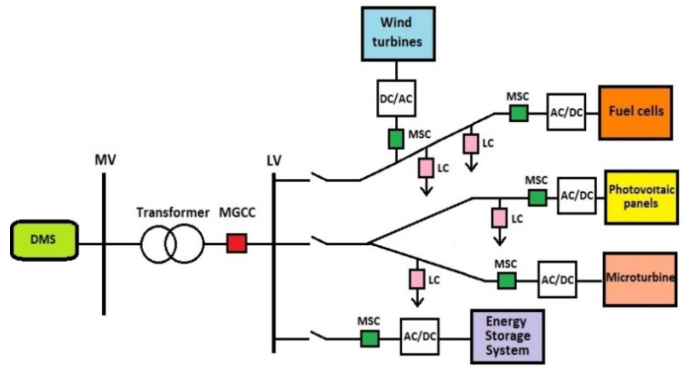


Fig. 11. An example of the hierarchical control layout of the architecture and structure of the MG with MGCC and MSC [13].

Primary regulation in the framework of hierarchical management of the MG is based on the control of the load distribution between the production units (DESs) in the MG and is primarily aimed at controlling voltage and frequency control at the local level. In the context of further hierarchical control of the MG, the secondary regulation performs actions for the purpose of correction (concretely, reduction) and/or complete elimination of the failures in the established state that occurred after primary control, and is primarily directed to frequency control and voltage control. In the final process of hierarchical control, tertiary regulation performs optimum aggregate engagement and control of flows (exchange) of energy between the MG and the MDG for optimal consumption, and aims to optimize the operation of the MG in the grid-connected and island mode. Detailed in [14].

## IV. Distributed Energy Sources In The Microgrid Concept "FTN NS"

Following the modern trends of intensive research and development, promotion and use of RESs, the application of EE, and clean energy technologies, the Faculty of Technical Sciences Novi Sad has developed the idea concept of plan and design of the microgrid (MG) "FTN NS".

The idea concept of the plan and design of the MG "FTN NS" is based on the application of the following different types of DESs and distributed electricity generation technologies and consists of the following:

1. photovoltaic power plant "FTN NS 1",
2. photovoltaic power plant "FTN NS 2",
3. wind power plant "FTN NS",
4. combined heat and power plant "FTN NS",
5. electric vehicle "FTN NS 1", and
6. electric vehicle "FTN NS 2".

### A. Photovoltaic power plant "FTN NS 1"

Within the framework of the plan and design of the MG "FTN NS", which is based on the application of different types of DESs, there is a photovoltaic (PV) power plant "FTN NS 1".

In terms of microlocation, the PV power plant "FTN NS 1" is installed on a flat roof of the building of the FTN, the geographic coordinates of the microlocation of the building are 45.246259 ° for latitude and 19.851335 ° for the geographical length [7]. For the purpose of better illustration, the satellite view of the position and appearance of the micro-location of the PV power plant "FTN NS 1" is shown in Fig. 12.

In terms of orientation and angle of inclination, the PV panels in the PV power plant "FTN NS 1" are oriented to the south at a tilting angle of 33 ° in relation to the horizon, in order to enable and ensure the maximum production of electricity of the PV power plant.


Fig. 12. Microlocation of the PV power plant "FTN NS 1" [7].

In terms of construction, the PV power plant "FTN NS 1" has a nominal output of 9.6 kWp and consists of the following main parts:

1. 40 PV panels,
2. 1 PV string inverter (DC/AC power converter),
3. 1 AC distribution box,
4. bidirectional meter, and
5. communication control devices and measuring equipment.

The block diagram of the PV power plant "FTN NS 1" within the framework of the plan and design of the MG "FTN NS 1" is shown in Fig. 13.

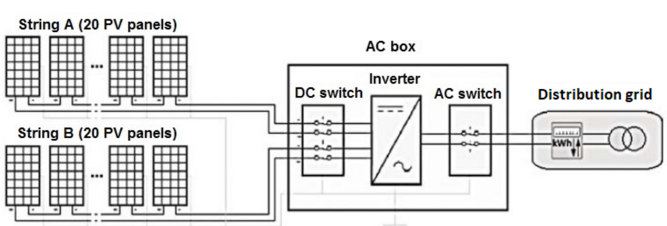


Fig. 13. Block diagram of the PV power plant "FTN NS 1".

In the process of designing and planning PV power plant "FTN NS 1", PV panels were formed and realized in two strings, each string consisting of 20 series connected PV panels (polycrystalline, nominal output power 240 W, module efficiency 14.66%) which are further connected to the DC inputs of the PV string inverter with the maximum power point tracking (MPPT). Detailed technical specifications and characteristics of used PV panels and PV string inverter in the PV power plant "FTN NS 1" are given in [15]-[16].

The AC distribution box is an integral part of the PV power plant "FTN NS 1", which houses a PV inverter string, one-way and alternating switching and protection devices and equipment (overvoltage protection, overcurrent protection, fuses, etc.) in order to enable and provide maximum reliability, security and protection of PV power plant and electricity consumers.

Since the PV power plant "FTN NS 1" is realized in the concept of "ON-grid" ("grid-tie"), the bidirectional meter is one of the components of the solar energy system. Bidirectional meter represents the PCC of the PV power plant and the MDG, where the measurement of the delivered energy into the MDG (more precisely, the electricity produced in the PV power plant) and the electricity from the MDG is carried out.

Communication control devices and measuring equipment within the PV power plant "FTN NS 1" enable and provide remote (internet) access to the portal of the PV power plant in real time, monitoring and control, as well as preservation of technical and ambient data on the micro-location of the PV power plant (daily, annual, total and current generation of electricity, current and total emissions of GHG ($CO_2$), solar radiation intensity, PV panels temperature, air temperature, wind speed, etc.). Detailed technical specifications and characteristics of used communication control devices and measuring equipment in the PV power plant "FTN NS 1" are given in [17]-[18].

As one of the best evidence that the FTN successfully follows modern trends of research, development, promotion and use of clean energy technologies, is the fact that the PV power plant "FTN NS 1" represents the first grid-connected PV power plant in the Republic of Serbia and the first privileged producer of electrical energy converted from solar energy in Serbia.

### *B. Photovoltaic power plant "FTN NS 2"*

Within the framework of the plan and design of the MG "FTN NS", which is based on the application of different types of DESs, the PV power plant "FTN NS 2" is located.

In terms of microlocation, the PV power plant "FTN NS 2" is installed on a flat roof of the building of the Mechanical Institute within the Faculty of Technical Sciences, the geographic coordinates of the microlocation of the building are 45.246259 ° for latitude and 19.851335 ° for geographical length [7]. For the purpose of better illustration, the satellite view of the position and appearance of the micro-location of the PV power plant "FTN NS 2" is shown in Fig. 14.

In terms of orientation and angle of inclination, the PV panels in the PV power plant "FTN NS 2" are oriented to the south at a tilting angle of 20 ° in relation to the horizon (the main reasons for the slope of the roof and the position of surrounding buildings on the micro-location of the PV power plant) in order to enable and secure of the maximum electricity production of the PV power plant.

In terms of construction, the PV power plant "FTN NS 2" has a nominal output power of 16.3 kWp and consists of the following main parts:

1. 69 PV panels,
2. 2 PV string inverters i 8 microinverters,
3. 2 AC distribution boxes,
4. bidirectional meter, and
5. communication control devices and measuring equipment.


Fig. 14. Microlocation of the PV power plant “FTN NS 2” [7].

The block diagram of the PV power plant “FTN NS 2” within the framework of the plan and design of the MG “FTN NS“ is shown in Fig. 15.

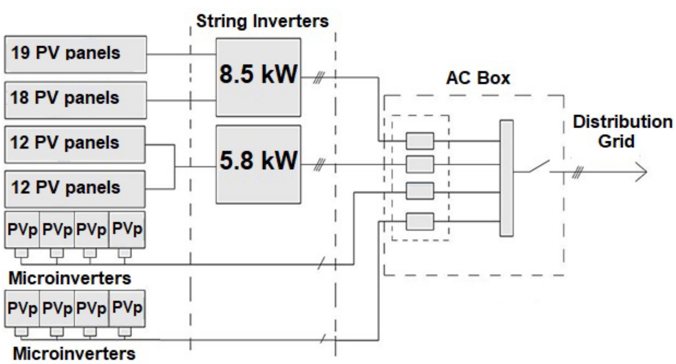


Fig. 15. Block diagram of the PV power plant “FTN NS 2”.

In the process of designing and planning PV power plant “FTN NS 2”, PV panels were formed and implemented in four strings, the first string consisting of 19 series connected PV panels, the second string consisting of 18 PV panels, while the third and fourth string consist each of 12 series connected PV panels. With regard to the concept of connection and realization, the first and second string connected to the one-way inputs of the PV string inverter of nominal output power of 8.5 kW with the MPPT inputs, the third and fourth string are connected to the single-phase inputs of the PV string inverter of nominal output power 5.8 kW with the MPPT, while each of the remaining 8 PV panels is connected to 8 microinverters.

Compared to the PV power plant “FTN NS 1” in which one type of PV panels (polycrystalline silicon) and one PV string inverter are installed, three PV panels (monocrystalline silicon, polycrystalline silicon, and thin film silicon) and two types of PV inverters (string inverters and microinverters). Detailed technical specifications and characteristics of used PV panels and PV inverters in the PV power plant “FTN NS 2” are given in [15], [19]-[23]. The technical characteristics and specifications of AC distribution boxes, bidirectional meters, communication control devices and measuring equipment in the PV power plant “FTN NS 2” are practically identical to those of the PV power plant “FTN NS 1”, which justifies the omission of further detailed descriptions.

### *C. Wind power plant “FTN NS”*

Within the framework of the plan and design of the MG “FTN NS”, which is based on the application of different types of DESs, there is a wind power plant (WPP) “FTN NS”.

In terms of microlocation, the WPP “FTN NS“ installation is planned on a flat roof of the building of the Faculty of Technical Sciences, the geographic coordinates of the microlocation of the building are 45.246073 ° for latitude and 19.851939 ° for the geographical longitude [7]. For the purpose of better illustration, the satellite view of the position and appearance of the micro-location of the WPP “FTN NS“ is shown in Fig. 16.


Fig. 16. Microlocation of the WPP “FTN NS” [7].

In terms of construction and design, the wind power plant “FTN NS” has a nominal output of 2 kW and consists of the following main parts:

1. wind turbine (wind generator),
2. inverter (DC/AC power converter),

3. AC box,
4. bidirectional meter, and
5. communication control devices and measuring equipment.

The block diagram of the WPP "FTN NS" in the framework of the plan and design of the MG "FTN NS" is shown in Fig. 17.

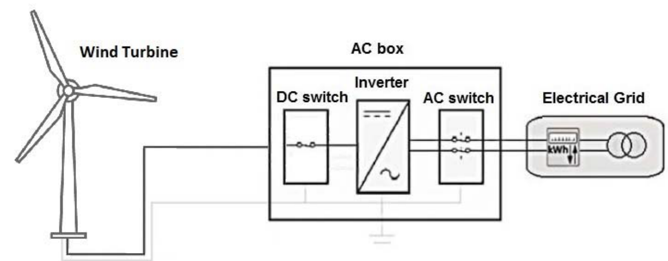


Fig. 17. Block diagram of the WPP "FTN NS".

With regard to the technical specifications of the main parts, equipment and components, within the WPP "FTN NS" is planned to install and use a wind turbine with a nominal output of 2 kW, a maximum output power of 2.95 kW, initial wind speed (cut-in speed) 2.5 m/s, working wind speed from 3 m/s to 25 m/s, nominal wind speed 8 m/s, maximum rotational speed 400 rpm and average average wind speed of 5 m/s is 4,672 kWh. The detailed technical characteristics of the WPP "FTN NS" are given in [24].

### *D. Combined heat and power plant "FTN NS"*

Within the framework of the plan and design of the MG "FTN NS", which is based on the application of different types of DESs, the combined heat and power (CHP) power plant "FTN NS" is located.

In terms of microlocation, the CHP plant "FTN NS" is planned in the building of the Mechanical Institute of the Faculty of Technical Sciences Novi Sad.

In terms of design, the CHP power plant "FTN NS" has a nominal output of 10 kW and consists of the following main parts:

1. combined heat and power generator,
2. distribution panel,
3. system controller,
4. heat and power devices and equipment.
5. communication control devices and measuring equipment.

A block diagram of the CHP power plant "FTN NS" within the framework of the MG "FTN NS" is shown in Fig. 18.

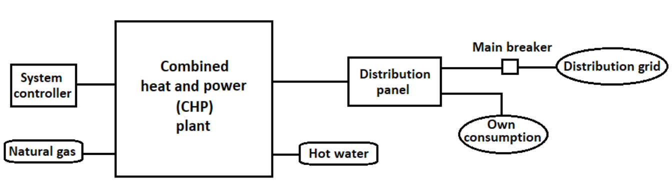


Fig. 18. Block diagram of the CHP power plant "FTN NS".

In terms of the plan and design of the CHP power plant "FTN NS", the following technical characteristics are provided: the nominal output power 10 kWe, the phase current 14 A, the recovered heat 17.5 kWt, the water inlet/outlet temperature 80°C/60°C, the total efficiency 86.5%, efficiency of electricity production 31.5%, efficiency of heat recovery 55%. The detailed technical characteristics of the CHP power plant "FTN NS" are given in [25].

### *E. Electric vehicle "FTN NS 1"*

Within the framework of the plan and design of the concept of the MG "FTN NS", which is based on the application of different types of DESs, there is an electric vehicle EV "FTN NS 1".

The EV "FTN NS 1" has power output of 4 kW (nominal voltage 48V, nominal current 104 A) and other technical characteristics of the engine system that enable and provide short distance driving of up to about 60 km. The power supply of the EV "FTN NS 1" is carried out by DC voltage 48 V by series connection of 5 batteries with a capacity of 145 Ah and a voltage of 12 V and 100 Ah and a voltage of 8 V, while the drive is a DC motor with a series-wound of a nominal speed of 2800 rpm. The detailed technical characteristics of the EV "FTN NS 1" are given in [26]. A block diagram of the drive of a DC motor of the EV "FTN NS 1" is shown in Fig. 19.

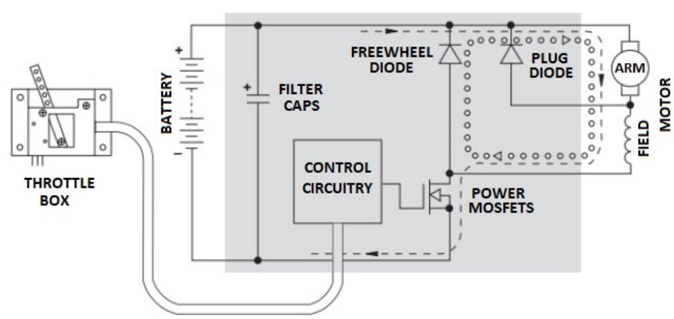


Fig. 19. Block diagram of the EV "FTN NS 1" [26].

### *F. Electric vehicle "FTN NS 2"*

Within the framework of the plan and design of the concept of the MG "FTN NS", which is based on the application of different types of DESs, there is an electric vehicle EV "FTN NS 2".

The EV "FTN NS 2" has a power output of 2.5 kW and technical characteristics of the engine system that provide and enable short-distance driving up to about 60 km. The power supply of the EV "FTN NS 2" is carried out by a DC voltage of 48 V by means batteries with a capacity of 55 Ah and a voltage of 8 V, while the drive consists of 4 permanent magnet synchronous motors, one mounted in each wheel, so that the EV "FTN NS 2" represents actually an four-wheel drive (4x4) electric vehicle. The detailed technical characteristics of the EV "FTN NS 1" are given in [26]. A block diagram of the 4 AC motor drive of the EV "FTN NS 2" is shown in Fig. 20.

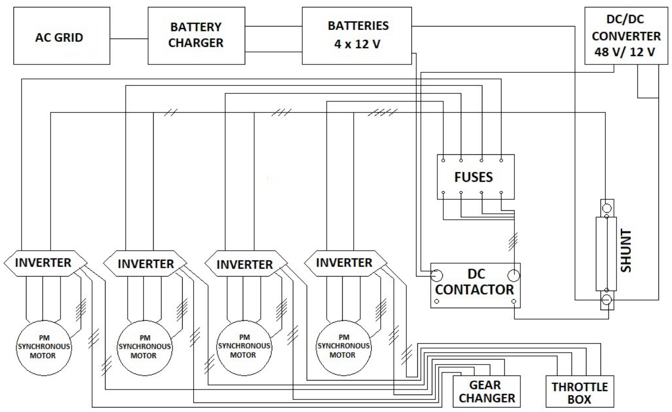


Fig. 20. Block diagram of the EV “FTN NS 2” [26].

### *G. Battery energy storage system*

In order to provide a backup power supply to electric consumers, within the framework of the concept of the MG “FTN NS” based on different types of DERs, the installation of the battery energy storage system is also planned. The main task and goal of the battery storage system is to enable and provide critical consumer power supply for at least 3 hours during an planned/unplanned interruption/outage. In order to meet this requirement, the application of 15 Absorbent Glass Matt Valve Regulated Lead Acid (AGM VRLA) batteries with a capacity of 200 Ah and a voltage of 12 V is planned and designed within the concept of the MG “FTN NS“, whose connection provides and enables total capacity of 36 kWh of electricity.

## V. Techno-Economic and Ecological Analysis of the MG “FTN NS” concept

In order to verify the feasibility of the realization of the plan and the design of the MG “FTN NS”, and the detailed consideration of the technical, economic and ecological aspects of the application of various DESs, the techno-economic and ecological analysis is carried out.

### *A. Cost and Revenues of a MG*

In the process of planning and designing the construction of power plants for the production of electricity and heat from RES, the analysis of technical, economic and ecological factors are of particular importance. For this reason, techno-economic and ecological analysis is carried out. It defines, analyzes and processes different types of costs and revenues of power plants for the production of electricity and heat from renewable sources.

Within the framework of techno-economic and ecological analysis, the total costs are most often defined and processed according to the following formula:

$$C_T = C_I + C_{O\&M} \tag{1}$$

where $C_T$ represents total costs [€], $C_I$ investment costs [€], and $C_{O\&M}$ operation and maintenance costs [€]. In most cases, decommissioning costs are part of the investment costs and are treated in this way in this paper.

Investment costs include the capital costs of the site (land), the costs of making and issuing construction, energy and environmental permits, the design of the idea and the main project, as well as the costs of procuring the equipment and devices of the RES power plant. Operational and maintenance costs include the cost of operation and the costs of planned and unplanned interventions, and are most often counted on an annual level as a certain percentage of the investment costs.

Within the framework of techno-economic and ecological analysis, total revenues are most often defined and processed according to the following equation:

$$R_T = R_{IM} + R_{GHG} \tag{2}$$

where $R_T$ represents total revenues [€], $R_{IM}$ revenues from electricity and heat generation through economic incentive measures (FIT) [€], and $R_{GHG}$ revenues from the avoidance of GHG emissions through ecological-economic incentive measures (e.g. carbon taxes) [€].

The revenues from electricity ($R_{IM}$) can be calculated on the basis of the following mathematical relation:

$$R_{IM} = E_P \cdot P_{IM} \tag{3}$$

where $E_P$ represents the amount of electricity and/or heat produced from particular type of RES power plant [kWh], $P_{IM}$ price of the incentive measure for particular type of RES power plant [c€/kWh].

The revenues from the avoidance of GHG emissions ($I_{GHG}$) can be calculated on the basis of the following mathematical relation:

$$R_{GHG} = A_{GHG} \cdot P_{GHG} \tag{4}$$

where $A_{GHG}$ represents the amount of GHG emission avoided by using of certain type of RES power plant [$kgCO_2$], $P_{GHG}$ price of the incentive measure for GHG emissions avoidance [€/$kgCO_2$]. In the world and in European countries, two main ecological and economic mechanisms used to encourage the avoidance of GHG emissions are emission trading systems and carbon tax [27]. Revenues from the avoidance of GHG emissions are calculated according to the (4) and the assumption that the carbon tax is 20 €/tonne CO2.

After detailed verification and determination of the techno-economic and ecological aspects of the proposed solution of the MG at a certain micro-location, it is necessary to determine the factor of the return of the investment (ROI) factor in the MG.

The return of investment factor in the MG is calculated on the basis of the following mathematical formula:

$$ROI = \frac{R_T - C_T}{C_T} \cdot 100\% \tag{5}$$

where $ROI$ represents the return factor of the investment in the MG, $R_T$ represents total revenues of the realization of the

MG, and $C_T$ represents total costs of the realization of the MG.

A detailed techno-economic and ecological analysis of the aspects of the application of various DESs for the case study of the MG "FTN NS" is given below.

### *B. Cost and Revenues of the microgrid "FTN NS"*

After detailed analysis and processing of technical characteristics of different types of DESs and realization of their integration within the framework of the MG "FTN NS" design and plan, in order to obtain a wider picture and detailed results, technical-economic and ecological analysis of the aspects of the proposed concept was carried out.

Techno-economic and ecological analysis of the aspects of the application of different DESs within the framework of plan and design of the MG "FTN NS" consists of and is defined on the basis of the following two parameters:

1. total costs, and
2. total revenues.

The total costs actually represent techno-economic costs of each individual DES in the MG "FTN NS". Techno-economic costs consist of the investment costs and operation and maintenance costs of each individual DES in MG "FTN NS". The results of the techno-economic analysis of techno-economic costs in terms of the application of different DESs in the MG "FTN NS" at annual and life span period (25-year) are given in Table I.

TABLE I
TECHNO-ECONOMIC COSTS OF THE MG "FTN NS"

| Type of DES | Investment costs [€] | Operation and management costs [€] |
|---|---|---|
| *PV power plant "FTN NS 1"* | 17,000.00 | 1,000.00 |
| *PV power plant "FTN NS 2"* | 27,000.00 | 1,000.00 |
| *Wind power plant "FTN NS"* | 3,750.00 | 750.00 |
| *CHP plant"FTN NS"* | 38,500.00 | 1,500.00 |
| *EV "FTN NS 1"* | 4,250.00 | 750.00 |
| *EV "FTN NS 2"* | 5,250.00 | 750.00 |
| *BESS "FTN NS"* | 6,300.00 | 0 |
| *MGCC* | 13,000.00 | 0 |
| *Total* | 115,050.00 | 5,750.00 |

Total revenues represent the techno-economic revenues and ecological-economic revenues of each individual DES in the MG "FTN NS". Techno-economic revenues consist of revenues generated through economic mechanisms for stimulating the production of electricity and heat from RESs, as well as ecological-economic revenues generated through economic mechanisms to encourage the avoidance of GHG emissions through the application of RESs.

The main parameters in the framework of the techno-economic analysis of techno-economic revenues are the amount

TABLE II
TECHNO-ECONOMIC REVENUES OF THE MG "FTN NS"

| Type of DES | Annual electricity production [kWh] | Annual income through incentive measures [€] | Life span electricity production [kWh] | Life span income through incentive measures [€] |
|---|---|---|---|---|
| *PV power plant "FTN NS 1"* | 11,346.53 | 2,609.72 | 283,663.25 | 65,243.00 |
| *PV power plant "FTN NS 2"* | 19,265.46 | 2,561.54 | 481,636.50 | 64,038.50 |
| *Wind power plant "FTN NS"* | 2,662.00 | 244.90 | 66,550.00 | 6,122.60 |
| *CHP plant"FTN NS"* | 32,850.00 | 4,538.955 | 985,500.00 | 136,168.65 |
| *EV "FTN NS 1"* | 0 | 0 | 0 | 0 |
| *EV "FTN NS 2"* | 0 | 0 | 0 | 0 |
| *BESS "FTN NS"* | 180.00 | 0 | 1,440.00 | 0 |
| *Total* | 66,309.99 | 9,955.115 | 1,818,789.75 | 271,572.75 |

TABLE III
ECOLOGICAL-ECONOMIC REVENUES OF THE MG "FTN NS"

| Type of DES | Annual GHG emissions avoided [kg$CO_2$] | Annual income through ecological-economic incentive measures [€] | Life cycle GHG emissions avoided [kg$CO_2$] | Life span income through ecological-economic incentive measures [€] |
|---|---|---|---|---|
| *PV power plant "FTN NS 1"* | 7,970.43 | 158.81 | 199,260.75 | 3,795.25 |
| *PV power plant "FTN NS 2"* | 13,533.12 | 270.66 | 338,328.00 | 6,766.50 |
| *Wind power plant "FTN NS"* | 1,597.20 | 31.94 | 39,930.00 | 798.50 |
| *CHP plant"FTN NS"* | 29,170.80 | 583.41 | 875,124.00 | 17,502.30 |
| *EV "FTN NS 1"* | 970.71 | 19.41 | 7,765.68 | 485.25 |
| *EV "FTN NS 2"* | 970.71 | 19.41 | 7,765.68 | 485.25 |
| *BESS "FTN NS"* | 198.00 | 0* | 1,440.00 | 0* |
| *Total* | 54,410.97 | 1,083.64 | 1,469,614.11 | 29,833.05 |

of electricity produced for DESs [kWh] and the amount of incentive purchase price for the production of electricity from different RESs [c€/kWh], which determines the techno-economic revenue of the microgrid at annual and life span period. In the Republic of Serbia, the Regulation on incentive measures for the production of electric energy from renewable resources and from high-efficiency electricity and thermal energy cogeneration is currently in force [28]. The results of the techno-economic analysis in terms of techno-economic revenues in terms of the application of different DESs in the MG "FTN NS" at annual and life span period are given in Table II.

The main parameters in the framework of the techno-economic analysis of ecological-economic revenues are the amount of GHG emissions (specifically CO2) avoided by the use of different DESs [kgCO2] and the incentive price for avoiding GHG emissions using RESs [€/tCO2], which determines the ecological-economic revenues of the MG "FTN NS" at the annual and the lifespan period. The results of the techno-economic analysis of ecological-economic revenues in terms of the application of different DESs in the MG "FTN NS" at annual and life span period are given in Table III.

## VI. Discussion

Based on the ROI factor calculation, the results of the carried out techno-economic and ecological analysis of the feasibility of the plan and design of the various types of DES in the MG "FTN NS" and its integration into the MDG show that the total costs of the realization of the MG "FTN NS" are 120,800 €, while the total techno-economic revenue from incentive measures for the production of electricity from various DESs and ecological-economic revenues from incentive measures to avoid GHG emissions amounts to 271,572.75 € (the worst case, without a carbon tax) and 301,405.80 € (the best case, with a carbon tax).

The results of the calculated return of investment (ROI) factor show that at the end of the power purchase agreement (12-year incentive period) from the different DESs in the MG "FTN NS" a profit of 12.41 % (the worst case, with no carbon tax) and 24.75 % (the best case, with a carbon tax) can be realized. Based on the obtained results of the techno-economic and ecological analysis of the feasibility of the plan and design of MG FTN NS and its integration into the MDG, it can be noticed that in the case of contract extension to the end of the life of distributed energy sources in MG FTN NS the value of total revenues is significantly higher the amount of the total cost of realization, which the MG "FTN NS" proposal makes even more techno-economic and ecological justified solution.

## VII. Conclusion

This paper presents the proposal of different types of the distributed energy sources, whose integration is and will be realized in the university campus within the plan and design of the microgrid at Faculty of Technical Sciences Novi Sad. In order to verify the feasibility of implementation of the proposed microgrid concept, a techno-economic and ecological analysis of the aspects of the application was carried out. The results of the work have reached the conclusion that at the end of power purchase agreement (12-year incentive period) and at the end of the life span of the all distributed energy sources in the microgrid in the university campus, the total revenues are higher than the total costs, and that the realization of the proposed microgrid concept is technical, economical, and ecological justified. Further research will be focused on the aspects of the integration of the distributed energy sources into microgrid, the stability and reliability of their work, the problem of optimizing the operation and control of distributed energy sources in microgrid, as well as aspects of the market and the internal aspects of the microgrid concept (variable energy price, vehicle to grid concept, peak shaving, backup power, etc.).

## Acknowledgment

This paper is a result of the scientific project No. III 42004 of Integrated and Interdisciplinary Research (narrow research field: Energy, Mining and Energy Efficiency) entitled "Smart Electricity Distribution Grids Based on Distribution Management System and Distributed Generation", funded by Republic of Serbia, Ministry of Education, Science and Technological Development.

## References

[1] N. Hatziargyriou, *Microgrids: Architectures and Control*, Wiley IEEE-Press, March 2014.

[2] S. Chowdhury, S. P. Chowdhury and P. Crossley, *Microgrids and Active Distribution Networks*, IET Renewable Energy, Series 6, The Institution of Engineering and Technology, 2009.

[3] H. Bevrani, B. Francois, T. Ise, *Microgrids Dynamics and Control*, Wiley IEEE Press, 2017.

[4] Doosan GridTech, What is Microgrid?, 2018, www.doosangridtech.com/faq/microgrid/ (Date accessed: 13.10.2018.)

[5] Republic of Serbia, Republic Hydrometeorological Service of Serbia http://www.hidmet.gov.rs/latin/meteorologija/klimatologija_srbije.php (Date accessed: 11.10.2018.)

[6] Ministry of Mining and Energy of the Republic of Serbia., *Energy Sector Development Strategy of the Republic of Serbia for the period by 2025 with projections by 2030*, Belgrade, Serbia, 2016.

[7] Google Maps, www.google.com/maps (Date accessed: 11.10.2018.)

[8] P. Gburčik, "Study of energy potential of the Serbia for the use of solar radiation and wind energy", Ministry of Science and Environmental Protection of the RS, National Energy Efficiency Program, EE704-1052A, Belgrade, Serbia, 2004.

[9] M. Lambic et. al., "A Study on Assessment of the Total Solar Resource - Solar Atlas and the Possibility of Production and the Use of Solar Energy on the territory Vojvodina", Provincial Secretariat for Energy and Mineral Resources, Novi Sad, September 2011. http://www.psemr.vojvodina.gov.rs/ (Date accessed: 12.10.2018.)

[10] R. Putnik et. al, "The possibility of using wind energy for electricity generation", Electric Power Industry of Serbia (EPS), Belgrade, Serbia, 2002. (in Serbian)

[11] V. Katić, "Wind Atlas of Autonomous Province Vojvodina, A Research Project Report, Provincial Secretariat for Energy and Mineral Resources of AP Vojvodina", Novi Sad, 2008. (in Serbian)

[12] Berkeley Lab, Microgrid in Berkeley Lab, 2018, https://building-microgrid.lbl.gov/about-microgrids (Date accessed: 13.10.2018.)

[13] A. G. Tsikalakis, N. D. Hatziargyriou, "Centralized Control for Optimizing Microgrids Operation," *IEEE Transactions on Energy Conversion*, Vol

23, No. 1, pp. 241-248, March 2008.

[14] M. J. Guerrero, C. J. Vasquez, J. Matas, L. García de Vicuna, M. Castilla, "Hierarchical Control of Droop-Controlled AC and DC Microgrids - A General Approach Toward Standardization" *IEEE Transactions on Industrial Electronics*, Vol. 58, No. 1, pp. 158-172, 2010.

[15] Jinko Solar, JKM250P-60, Polycristalline Module 230-250 Watt, https://jinkosolar.com/ftp/US-MKT-250P_v1.0_rev2013.pdf (Date accessed: 13.10.2018.)

[16] SMA Solar Technology AG, Operating Manual SUNNY TRIPOWER 5000TL/6000TL/7000TL/8000TL/9000TL/ 10000TL/12000TL, http://files.sma.de/dl/8552/STP8-17TL-IA-en-31.pdf (Date accessed: 13.10.2018.)

[17] SMA Solar Technology AG, Sunny WebBox with Bluetooth Wireless Technology, http://files.sma.de/dl/11567/WEBBOXBT-DEN113213W.pdf (Date accessed: 13.10.2018.)

[18] SMA Solar Technology AG, Sunny SensorBox – The weather station for PV plants, http://files.sma.de/dl/4148/SENSORBOX-DEN103131W.pdf (Date accessed: 13.10.2018.)

[19] Yingli Green Energy Holding Co., Ltd., Yingli Panda 60 Cell Series Module Datasheet, 2012, http://www.yinglisolar.com/assets/uploads/products/downloads/2012_PANDA_60.pdf (Date accessed: 13.10.2018.)

[20] Yingli Green Energy Holding Co., Ltd., Yingli 60 Cell 40 mm Series, Datasheet Yingli Solar, 2012, http://www.yinglisolar.com/assets/uploads/products/downloads/YGE_60_Cell_Series_EN.pdf (Date accessed: 13.10.2018.)

[21] Würth Solar GmbH & Co. KG, GeneCIS Solar Module 80W, WSG0036E080,2008,http://www.vindogsol.dk/GeneCIS%20modul%2080%20Wp%20datablad.pdf (Date accessed: 13.10.2018.)

[22] ABB, ABB solar inverters, ABB string inverters, Product Manual TRIO-5.8/7.5/8.5-TL-OUTD (5.8 to 8.5 kW) string inverters, https://library.e.abb.com/public/a201fd491f1a14ee85257dab0035c818/TRIO-5.8_7.5_8.5-TL-OUTD-Product%20manual%20EN-RevD.pdf, (Date accessed: 13.10.2018.)

[23] ABB, ABB solar inverters, Product manual MICRO-0.25/0.3/0.3HV-I-OUTD-US-208/240, 2014, https://library.e.abb.com/public/3b4b2359a4986e2685257dff005e1834/MICRO-0.25-0.3-0.3HV-Rev0.1.pdf, (Date accessed: 13.10.2018.)

[24] SENWEI ENERGY TECHNOLOGY INC., SW-2KW Wind Turbine, 2018,http://www.windpowercn.com/products/21.html, (Date accessed: 14.10.2018.)

[25] YANMAR ENERGY SYSTEM CO., LTD., CP Series Gas Engine Micro Cogeneration System, 2015, https://www.yanmar.com/media/global/2015/catalog/cp.pdf (Date accessed: 17.10.2018.)

[26] V. A. Katić, Z. Čorba, B. Dumnić, D. Milićević, B. Popadić, "Small electric cars – testing basic drive characteristics", Scientific-professional Symposium Energy Efficiency – ENEF 2013, Banja Luka, 22-23 November 2013. (In Serbian)

[27] World Bank, Pricing Carbon – What is Carbon Pricing?, 2018, http://www.worldbank.org/en/programs/pricing-carbon (Date accessed: 13.10.2018.)

[28] Ministry of Mining and Energy of the Republic of Serbia., "The Regulation on Incentive Measures for the Production of Electric Energy from Renewable Resources and from High-Efficiency Electricity and Thermal Energy Cogeneration" (*"Official Gazette of the Republic of Serbia", No. 091/2018*), Belgrade, Serbia, 2018.

# Preparation of Papers for Electronics (September 2011)

First A. Author, Second B. Author, and Third C. Author

***Abstract*—These instructions give you guidelines for preparing papers for ELECTRONICS journal. Use this document as a template if you are using Microsoft *Word* 6.0 or later. Otherwise, use this document as an instruction set. The electronic file of your paper will be formatted further. Define all symbols used in the abstract. Do not cite references in the abstract. Do not delete the blank line immediately above the abstract; it sets the footnote at the bottom of this column.**

***Index Terms*—About four key words or phrases in alphabetical order, separated by commas.**

*Paper Classification*
*DOI: 10.7251/ELSxxxxxxxx*

## I. Introduction

THIS document is a template for Microsoft *Word* versions 6.0 or later.

When you open the file, select "Page Layout" from the "View" menu in the menu bar (View | Page Layout), which allows you to see the footnotes. Then, type over sections of file or cut and paste from another document and use markup styles. The pull-down style menu is at the left of the Formatting Toolbar at the top of your *Word* window (for example, the style at this point in the document is "Text"). Highlight a section that you want to designate with a certain style, then select the appropriate name on the style menu. The style will adjust your fonts and line spacing. **Do not change the font sizes or line spacing to squeeze more text into a limited number of pages.** Use italics for emphasis; do not underline. The length of the manuscript is limited to the maximum of 15 pages.

To insert images in *Word,* position the cursor at the insertion point and either use Insert | Picture | From File or copy the image to the Windows clipboard and then Edit | Paste Special | Picture (with "float over text" unchecked).

We will do the final formatting of your paper.

## II. Procedure for Paper Submission

### *A. Review Stage*

The manuscripts are to be submitted using the Electronics Journal online submission system – accessible from Journal's homepage. Prepare it in two-column format as shown in this template. Place all figures and tables at the end of the paper (after the references) on separate page(s). Figures and tables must have the same caption names as referenced in the text. Only PDF format of the manuscript is allowed at the review stage. Please, check if all fonts are embedded and subset and that the quality of diagrams, illustrations, and graphics is satisfactory. Failing to provide above listed requirements is a valid reason for rejection.

### *B. Final Stage*

When you submit your final version (after your paper has been accepted), prepare it in two-column format, including figures and tables in accordance with this template. Pack all of your files (manuscript source file in *Word*, figures, and manuscript PDF form) within one archive file (you may use any of the available file compression tools: *WinZip*, *WinRAR*, *7-Zip*, etc.). Do not forget to provide the manuscript converted in PDF format that will be used as a reference for final formatting of your paper. Figures should be named as referenced in the manuscript (e.g. *fig1.eps*, *fig2.tif*, etc.)

### *C. Figures and Tables*

Format and save your graphic images using a suitable graphics processing program and adjusts the resolution settings. We accept images in the following formats: PS, EPS, TIFF, GIF, and PNG. Additionally, it is allowed to use images generated by using one of the following software tools: Microsoft Word, Microsoft PowerPoint, or Microsoft Excel. The resolution of a RGB color file should be 400 dpi. Please note that JPG and other lossy-compressed image formats are not allowed. Use available software tools to convert these images to appropriate format.

Image quality is very important to how yours graphics will reproduce. Even though we can accept graphics in many formats, we cannot improve your graphics if they are poor quality when we receive them. If your graphic looks low in

Manuscript received 15 September 2011 (write the date when you have first sent the manuscript for review). Received in revised form 20 October 2011 (write the date when you have sent the manuscript in its revised form if revisions required for your paper after review).

(Place here any sponsor and financial support acknowledgments).

F. A. Author is with the Faculty of Electrical Engineering, University of Banja Luka, Banja Luka, Bosnia and Herzegovina (corresponding author to provide phone: +387-51-222-333; fax: +387-51-111-222; e-mail: author@etfbl.net).

S. B. Author was with Faculty of Technical Sciences, University of Novi Sad, Novi Sad, Serbia. He is now with the Institute "Mihailo Pupin", Belgrade, Serbia (e-mail: author@pupin.rs).

T. C. Author is with the School of Electrical Engineering, University of Belgrade, Belgrade, Serbia, on leave from the Faculty of Electronic Engineering, University of Niš, Niš, Serbia (e-mail: author@elfak.ni.ac.rs).

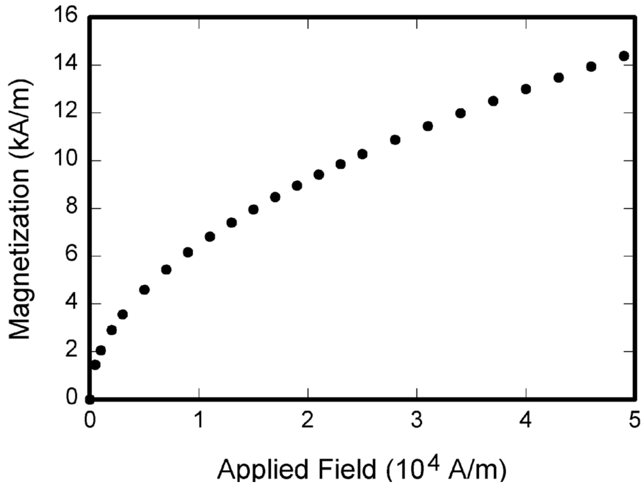

Fig. 1. Magnetization as a function of applied field. Note that "Fig." is abbreviated. There is a period after the figure number, followed by two spaces. It is good practice to explain the significance of the figure in the caption.

quality on your printer or monitor, please keep in mind that cannot improve the quality after submission.

If you are importing your graphics into this Word template, please use the following steps:

Under the option EDIT select PASTE SPECIAL. A dialog box will open, select paste picture, then click OK. Your figure should now be in the Word Document.

If you are preparing images in TIFF, EPS, or PS format, note the following. High-contrast line figures and tables should be prepared with 600 dpi resolution and saved with no compression, 1 bit per pixel (monochrome).

Photographs and grayscale figures should be prepared with 300 dpi resolution and saved with no compression, 8 bits per pixel (grayscale).

Most charts graphs and tables are one column wide (3 1/2 inches or 21 picas) or two-column width (7 1/16 inches, 43 picas wide). We recommend that you avoid sizing figures less than one column wide, as extreme enlargements may distort your images and result in poor reproduction. Therefore, it is better if the image is slightly larger, as a minor reduction in size should not have an adverse affect the quality of the image.

## III. Math

If you are using *Word,* use either the Microsoft Equation Editor or the *MathType* add-on (http://www.mathtype.com) for equations in your paper (Insert | Object | Create New | Microsoft Equation *or* MathType Equation). "Float over text" should *not* be selected.

## IV. Units

Use either SI (MKS) or CGS as primary units. (SI units are strongly encouraged.) English units may be used as secondary units (in parentheses). **This applies to papers in data storage.** For example, write "15 Gb/cm² (100 Gb/in²)." An exception

TABLE I
Units for Magnetic Properties

| Symbol | Quantity | Conversion from Gaussian and CGS EMU to SI [a] |
|---|---|---|
| $\Phi$ | magnetic flux | $1\ \mathrm{Mx} \rightarrow 10^{-8}\ \mathrm{Wb} = 10^{-8}\ \mathrm{V\cdot s}$ |
| $B$ | magnetic flux density, magnetic induction | $1\ \mathrm{G} \rightarrow 10^{-4}\ \mathrm{T} = 10^{-4}\ \mathrm{Wb/m^2}$ |
| $H$ | magnetic field strength | $1\ \mathrm{Oe} \rightarrow 10^3/(4\pi)\ \mathrm{A/m}$ |
| $m$ | magnetic moment | $1\ \mathrm{erg/G} = 1\ \mathrm{emu} \rightarrow 10^{-3}\ \mathrm{A\cdot m^2} = 10^{-3}\ \mathrm{J/T}$ |
| $M$ | magnetization | $1\ \mathrm{erg/(G\cdot cm^3)} = 1\ \mathrm{emu/cm^3} \rightarrow 10^3\ \mathrm{A/m}$ |
| $4\pi M$ | magnetization | $1\ \mathrm{G} \rightarrow 10^3/(4\pi)\ \mathrm{A/m}$ |
| $\sigma$ | specific magnetization | $1\ \mathrm{erg/(G\cdot g)} = 1\ \mathrm{emu/g} \rightarrow 1\ \mathrm{A\cdot m^2/kg}$ |
| $j$ | magnetic dipole moment | $1\ \mathrm{erg/G} = 1\ \mathrm{emu} \rightarrow 4\pi \times 10^{-10}\ \mathrm{Wb\cdot m}$ |
| $J$ | magnetic polarization | $1\ \mathrm{erg/(G\cdot cm^3)} = 1\ \mathrm{emu/cm^3} \rightarrow 4\pi \times 10^{-4}\ \mathrm{T}$ |
| $\chi, \kappa$ | susceptibility | $1 \rightarrow 4\pi$ |
| $\chi_\rho$ | mass susceptibility | $1\ \mathrm{cm^3/g} \rightarrow 4\pi \times 10^{-3}\ \mathrm{m^3/kg}$ |
| $\mu$ | permeability | $1 \rightarrow 4\pi \times 10^{-7}\ \mathrm{H/m} = 4\pi \times 10^{-7}\ \mathrm{Wb/(A\cdot m)}$ |
| $\mu_r$ | relative permeability | $\mu \rightarrow \mu_r$ |
| $w, W$ | energy density | $1\ \mathrm{erg/cm^3} \rightarrow 10^{-1}\ \mathrm{J/m^3}$ |
| $N, D$ | demagnetizing factor | $1 \rightarrow 1/(4\pi)$ |

Vertical lines are optional in tables. Statements that serve as captions for the entire table do not need footnote letters.
[a]Gaussian units are the same as cgs emu for magnetostatics; Mx = maxwell, G = gauss, Oe = oersted; Wb = weber, V = volt, s = second, T = tesla, m = meter, A = ampere, J = joule, kg = kilogram, H = henry.

is when English units are used as identifiers in trade, such as "3½-in disk drive." Avoid combining SI and CGS units, such as current in amperes and magnetic field in oersteds. This often leads to confusion because equations do not balance dimensionally. If you must use mixed units, clearly state the units for each quantity in an equation.

The SI unit for magnetic field strength $H$ is A/m. However, if you wish to use units of T, either refer to magnetic flux density $B$ or magnetic field strength symbolized as $\mu_0 H$. Use the center dot to separate compound units, e.g., "$\mathrm{A\cdot m^2}$."

## V. Helpful Hints

### *A. Figures and Tables*

Because we will do the final formatting of your paper, you do not need to position figures and tables at the top and bottom of each column. In fact, all figures, figure captions, and tables can be at the end of the paper. Large figures and tables may span both columns. Place figure captions below the figures; place table titles above the tables. If your figure has two parts, include the labels "(a)" and "(b)" as part of the artwork. Please verify that the figures and tables you mention in the text actually exist. **Please do not include captions as part of the figures. Do not put captions in "text boxes" linked to the figures. Do not put borders around the outside of your figures.** Use the abbreviation "Fig." even at the beginning of a sentence. Do not abbreviate "Table." Tables are numbered with Roman numerals.

Color printing of figures is not available Do not use color unless it is necessary for the proper interpretation of your figures.

Figure axis labels are often a source of confusion. Use words rather than symbols. As an example, write the quantity "Magnetization," or "Magnetization *M*," not just "*M*." Put units in parentheses. Do not label axes only with units. As in Fig. 1, for example, write "Magnetization (A/m)" or "Magnetization ($A \cdot m^{-1}$)," not just "A/m." Do not label axes with a ratio of quantities and units. For example, write "Temperature (K)," not "Temperature/K."

Multipliers can be especially confusing. Write "Magnetization (kA/m)" or "Magnetization ($10^3$ A/m)." Do not write "Magnetization (A/m) x 1000" because the reader would not know whether the top axis label in Fig. 1 meant 16000 A/m or 0.016 A/m. Figure labels should be legible, approximately 8 to 12 point type.

### *B. References*

Number citations consecutively in square brackets [1]. The sentence punctuation follows the brackets [2]. Multiple references [2], [3] are each numbered with separate brackets [1]–[3]. When citing a section in a book, please give the relevant page numbers [2]. In sentences, refer simply to the reference number, as in [3]. Do not use "Ref. [3]" or "reference [3]" except at the beginning of a sentence: "Reference [3] shows ... ." Please do not use automatic endnotes in *Word*, rather, type the reference list at the end of the paper using the "References" style.

Number footnotes separately in superscripts (Insert | Footnote).[1] Place the actual footnote at the bottom of the column in which it is cited; do not put footnotes in the reference list (endnotes). Use letters for table footnotes (see Table I).

Please note that the references at the end of this document are in the preferred referencing style. Give all authors' names; do not use "*et al*." unless there are six authors or more. Use a space after authors' initials. Papers that have not been published should be cited as "unpublished" [4]. Papers that have been accepted for publication, but not yet specified for an issue should be cited as "to be published" [5]. Papers that have been submitted for publication should be cited as "submitted for publication" [6]. Please give affiliations and addresses for private communications [7].

Capitalize only the first word in a paper title, except for proper nouns and element symbols. For papers published in translation journals, please give the English citation first, followed by the original foreign-language citation [8]. All references **must be** written in Roman alphabet.

### *C. Abbreviations and Acronyms*

Define abbreviations and acronyms the first time they are used in the text, even after they have already been defined in the abstract. Abbreviations such as IEEE, SI, ac, and dc do not have to be defined. Abbreviations that incorporate periods should not have spaces: write "C.N.R.S.," not "C. N. R. S." Do not use abbreviations in the title unless they are unavoidable (for example, "IEEE" in the title of this article).

### *D. Equations*

Number equations consecutively with equation numbers in parentheses flush with the right margin, as in (1). First use the equation editor to create the equation. Then select the "Equation" markup style. Press the tab key and write the equation number in parentheses. To make your equations more compact, you may use the solidus ( / ), the exp function, or appropriate exponents. Use parentheses to avoid ambiguities in denominators. Punctuate equations when they are part of a sentence, as in

$$\begin{aligned} \int_0^{r_2} F(r,\varphi)\, dr\, d\varphi = [\sigma r_2 / (2\mu_0)] \\ \cdot \int_0^{\infty} \exp(-\lambda |z_j - z_i|)\, \lambda^{-1} J_1(\lambda r_2)\, J_0(\lambda r_i)\, d\lambda . \end{aligned} \tag{1}$$

Be sure that the symbols in your equation have been defined before the equation appears or immediately following. Italicize symbols (*T* might refer to temperature, but T is the unit tesla). Refer to "(1)," not "Eq. (1)" or "equation (1)," except at the beginning of a sentence: "Equation (1) is ... ."

### *E. Other Recommendations*

Use one space after periods and colons. Hyphenate complex modifiers: "zero-field-cooled magnetization." Avoid dangling participles, such as, "Using (1), the potential was calculated." [It is not clear who or what used (1).] Write instead, "The potential was calculated by using (1)," or "Using (1), we calculated the potential."

Use a zero before decimal points: "0.25," not ".25." Use "$cm^3$," not "cc." Indicate sample dimensions as "0.1 cm x 0.2 cm," not "0.1 x 0.2 $cm^2$." The abbreviation for "seconds" is "s," not "sec." Do not mix complete spellings and abbreviations of units: use "$Wb/m^2$" or "webers per square meter," not "webers/$m^2$." When expressing a range of values, write "7 to 9" or "7-9," not "7~9."

A parenthetical statement at the end of a sentence is punctuated outside of the closing parenthesis (like this). (A parenthetical sentence is punctuated within the parentheses.) In American English, periods and commas are within quotation marks, like "this period." Other punctuation is "outside"! Avoid contractions; for example, write "do not" instead of "don't." The serial comma is preferred: "A, B, and C" instead of "A, B and C."

If you wish, you may write in the first person singular or plural and use the active voice ("I observed that ..." or "We observed that ..." instead of "It was observed that ..."). Remember to check spelling. If your native language is not English, please get a native English-speaking colleague to carefully proofread your paper.

[1] It is recommended that footnotes be avoided (except for the unnumbered footnote with the receipt date and authors' affiliations on the first page). Instead, try to integrate the footnote information into the text.

## VI. Some Common Mistakes

The word "data" is plural, not singular. The subscript for the permeability of vacuum $\mu_0$ is zero, not a lowercase letter "o." The term for residual magnetization is "remanence"; the adjective is "remanent"; do not write "remnance" or "remnant." Use the word "micrometer" instead of "micron." A graph within a graph is an "inset," not an "insert." The word "alternatively" is preferred to the word "alternately" (unless you really mean something that alternates). Use the word "whereas" instead of "while" (unless you are referring to simultaneous events). Do not use the word "essentially" to mean "approximately" or "effectively." Do not use the word "issue" as a euphemism for "problem." When compositions are not specified, separate chemical symbols by en-dashes; for example, "NiMn" indicates the intermetallic compound $Ni_{0.5}Mn_{0.5}$ whereas "Ni–Mn" indicates an alloy of some composition $Ni_xMn_{1-x}$.

Be aware of the different meanings of the homophones "affect" (usually a verb) and "effect" (usually a noun), "complement" and "compliment," "discreet" and "discrete," "principal" (e.g., "principal investigator") and "principle" (e.g., "principle of measurement"). Do not confuse "imply" and "infer."

Prefixes such as "non," "sub," "micro," "multi," and "ultra" are not independent words; they should be joined to the words they modify, usually without a hyphen. There is no period after the "et" in the Latin abbreviation "*et al.*" (it is also italicized). The abbreviation "i.e.," means "that is," and the abbreviation "e.g.," means "for example" (these abbreviations are not italicized).

An excellent style manual and source of information for science writers is [9].

## VII. Editorial Policy

Each manuscript submitted is subjected to the following review procedure:

- It is reviewed by the editor for general suitability for this publication
- If it is judged suitable, two reviewers are selected and a single-blinded review process takes place
- Based on the recommendations of the reviewers, the editor then decides whether the particular paper should be accepted as is, revised or rejected.

Do not submit a paper you have submitted or published elsewhere. Do not publish "preliminary" data or results. The submitting author is responsible for obtaining agreement of all coauthors and any consent required from sponsors before submitting a paper. It is the obligation of the authors to cite relevant prior work.

Every paper submitted to "Electronics" journal are single-blind reviewed. For conference-related papers, the decision to accept or reject a paper is made by the conference editors and publications committee; the recommendations of the referees are advisory only. Undecipherable English is a valid reason for rejection.

## VIII. Publication Principles

The contents of "Electronics" are peer-reviewed and archival. The "Electronics" publishes scholarly articles of archival value as well as tutorial expositions and critical reviews of classical subjects and topics of current interest.

Authors should consider the following points:

1) Technical papers submitted for publication must advance the state of knowledge and must cite relevant prior work.
2) The length of a submitted paper should be commensurate with the importance, or appropriate to the complexity, of the work. For example, an obvious extension of previously published work might not be appropriate for publication or might be adequately treated in just a few pages.
3) Authors must convince both peer reviewers and the editors of the scientific and technical merit of a paper; the standards of proof are higher when extraordinary or unexpected results are reported.
4) Because replication is required for scientific progress, papers submitted for publication must provide sufficient information to allow readers to perform similar experiments or calculations and use the reported results. Although not everything need be disclosed, a paper must contain new, useable, and fully described information. For example, a specimen's chemical composition need not be reported if the main purpose of a paper is to introduce a new measurement technique. Authors should expect to be challenged by reviewers if the results are not supported by adequate data and critical details.
5) Papers that describe ongoing work or announce the latest technical achievement, which are suitable for presentation at a professional conference, may not be appropriate for publication in "Electronics".

## IX. Conclusion

A conclusion section is not required. Although a conclusion may review the main points of the paper, do not replicate the abstract as the conclusion. A conclusion might elaborate on the importance of the work or suggest applications and extensions.

## Appendix

Appendixes, if needed, appear before the acknowledgment.

## Acknowledgment

The preferred spelling of the word "acknowledgment" in American English is without an "e" after the "g." Use the singular heading even if you have many acknowledgments. Avoid expressions such as "One of us (S.B.A.) would like to thank ... ." Instead, write "F. A. Author thanks ... ." **Sponsor and financial support acknowledgments are placed in the unnumbered footnote on the first page, not here.**

## References

[1] G. O. Young, “Synthetic structure of industrial plastics (Book style with paper title and editor),” in *Plastics*, 2nd ed. vol. 3, J. Peters, Ed. New York: McGraw-Hill, 1964, pp. 15–64.

[2] W.-K. Chen, *Linear Networks and Systems* (Book style). Belmont, CA: Wadsworth, 1993, pp. 123–135.

[3] H. Poor, *An Introduction to Signal Detection and Estimation*. New York: Springer-Verlag, 1985, ch. 4.

[4] B. Smith, “An approach to graphs of linear forms (Unpublished work style),” unpublished.

[5] E. H. Miller, “A note on reflector arrays (Periodical style—Accepted for publication),” *IEEE Trans. Antennas Propagat.*, to be published.

[6] J. Wang, “Fundamentals of erbium-doped fiber amplifiers arrays (Periodical style—Submitted for publication),” *IEEE J. Quantum Electron.*, submitted for publication.

[7] C. J. Kaufman, Rocky Mountain Research Lab., Boulder, CO, private communication, May 1995.

[8] Y. Yorozu, M. Hirano, K. Oka, and Y. Tagawa, “Electron spectroscopy studies on magneto-optical media and plastic substrate interfaces (Translation Journals style),” *IEEE Transl. J. Magn.Jpn.*, vol. 2, Aug. 1987, pp. 740–741 [*Dig. 9th Annu. Conf. Magnetics* Japan, 1982, p. 301].

[9] M. Young, *The Techincal Writers Handbook.* Mill Valley, CA: University Science, 1989.

[10] J. U. Duncombe, “Infrared navigation—Part I: An assessment of feasibility (Periodical style),” *IEEE Trans. Electron Devices*, vol. ED-11, pp. 34–39, Jan. 1959.

[11] S. Chen, B. Mulgrew, and P. M. Grant, “A clustering technique for digital communications channel equalization using radial basis function networks,” *IEEE Trans. Neural Networks*, vol. 4, pp. 570–578, Jul. 1993.

[12] R. W. Lucky, “Automatic equalization for digital communication,” *Bell Syst. Tech. J.*, vol. 44, no. 4, pp. 547–588, Apr. 1965.

[13] S. P. Bingulac, “On the compatibility of adaptive controllers (Published Conference Proceedings style),” in *Proc. 4th Annu. Allerton Conf. Circuits and Systems Theory*, New York, 1994, pp. 8–16.

[14] G. R. Faulhaber, “Design of service systems with priority reservation,” in *Conf. Rec. 1995 IEEE Int. Conf. Communications,* pp. 3–8.

[15] W. D. Doyle, “Magnetization reversal in films with biaxial anisotropy,” in *1987 Proc. INTERMAG Conf.*, pp. 2.2-1–2.2-6.

[16] G. W. Juette and L. E. Zeffanella, “Radio noise currents n short sections on bundle conductors (Presented Conference Paper style),” presented at the IEEE Summer power Meeting, Dallas, TX, Jun. 22–27, 1990, Paper 90 SM 690-0 PWRS.

[17] J. G. Kreifeldt, “An analysis of surface-detected EMG as an amplitude-modulated noise,” presented at the 1989 Int. Conf. Medicine and Biological Engineering, Chicago, IL.

[18] J. Williams, “Narrow-band analyzer (Thesis or Dissertation style),” Ph.D. dissertation, Dept. Elect. Eng., Harvard Univ., Cambridge, MA, 1993.

[19] N. Kawasaki, “Parametric study of thermal and chemical nonequilibrium nozzle flow,” M.S. thesis, Dept. Electron. Eng., Osaka Univ., Osaka, Japan, 1993.

[20] J. P. Wilkinson, “Nonlinear resonant circuit devices (Patent style),” U.S. Patent 3 624 12, July 16, 1990.

*[21] IEEE Criteria for Class IE Electric Systems* (Standards style), IEEE Standard 308, 1969.

*[22] Letter Symbols for Quantities*, ANSI Standard Y10.5-1968.

[23] R. E. Haskell and C. T. Case, “Transient signal propagation in lossless isotropic plasmas (Report style),” USAF Cambridge Res. Lab., Cambridge, MA Rep. ARCRL-66-234 (II), 1994, vol. 2.

[24] E. E. Reber, R. L. Michell, and C. J. Carter, “Oxygen absorption in the Earth’s atmosphere,” Aerospace Corp., Los Angeles, CA, Tech. Rep. TR-0200 (420-46)-3, Nov. 1988.

[25] (Handbook style) *Transmission Systems for Communications,* 3rd ed., Western Electric Co., Winston-Salem, NC, 1985, pp. 44–60.

[26] *Motorola Semiconductor Data Manual,* Motorola Semiconductor Products Inc., Phoenix, AZ, 1989.

[27] (Basic Book/Monograph Online Sources) J. K. Author. (year, month, day). *Title* (edition) [Type of medium]. Volume (issue). Available: http://www.(URL)

[28] J. Jones. (1991, May 10). Networks (2nd ed.) [Online]. Available: http://www.atm.com

[29] (Journal Online Sources style) K. Author. (year, month). Title. *Journal* [Type of medium]. Volume(issue), paging if given. Available: http://www.(URL)

[30] R. J. Vidmar. (1992, August). On the use of atmospheric plasmas as electromagnetic reflectors. *IEEE Trans. Plasma Sci.* [Online]. *21(3).* pp. 876–880. Available: http://www.halcyon.com/pub/journals/21ps03-vidmar

# Information for Authors

### *Editorial objectives*

In the journal ”Electronics”, the scientific papers from different fields of electronics and electrical engineering in the broadest sense are published. Main topics are electronics, automatics, telecommunications, computer techniques, power engineering, nuclear and medical electronics, analysis and synthesis of electronic circuits and systems, new technologies and materials in electronics etc. The main emphasis of papers should be on methods and new techniques, or the application of existing techniques in a novel way.

### *The reviewing process*

Each manuscript submitted is subjected to the following review procedures:

- It is reviewed by the editor for general suitability for this publication;
- If it is judged suitable, two reviewers are selected and a double-blind review process takes place;
- Based on the recommendations of the reviewers, the editor then decides whether the particular paper should be accepted as it is, revised or rejected.

### *Submissions Process*

The manuscripts are to be submitted using the Electronics Journal online submission system – accessible from Journal’s homepage.

Manuscripts have to be prepared in accordance with the instructions given in the template for paper preparation that can be found on the journal’s web page (www.els-journal.etf.unibl.org).

**Authors should note that proofs are not supplied prior to publication and ensure that the paper submitted is complete and in its final form.**

### *Copyright*

Articles submitted to the journal should be original contributions and should not be under consideration for any other publication at the same time. Authors submitting articles for publication warrant that the work is not an infringement of any existing copyright and will indemnify the publisher against any breach of such warranty. For ease of dissemination and to ensure proper policing of use, papers and contributions become the legal copyright of the publisher unless otherwise agreed.

# ELECTRONICS, VOL. 23, NO. 1, JUNE 2019




**ISSN 1450-5843**
**UDK 621.38**